TECHNISCHE UNIVERSITÄT WIEN

INSTITUT FÜR MECHANIK UND MECHATRONIK

Diploma Thesis

Modelling the Human Control of a Steer-by-Wire Bicycle

carried out for the purpose of obtaining the academic degree of Diplom-Ingenieur (Dipl.-Ing. or DI) under the supervision of

Senior Lecturer Dipl.-Ing. Dr.techn. Florian Klinger
Institute of Mechanics and Mechatronics

with co-supervision from

Ao.Univ.Prof. Dipl.-Ing. Dr.techn. Manfred Plöchl
Institute of Mechanics and Mechatronics

submitted at the TU Wien
Faculty of Mechanical and Industrial Engineering

Michael Ruttmann
11909827
066 445

I acknowledge that I am only authorised to publish my thesis with the title

Diploma Thesis

with the approval of the examination board.

Statutory Declaration

I declare on oath that this thesis was written by myself in accordance with the recognized principles of academic writing. All resources used, in particular the underlying literature, are named and listed in this thesis. The passages taken verbatim from the sources are labeled as such.

The topic of this thesis has not been submitted by me in any form as an examination paper to an assessor either in Austria or abroad. This thesis is identical to the thesis assessed by the assessors.

Wien, Monday 24th March, 2025 Michael Ruttmann

Kurzfassung

Diese Arbeit behandelt die Modellierung der menschlichen Führung eines Steer-by-Wire Fahrrades. Das Steuern und Stabilisieren eines Fahrrades ist eine auf den ersten Blick einfache Tätigkeit, die bei genauerer Betrachtung jedoch erhebliche Ansprüche an den Menschen stellt: es verlangt die sensorische Auffassung des aktuellen Fahrzustandes, die Planung einer gewünschten Fahrtrajektorie unter Berücksichtigung des dynamischen Verhaltens des Fahrrades, sowie die anschließende Umwandlung dessen in adäquate Eingaben durch den Menschen, welche insbesondere in Form von auf den Lenker aufgebrachten Kräften erfolgt. Das daraus resultierende Lenkmoment stellt die wesentliche Stellgröße zum Führen eines Fahrrades dar.

Am Forschungsbereich für Technische Dynamik und Fahrzeugdynamik wird ein Steer-by-Wire Fahrrad aufgebaut, mit welchem die Interaktion zwischen Mensch und Fahrrad vertieft untersucht werden soll. Im Zuge dieser Diplomarbeit erfolgt die simulationsbasierte Auslegung der Funktionen des Systems. Hierzu wurde ein bestehendes Mehrkörpersimulationsmodell des Fahrrads samt den Komponenten des Steer-by-Wire Systems um ein Fahrermodel erweitert, welche basierend auf vorgegebenen Fahrtrajektorien die Lenkeingaben des menschlichen Fahrers bzw. der menschlichen Fahrerin modelliert. Es wurden dabei zwei Ansätze implementiert: ein Fahrrad-Fahrermodell, das unmittelbar ein Lenkmoment ausgibt, sowie ein PKW-Fahrermodell, das die Steuerung des Fahrrades über ein Lenkrad und die Vorgabe von Lenkwinkeln abbildet; die Umwandlung in ein geeignetes Lenkmoment erfolgt dann durch das Steer-by-Wire System. In beiden Fällen werden die Lenkeingaben an einen Stabilisierungsregler übermittelt, der einerseits diese Eingaben mittels Folgeregelung an die Gabel überträgt, und andererseits den Fahrzustand (sofern erforderlich) stabilisiert.

Durch die mechanische Entkopplung von Gabel und Lenker erfolgt bei einem Steer-by-Wire Systemkeine unmittelbare Rückmeldung an den Fahrer bzw. die Fahrerin; zur Generierung eines entsprechenden Feedbacks wurde ein Ansatz entworfen, der dem Fahrer(modell) ein zur Eingabe und zum aktuellen Fahrzustand passendes Feedbackmoment liefert. Die einzelnen Funktionen des Steer-by-Wire Systems sind modular aufgebaut, und die Parameter der jeweiligen Regelsysteme wurden anhand des Simulationsmodells abgestimmt. Abschließend werden die Funktionen des Steer-by-Wire Systems anhand ausgewählter Teststrecken in der Simulationsumgebung dargestellt und untersucht. Die Ergebnisse dieser Untersuchungen sollen die Grundlage für die spätere Umsetzung eines Prototyps bilden.

Abstract

This thesis discusses the modelling of the human control of a Steer-by-Wire bicycle. Steering and stabilizing a bicycle is a task that appears simple at first glance but, upon closer examination, puts significant demands on the human operator: It demands the accurate sensory perception of the current dynamical state of the bicycle, the precise planning of a desired trajectory while accounting for the dynamic behavior of the bicycle, and the transformation of this plan into appropriate human inputs, primarily in the form of forces exerted on the handlebars. The resulting steering torque is the crucial control variable for guiding the bicycle.

At the Research Unit for Technical Dynamics and Vehicle Dynamics, a Steer-by-Wire bicycle is being developed to investigate the interaction between humans and bicycles. As part of this thesis, the simulation-based design of the system's functionalities is carried out. To this end, an existing multi-body simulation model of the bicycle, including the components of the Steer-by-Wire system, was extended by a rider model that simulates the steering inputs of a human rider based on predefined trajectories. Two approaches were implemented: a bicycle-rider model that gives a steer torque as output, and a car-driver model that simulates the control of the bicycle with a steering wheel by providing steering wheel angle courses, where the assignment of the steering wheel angle to an appropriate steering torque is performed by the Steer-by-Wire system. In both cases, the steering inputs are transmitted to a stabilization controller, which transfers these inputs to the fork using a follow-up control algorithm and, if necessary, stabilizes the riding state.

Due to the mechanical decoupling of the fork and the handlebar in a Steer-by-Wire system, there exists no immediate feedback to the rider by the steering. An approach was designed to provide the rider (model) with a feedback torque that corresponds to the input and the current dynamical bicycle state. The individual functions of the Steer-by-Wire system are modularly designed, and the parameters of the respective control systems were fine-tuned based on the simulation model. Finally, the functions of the Steer-by-Wire system are demonstrated and analyzed using selected test trajectories in the simulation environment. The results of these investigations are intended to form the base for an actual future prototype.

Danksagung

Zuallererst möchte ich mich bei meinem Hauptbetreuer Herrn Senior Lecturer Dipl.-Ing. Dr.techn. Florian Klinger bedanken, welcher stets ein offenes Ohr für meine Fragen und Anliegen hatte und mir genug Freiraum gab, dieser Arbeit einen persönlichen Stempel aufzudrücken, mit wertvollen Impulsen und Hinweisen unterstützte, wenn es Bedarf gab. Vielen Dank für die zahlreichen interessanten Meetings, in denen ich vieles von Ihnen lernen durfte und wo massenhaft spannende Gespräche entstanden. Weiters möchte ich meinem Zweitbetreuer Ao.Univ.Prof. Dipl.-Ing. Dr.techn. Manfred Plöchl bedanken, welcher ebenso stets für Fragen offen war und die Idee für diese Arbeit gab. Ihr beide ward die Stützräder dieser akademischen Radfahrt, welche mich zur Vollbringung dieser Arbeit geführt haben.

Weiters möchte ich mich bei den wichtigsten Personen in meinem Leben bedanken: meinen Eltern Sandra und Willibald. Meiner Mutter möchte ich für ihre empathische, einfühlsame Art danken. Du hattest und hast immer ein offenes Ohr für meine Probleme, egal ob akademischer oder privater Natur, egal ob irgendwie deinen Interessen entsprechend oder nicht. Ich konnte mich darauf verlassen bei dir Zuspruch, Rat und auch Kritik zu bekommen. Du wusstest stets, was im jeweiligen Moment angebracht war und was mir auf meinem Weg half. Ich hoffe ich konnte, kann und werde dir noch oftmals auf gleicher Weise behilflich sein.
Meinem Vater möchte ich Bewunderung für sein Durchhaltevermögen und für seine technische Finesse aussprechen. Auch beim erstmaligen Ausführen von Aufgaben schaffst du es diese mit Bravour zu bewältigen, egal wie kompliziert und langwierig diese sein mag. Du motivierst mich und zeigst mir, dass man alles im Leben erreichen kann, solange man fokussiert und zielstrebig bleibt.
Ihr seid meine größten Vorbilder, meine engsten Mitstreiter und vor allem meine ersten Unterstützer. Ich wünsche allen Menschen dieser Welt den Beistand, die Liebe und die Zuneigung die ich durch euch erfahre. Ich werde euch ewig dankbar sein.

Meiner Schwester Lisa möchte ich für ihre lustige, aufmerksame und liebvolle Art danken. Ich weiß, dass ich in dir eine Person habe, bei der ich bedingungslos ich selbst sein kann. Du bist meine beste Freundin, mein Laufkumpel und mein liebster Quälgeist. Danke für alles.

Auch meiner weiteren Familie bin ich zu Dank verpflichtet. Durch euch konnte ich meinen Fokus gelegentlich von der Universität auf die anderen wichtigen Dinge im Leben richten.

Weiters möchte ich mich bei Tobias, Karl, Maximilian, Patrick, Laura, Sara und Theresa für unsere Freundschaft bedanken. Ihr seid die Menschen, die mir das Leben in Wien versüßen konnten. Zusätzlich möchte ich Felix, Andreas, Martin, Andre, Richard und Oliver für die langjährige Unterstützung aus der Heimat danken. Auch ihr habt einen Teil zu dieser Arbeit beigetragen.

I'm also thankful for my companions Lorenz, Matthias, Luca, Tommy and Fabian which were always available to help me with questions about our field of work and listened to all my bad jokes. Thanks for all the recommendations I've received, insightful conversation we had and giggles we shared.

Zuletzt möchte ich mich bei meiner Freundin Viktoria bedanken. Du bist meine mentale Stütze und meine Motivatorin. Ich möchte dir für alle liebsamen Worte und tiefen Gespräche danken, die mich zur Fertigstellung dieser Arbeit trieben.

Wir haben es geschafft.
Danke.

Contents

Nomenclature

Typeset

Notation	Description
a, b, c	Scalar quantities (non-bold symbols)
$\boldsymbol{a}, \boldsymbol{b}, \boldsymbol{c}$	Vector quantities (bold, lower case letters)
a_i, b_i, c_i	i-th component of a vector
$\boldsymbol{A}, \boldsymbol{B}, \boldsymbol{C}$	Matrix quantities (bold, capital letters)
A_{ij}, B_{ij}, C_{ij}	Entry at the i-th row and j-th column of the matrix with the same character
$\mathbf{e}_i$	Unit vector in direction of vector i

Mathematical quantities

Scalars

Symbol	Description
G_{ij}	Transfer function relation between input j and output i
K_{ij}	Transfer function at $s = 0$ between input j and output i
K_x	Gain related to variable x
$\boldsymbol{x}$	State vector
$\boldsymbol{A}$	System matrix
$\boldsymbol{b}$	Input vector
$\boldsymbol{c}$	Output vector
d	Feedthrough gain
e	Control difference
$\boldsymbol{f}$	Disturbance vector
u	Input variable
$\boldsymbol{k}^{\mathrm{T}}$	State feedback gain vector
K_w	Preamplification gain of state feedback control
s	Laplace frequency variable
z	z-Transform frequency variable
$Y(s)$	Numerator polynomial of G
$U(s)$	Denominator polynomial of G
Δx	Difference between actual and desired quantity x
$\boldsymbol{I}$	Identity matrix
$\boldsymbol{r}_{PQ}$	Vector $\boldsymbol{r}$ pointing from point Q to point P
$\mathcal{L}\{\ldots\}$	Laplace operator

Physical quantities

Symbol	Unit	Description
x, y, z	m	Translational degrees of freedom (absolute)
u, v, w	m/s	Velocities in the respective directions (absolute)
$\varphi, \vartheta, \psi, \delta$	1	Rotational degrees of freedom (roll, pitch, yaw, steer)
$\dot{\varphi}, \dot{\vartheta}, r, \dot{\delta}$	1/s	Rotational velocities (roll, pitch, yaw, steer)
v_y	m/s	Lateral velocity
T_A	s	Anticipation time
T_s	s	Sampling time period
f_s	1/s	Sampling frequency
V_m	-	Controller static gain
T_v	s	Lead time constant
T_n	s	Lag time constant
ρ	m	Curvature radius of the trajectory
κ	1/m	Curvature of the trajectory
α	1	Stationary side slip angle
γ	1	Stationary camber angle
α'	1	Transient side slip angle
γ'	1	Transient camber angle
F_x	N	Longitudinal tire force
F_y	N	Lateral tire force
F_z	N	Normal tire force
M_x	Nm	Tire roll moment
M_y	Nm	Tire rolling resistance torque
M_z	Nm	Tire restoring moment
T_δ	Nm	Steer torque

Indices

Symbol	Description
d	Desired value of respective quantity
0	Initial value of respective quantity
$\perp$	Perpendicular to trajectory
$f\|r$	Front or rear wheel quantity
ff	Quantity for feedforward control
fb	Quantity for feedback control
$\|P$	Index suffix to locate a quantity to Point P
T	Total values
act	Actual quantities
max	Maximum quantity

Acronyms

Acronym	Description
ÖAMTC	Österreichischer Automobil-, Motorrad- und Touring Club
WRI	World Resources Institute
MBS	Multi Body Systems
PID	Proportional Integral Derivative Controller
LQR	Linear-Quadratic Regulator
SbW	Steer by Wire
BM	Benchmark bicycle
COM	Center of mass
DOF	Degree of freedom
FEA	Finite Element Analysis

1 Introduction

1.1 A Brief History

1.1.1 Bicycle

Two-wheeled, man-powered vehicles were introduced by Karl von Drais in 1817 with his invention, the Draisine [1]. In the following years, the development of the Draisine into the modern bicycle added the pedal drive to the two-wheeler in 1840, followed by lighter constructions with larger front wheels, and finally, the pneumatic tire was introduced by John Dunlop to consolidate the bicycle in the public transport sector [2]. Further inventions and innovations led to the rise of the bicycle, which is why today around 75% of households in Austria own bicycles [3]. What has not changed over the years are the human operators, who need to power the vehicles with their muscles. Moreover, one has to obtain the ability to balance the vehicle in an upright position while following a desired path, which is quite challenging in the beginning, as most of us know from our early days.

The first attempts to mathematically describe the dynamics of a bicycle were published in 1869 in [4], wherein an inverted pendulum model was used to investigate basic dynamic properties of single-track vehicles. In addition, the need for countersteering to initiate a cornering maneuver in the opposite direction was mentioned. Today's 'standard' bicycle model was derived in 1899 by Whipple [5] and, independently, by Carvallo [6] in 1901. While Whipple derived the nonlinear equations and later considered the linearized version for upright cycling, Carvallo already derived the linear equations by assuming small perturbations around an upright free-running equilibrium [7]. A structured derivation, detailed analysis, and a comparison with a multi-body model were carried out by Meijaard et al. [8], which is seen as the established standard work for bicycle dynamics. Additionally, multi-body system (MBS) models exist, which allow the computation of the dynamics of the model in a numerical way.

If one aims to analyze the stability behavior of a bicycle, and considering the similarity of the system dynamics, publications on motorcycles and e-scooters could also be consulted. Especially motorcycle dynamics are a well-researched subject. Pacejka [9], for instance, provides a separate chapter on motorcycle dynamics in his book 'Tyre and Vehicle Dynamics.' Cossalter [10] and Lot and Sadauckas [11] dedicated entire books to the physical phenomena and mathematical modeling of motorcycles. Further researchers in the field of modeling two-wheeled vehicles are Arend Schwab, Matteo Massaro, and Robin Sharp, to name a few.

1.1.2 Rider Models

In order to influence a system to work in a desired way, typically a controller has to be used. In vehicle dynamics, the human is seen as a controller operating a vehicle. We use sensory inputs like visual, vestibular, and proprioceptive stimulations, which are processed by our brains and then transformed into an appropriate reaction [12]. Additionally to the control actions, the rider of a bicycle, motorcycle, or e-scooter also provides a significant contribution to the system's open-loop dynamics. This is due to the high relative mass and inertia of the rider compared to the ridden vehicle.

The first investigations into describing the control properties of humans were conducted by McRuer et al. in the 1960s while observing jet pilots [13], [14]. They found that the operator adjusts their dynamics according to the respective vehicle. These experimental results were analyzed and put into a describing function between a particular input and output. It contains a neuromuscular delay and parameters to vary the model's output reaction to given inputs. Despite the advanced age of McRuer's relation, it is still used in simple driver and rider models today, see e.g. [12], [15].

The tasks of controlling a bicycle are mostly split into three sections. The first task is to stabilize the vehicle, as a two-wheeled vehicle is unstable at low speeds. Secondly, the adjustment of the speed by braking and accelerating to adapt the velocity for upcoming maneuvers is necessary. The third task comprises the lateral guidance of the bicycle in order to follow a desired path. Most of the control strategies for rider modeling use an integrative concept where stabilization, speed tracking, and lateral control are combined into a single controller. Sharp [16], [17] and Schwab et al. [18] use optimal control theory with and without preview to model the rider. Other authors, such as Findlay and Moore [19] or Hess [20], use classic control-theoretic approaches. Another concept for controller design is splitting the tasks into designated controllers. Here, each individual control goal is tracked by a single controller. Commonly, the controllers are then cascaded. Edelmann et al. [21], as well as Haudum [22] and Gabriel et al. [23], use such approaches. With this method, it is necessary to synchronize the individual controllers.

Further control strategies, such as fuzzy control or inverse dynamics, used by various authors are mentioned in [12], which gives an excellent review of rider models in general.

1.1.3 Steer-by-Wire (SbW)

The idea of an X-by-Wire system was born in the aerospace industry, where the Concorde was the first commercial plane equipped with a Fly-by-Wire system [24]. Since the

Airbus A320, every *Airbus* plane has been equipped with a Fly-by-Wire system without a mechanical backup system. In modern passenger cars, the electronic gas pedal is commonly integrated. With it, the engines achieve faster reaction times to the driver's input, as the rate of change of the throttle position is considered. The motor controller acts in a predictive manner. Furthermore, the desired acceleration can be harmonized with the traction control system in order to prevent wheel slip. X-by-Wire systems, therefore, are already established in the transport sector and bring many advantages for control and assistance systems.

SbW systems for two-wheeled vehicles are not yet common. The development of steering assistance systems for motorcycles is still in its infancy, as Bartolozzi et al. emphasize [25]. Marumo [26] developed an SbW system for motorcycles. Even less has been done for bicycles. Very few publications were found for steer assist systems or SbW applications. Valenzano managed to stabilize a virtual multi-body bicycle model using state feedback control. Appelman [27] designed an SbW bicycle for research in his master's thesis. Dialynas [28] built and tested the bicycle afterward.

1.2 Motivation, Goals and Structure of the Thesis

Motivation and Goals of the Thesis

Riding a bicycle is a difficult task for a human. Guiding a vehicle that is unstable at lower velocity ranges whilst keeping the bicycle on a desired track and indicating turns to traffic partners while doing the respective visual checks for the turn is a challenge by itself. Handing all of these tasks to novice or inexperienced operators has led to accidents. The *Österreichischer Automobil-, Motorrad- und Touring Club* (ÖAMTC) published a news article in 2023 [29], where they list the numbers of traffic accidents over the last ten years. Specialists of the ÖAMTC concluded that most of the accidents are single-vehicle accidents. These have increased most significantly over the last ten years compared to other types of accidents. This is due to the rise of electric-powered bicycles (E-bikes) [29], since humans who were not used to riding a bike regained the desire to do so.

The combination of inexperienced riders and complicated tasks, which need to be coordinated simultaneously, has led to the rapid increase in road accidents.

This naturally leads to the question of how to lower the number of accidents effectively. One possibility to lower the complexity of a bicycle ride for its rider is to ease the use of the bicycle. Here, the dynamics of the bicycle can be slowed by adjusting the inertia and tire properties as well as the geometry of the construction. By shifting the system's

dynamics, the bicycle will react more moderately to inputs and will therefore extend the reaction time for its operators [30] and increase stability.

The second possibility to support the rider whilst riding is active assistance systems. The SbW system in this thesis is able to increase stability, slow down the dynamics and adjust the input-output behavior to the rider's desire. If the stabilization task whilst riding a bicycle is done by the SbW system, the rider only has to steer to follow a trajectory. An entirely different way to maneuver a bicycle is created.

The goal of this thesis is to answer the question *'How can the possibilities of the Steer-by-Wire system be assessed using the virtual multi-body model, and how could a possible parameterization look like?'* For that, a suitable rider model needs to be introduced to simulate inputs for the existing model of the SbW bicycle. Using these inputs, the performance of the Steer-by-Wire system will be assessed.

In Fig. 1.1, the principal layout of a rider model operating a Steer-by-Wire bicycle is illustrated. It consists of three main parts: The rider model, the Steer-by-Wire system, and the bicycle model. The single module blocks are clustered by colored boxes representing the three main parts. The lines connecting the module blocks symbolize an information transfer. The quantities above the lines reaching from one of the three main parts to another show the quantities passed at the interface between the main blocks. The lines inside a certain block are intrinsic or intermediate quantities. The red block represents the rider model. The rider model uses the curvature κ of the trajectory and the position of the rider model relative to the trajectory $y_\perp$, computed using the states of the bicycle model $\boldsymbol{x}$, to form a desired roll angle φ_d, composed of the feedforward roll angle φ_{ff} and the feedback roll angle φ_{fb}, and applies a respective steer torque T_r or prescribes a respective steering wheel angle δ_{SW} at the Steer-by-Wire interface. The Steer-by-Wire system is shaded in blue. The input unit computes the reference variable y_d for the stabilization controller and a feedback torque for the rider. The stabilizing controller tracks and stabilizes the reference variable by applying a steer torque T_δ at the fork of the bicycle. The steer torque is computed using state feedback control, where the stabilizing controller requires the bicycle model states $\boldsymbol{x}$. The bicycle model reacts to the respective steer torque input with the dynamics of the respective bicycle model in use.

Structure of the Thesis

The Introduction will end with a brief literature review. The literature review was performed to discuss the required aspects of bicycle dynamics from the perspective of rider modelling. Afterwards, the thesis proceeds to introduce the main parts in Fig. 1.1 as follows:

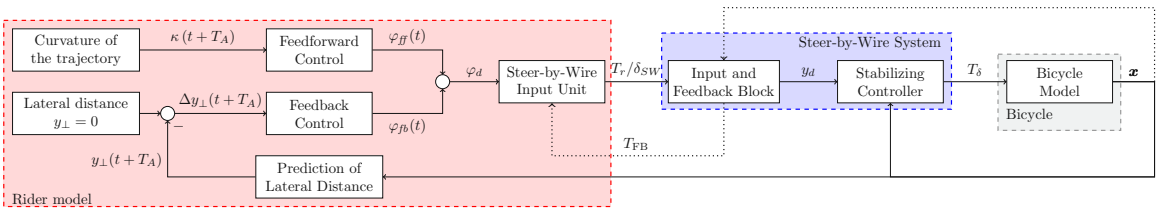

Figure 1.1: Layout of the Steer-by-Wire bicycle model controlled by a path-tracking rider control model.

In Chapter 2, the fundamental mathematical models are introduced. This was necessary to fully understand the problems and their solutions later on. The individual components—bicycle model, rider model, and SbW system—are introduced subsequently. The description of the bicycle dynamics begins with the simplest model, the Carvallo-Whipple model, also called the benchmark bicycle model. Later on, a tire model was added to the bicycle model using the relations of Ott [31]. Since both models only contain the necessary assemblies of regular bicycles, the SbW system is introduced, and its design as well as its influence on the dynamics are explained briefly. In order to obtain a more realistic bicycle model, an existing MBS bicycle model was used. This will be referred to as the high-fidelity model. In order to compare the different models to each other, a stability analysis was performed for the straight-running condition.

In Chapter 3, a rider model was introduced that is able to laterally follow a track. In the beginning, it was discussed which inputs and outputs a bicycle rider uses to guide a bike. The rider model will then be broken into the respective individual components, the feedforward and feedback control levels. It was shown what information of the environment a human uses to form the desired control quantity, the roll angle φ_d. A comparison of two different approaches to obtaining the feedforward quantity is done. The difficulties in designing the feedback level, which originate from the non-minimum phase characteristic of the bicycle model's lateral dynamics, are mentioned. Furthermore, the control inputs of a bicycle rider model and a car driver model are designed. The considerations and drawbacks of the chosen rider model are also listed. In general, it can be said that the rider model was chosen for the sake of simplicity and easy parametrization.

In Chapter 4, the stabilizing controller of the SbW system, which was designed in a previous thesis [32], is introduced. At the beginning of this chapter, the ability of the steer torque applied by the stabilizing controller at the fork of the bicycle model to influence the bicycle model's movements was discussed. Afterwards, additional investigations of the stabilization controller are conducted, considering pole placement accuracy between the models used for controller design. Furthermore, a follow-up control algorithm was added to the initial stabilizing controller in order to allow reference variable tracking.

In Chapter 5, the interface between the rider control model and the stabilization controller is designed. Specifically, the input unit and the rider feedback system are introduced and discussed. These components are modeled using a model-based approach, incorporating findings from the literature to establish suitable relationships. These relationships transform the rider model inputs into a reference variable for the stabilizing controller to track and generate a feedback torque for the rider.

In Chapter 6, the results are shown. In the simulation preface, the simulation procedure using *Simpack 2024x* and *Matlab* in a Co-Simulation is explained. The parameter set of the simulations is then discussed, and important thoughts regarding the trajectory design are mentioned. Afterwards, the results are presented and discussed, all aiming to answer arising questions when reading this thesis and to test the individual components in Fig. 1.1. The thesis ends with the conclusion and a brief outlook.

1.3 Literature Review

The paper by Meijaard et al. [8] provides a detailed derivation of the equations of motion for the benchmark bicycle model using different approaches, extensive system analysis, and benchmarking against a multi-body bicycle model. The bicycle model discussed is identical to the models introduced independently by Carvallo [6] and Whipple [5]. The authors of [8] highlight that the nonlinear equations do not have a simple, compact form, which is why they are often linearized. However, the derivation of these linear equations is time-consuming and results in a set of nested functions, leading to a lack of cross-checking between publications. This paper was also used to gather kinematic relations for the benchmark bicycle model.

At the Institute of Mechanics and Mechatronics of the TU Wien, several diploma theses have been conducted on bicycle modelling. Klinger [33], Ott [31], Müller [34], Haudum [22], and Angrosch [35] all researched bicycle dynamics. The theses of Klinger [33], Ott [31], and Angrosch [35] focus on the modelling of high-speed wobble in bicycles. Klinger included the effect of human inertia terms using a 'hands-on' and 'hands-off' model to describe the effects on lateral dynamics. Ott performed a series of parameter variations, such as mass distribution, tire parameters, and bicycle geometry. Müller [34] focused on the general modelling of bicycle lateral dynamics, while Haudum [22] included the roll angle of the rider's body relative to the roll angle of the bicycle. Differences in modelling approaches exist, such as Klinger's use of the lateral velocity of the rear wheel contact point v_D compared to Haudum's use of the lateral velocity of point A, the projected center of mass of the frame onto the road surface, v_A. The kinematic relations for modelling the camber angle γ and the side slip angle α were obtained from [31]. The linear tire model used in this thesis is the motorcycle tire model of Pacejka [9], chosen due to the lack of acknowledged bicycle tire models. A brief review of available bicycle tire models and measurements is provided by Dressel [36].

To include a rider model that provides reasonable reactions to a trajectory in front of the rider to test the Steer-by-Wire system, literature on human control properties was reviewed. McRuer [13], [14] was the first to investigate control properties while studying jet pilot task handling. He developed a simple mathematical model of a human operating a vehicle, using system identification techniques to identify the following relations:

$$G_O(s) = G_p \cdot G_a = \frac{\omega_C}{s} \cdot \mathrm{e}^{\psi_R}, \tag{1.1}$$

$$G_p(s) = V_m \cdot \frac{1 + T_v\, s}{1 + T_n\, s} \cdot \mathrm{e}^{-s\tau}. \tag{1.2}$$

The first equation describes the ability of a human with transfer function G_p to operate a vehicle with transfer function G_a such that the open-loop transfer function G_O possesses local integral behavior and a phase reserve ψ_R near the open-loop crossover frequency ω_C. The second equation describes the human input-output relation, with static gain V_m, lead time constant T_v, lag time constant T_n, and neuromuscular time delay τ.

Van Lunteren [37] was the first to model bicycle riders specifically, investigating the influence of drugs on rider control. A comprehensive review of bicycle rider models is provided by Kooijman and Schwab [12], who categorized rider models into:

- Classical control system design,
- Optimal control,
- Other control approaches.

Moore [38] dedicated his PhD studies to investigating human control of bicycles. He identified the following general properties a human needs to operate a bicycle:

1. Visual feedback: The ability to recognize deviations from desired positions.
2. Vestibular feedback: The ability to sense rotations.
3. Proprioceptive feedback: The ability to perceive force and torque feedback and estimate future states.

Rider models should incorporate these properties, as well as physiological limits such as limited frequency bandwidth, force and torque output capabilities, and sensory and muscular delays. Sophisticated models should also account for factors like age, risk management, and situational properties such as stress and fatigue, as noted by Plöchl and Edelmann [39]. Problem-specific rider models, such as those in [40], [41], are used for traffic flow simulations.

Schwab et al. [42] demonstrated that rider control goals vary with velocity. Using model identification techniques and a grey-box model of an optimal linear rider control model,

they concluded that riders aim to minimize input amplitudes at low speeds and maximize trajectory tracking performance at high speeds.

The most important input a bicycle rider provides is the steering torque T_δ, as supported by [43]. This study used an instrumented bicycle to determine that steering torque is the primary input, with minimal upper body movement during normal tasks. Upper body movements were primarily used to keep the head upright, while knee movements increased at slow velocities to shift the center of mass. Aoki [44] confirmed that motorcycle riders primarily use steering torque, based on observations of the yaw rate transfer function.

The tasks of controlling a bicycle are divided into three levels: stabilization, lateral guidance, and speed control. Sharp [16], [17] and Schwab et al. [18] use optimal control theory with and without preview to model the rider within a single controller. Other authors, such as Findlay and Moore [19] and Hess [20], use classical control theoretic approaches. Alternatively, some models split the tasks into designated, cascaded controllers, where each controller aims to achieve its individual control goal. Examples include Edelmann et al. [21], Haudum [22], and Gabriel et al. [23].

Bicycle lateral dynamics exhibit non-minimum phase behavior, requiring careful treatment in rider modelling. General control theory literature often struggles with non-minimum phase systems, as noted by Lunze [45], who suggests:

- Preventing non-minimum phase behavior by selecting appropriate sensors and actuators.
- Eliminating non-minimum phase behavior using feedback from coupled subsystems.

Edelmann and Plöchl [46] addressed these challenges by designing a driver controller for a vehicle with similar dynamics to a bicycle. They concluded that the static gain of the McRuer pilot model must be small, and the anticipation time T_A large, to avoid cutting corners during curve entry. A supplemental feedforward control level is key to satisfactory lateral control performance [45].

To improve control performance, optimal preview controllers or model predictive controllers are recommended [23]. Kooijman and Schwab [12] reviewed various approaches for balancing bicycles and motorcycles, noting that optimal control strategies like LQR and H_∞ are unsuitable for the Steer-by-Wire system, as the dynamics cannot be impinged as desired. Haudum [22] found state feedback control to deliver the best overall performance.

Literature on active steering assistance systems for bicycles is scarce. A general introduction to assistive steering and steer by wire systems is given for automobiles by Pfeffer [24]. Active support systems for two-wheeled vehicles are still in their infancy, as emphasized by Bartolozzi et al. [25]. Marumo [26] developed a Steer-by-Wire system for motorcycles, but very few publications exist for bicycles. Appelman [27] designed

a Steer-by-Wire bicycle for research, while Valenzano [32] proposed a stabilization control algorithm using the pole placement method for a multi-body bicycle model. A few research units have built prototypes using active elements to control the roll angle of bicycles [28], [47].

Only one publication was found addressing rider models for Steer-by-Wire bicycles [23]. The dynamics of a stabilized bicycle are similar to those of the three-wheeled tilting vehicle investigated by Edelmann et al. [46], making the rider controller applicable to Steer-by-Wire bicycle design. Haudum [22] used designated controllers for the separate control tasks of a bicycle rider, employing the McRuer human control model for lateral guidance and a state feedback controller for stabilization. The lateral controller from Haudum's work is used in this thesis to provide inputs for the Steer-by-Wire bicycle. Haudum adapted the lateral dynamics car driver model of Mitschke [15], using its feedforward and feedback control levels to compute desired inputs and react to deviations from the desired path. The trajectory planning and 'task dependent' control levels were neglected.

2 Bicycle Models

The research object of interest in this thesis is the bicycle. As in learning to ride a bicycle, the fundamental dynamics of the vehicle need to be understood to perform further actions. The fundamental equations of three different mathematical bicycle models will be presented. The models vary in modeling depth. The different bicycle models are used for model-based controller design. The model should be as simple as possible to use as few parameters as necessary. The multi-body model was introduced to incorporate additional dynamics efficiently. The parameters of the bicycle models as well as the geometric and inertia parameters of the rider and the Steer-by-Wire system are given in Table A.1 in the Appendix.

2.1 Benchmark Bicycle Model (BM)

As already mentioned in the introduction, the first mathematical models of the lateral dynamic behavior of bicycles were presented independently by Carvallo and Whipple [7]. The respective bicycle model consists of four rigid bodies: the frame, the fork, and the front and rear tires with their respective masses m_m, m_H, m_f, and m_r. The tires are connected to the fork and the frame of the bicycle using frictionless rotary bearings. The fork and the frame are connected via an inclined, frictionless bearing. A rider is considered rigidly attached to the saddle of the frame assembly and therefore only adds mass m_R and inertia to the system. The geometry and mass distribution are computed according to the anthropometric model of Hanavan [48], and the human parameters are equal to those of Klinger [33], given in the Appendix. The system layout is depicted in Fig. 2.1.

The distance between the points of contact of the front and rear tires, in an upright position and with a vanishing steer angle, with the road is called the wheelbase l. The center of mass of the mainframe is located at a horizontal distance a_c from the front wheel and b_c from the rear wheel contact point. The relative distances between the rider's center of mass to the frame's center of mass and the fork's center of mass are referred to as a_r and a_H, respectively. The rider's center of mass is located h_R above the ground and therefore lies higher than the center of mass of the frame at height h_m and the fork's center of mass h_H. The center of mass offset of the fork is labeled e_H.

Due to the inclined steering assembly with inclination ε, the front wheel obtains a geometric trail t_c, which is the distance between the actual point of contact and the point of intersection of the steering axis with the roadway of the system in nominal configuration. The front and rear wheels have the respective radii r_f and r_r.

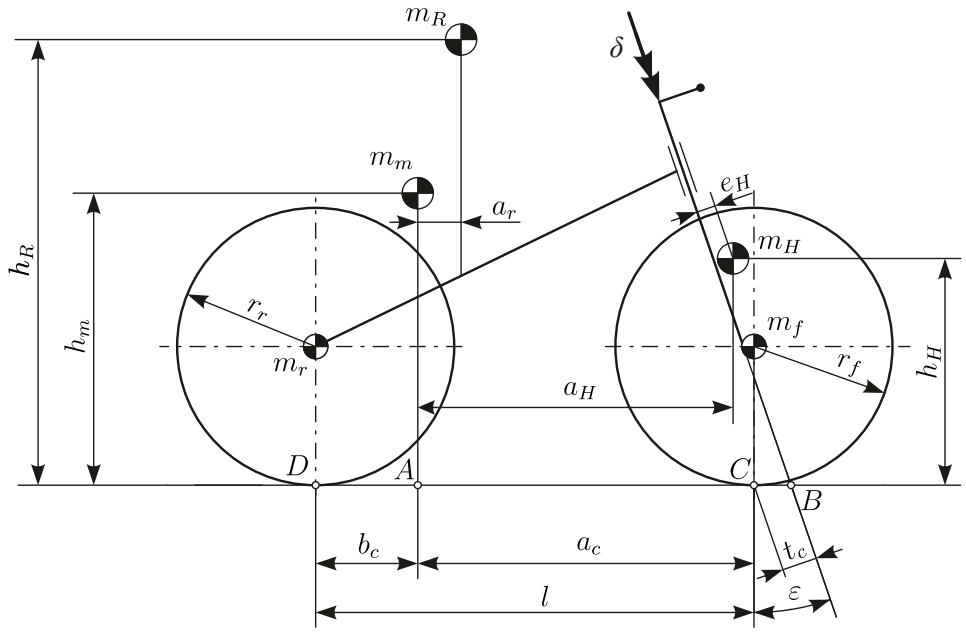

Figure 2.1: Bicycle model adapted from [22].

The described model has a seven-dimensional configuration space $\boldsymbol{S}$, three velocity degrees of freedom, and is conservative [8]:

$$\boldsymbol{S} = (x_D, y_D, \varphi, \psi, \delta, \theta_f, \theta_r)\,. \tag{2.1}$$

The position of the rear wheel contact point D in the x and y directions is labeled as x_D and y_D, respectively. The roll angle φ is the angle of the frame's plane to a vertical axis. The yaw angle ψ gives the orientation of the frame towards the x-axis of the global coordinate system. The steer angle δ is measured from the frame's plane in the direction of the steer axis. The rotational positions of the front and rear wheels are given by θ_f and θ_r, respectively.

The system is laterally symmetric. The wheels have knife-edge point contact with the ground. The tires cannot slip laterally or longitudinally, and the constraints are therefore non-holonomic. The movement of the tire thus follows its orientation. Considering the two non-holonomic constraints for each wheel, $\boldsymbol{S}$ reduces to $7 - 4 = 3$ accessible configurations:

$$\boldsymbol{S} = (\varphi, \delta, \theta_r)\,. \tag{2.2}$$

This is the minimum set of variables required to describe the motion of the bicycle with the assumed constraints. The variables in $\boldsymbol{S}$ could be chosen arbitrarily. The configuration space representation is therefore not unique.

Equations of Motion

The equations of motion were used from Ott [31]. Ott derived them using a multi-body approach and appropriately linearising them at the straight running condition $\varphi = \delta = 0$. The equations use a constant forward velocity u. This way the velocity is a parameter in the equations describing the lateral dynamics and the configuration space $\boldsymbol{S}$ degenerates, as the rotation of the rear wheel θ_r then is prescribed

$$\boldsymbol{S} = (\varphi, \delta)\,. \tag{2.3}$$

The parameter set of Klinger [33] was used to parameterize the bicycle and the rider model. The equations of motion of the respective state variable in Ott's notation read:

φ :

$$\begin{aligned} &I_{T_{xx|D}}\,\ddot{\varphi} + m_T h_T g\,\varphi + \left[I_{H_{\delta x_D}} + \frac{t_c}{l} I_{T_{xz|D}}\right]\ddot{\delta} + \\ &\left[G_1 \cos\varepsilon + \frac{t_c}{l}\left(-m_T h_T + G_T\right) + \frac{\cos\varepsilon}{l} I_{T_{xz|D}}\right] u\,\dot{\delta} + \\ &\left[-S_\delta g + \frac{\cos\varepsilon}{l}\left(-m_T h_T + G_T\right) u^2\right]\delta = 0 \end{aligned} \tag{2.4}$$

δ :

$$\begin{aligned} &\left[I_{H_{\delta x_D}} + \frac{t_c}{l} I_{T_{xz|D}}\right]\ddot{\varphi} - \left[G_1 \cos\varepsilon + \frac{t_c}{l} G_T\right] u\,\dot{\varphi} - S_\delta g\,\varphi + \\ &\left[I_{H_{\delta\delta}} + \frac{t_c}{l}\left(2 I_{H_{\delta z_D}} + \frac{t_c}{l} I_{T_{zz|D}}\right)\right]\ddot{\delta} + \\ &\left[k_\delta + \left(\frac{\cos\varepsilon}{l} I_{H_{\delta z_D}} + \frac{t_c}{l}\left(S_\delta + \frac{\cos\varepsilon}{l} I_{T_{zz|D}}\right)\right) u\right]\dot{\delta} + \\ &\left[c_\delta - S_\delta \sin\varepsilon\, g + \frac{\cos\varepsilon}{l}\left(S_\delta + G_1 \sin\varepsilon\right) u^2\right]\delta = T_\delta \end{aligned} \tag{2.5}$$

The quantities with index T describe total quantities like the total mass of the system m_T, the horizontal distance of the total center of mass to the rear wheel contact point x_T and the height of the total center of mass h_T. The physical quantities are represented in the vehicle-fixed coordinate system, see 2.4. The equations can also be written in matrix-vector notation. The generalized coordinates $\boldsymbol{q} = (\varphi, \delta)^{\mathrm{T}}$ and their derivatives are used. The terms in front of the generalized coordinates vector and the respective derivatives are gathered and put into matrices. The mass matrix $\boldsymbol{M}$ contains the mass and inertia terms in front of the second derivatives and is symmetric. The damping matrix $\boldsymbol{C}$ contains the damping terms and the terms of gyroscopic forces associated with the first derivatives. The stiffness matrix $\boldsymbol{K}$ contains the parameters in front of

the generalized coordinates vector. The forcing vector $\boldsymbol{f}$ is composed by the terms on the right side of the equations. The equations of motion then read

$$\boldsymbol{M}\ddot{\boldsymbol{q}} + \boldsymbol{C}\dot{\boldsymbol{q}} + \boldsymbol{K}\boldsymbol{q} = \boldsymbol{f}. \tag{2.6}$$

In particular, the terms of the damping matrix $\boldsymbol{C}$ and stiffness matrix $\boldsymbol{K}$ can be split up into their velocity dependent and independent parts, $\boldsymbol{C}_1$, $\boldsymbol{K}_2$ and $\boldsymbol{K}_0$, respectively,

$$\boldsymbol{M}\ddot{\boldsymbol{q}} + u\boldsymbol{C}\dot{\boldsymbol{q}} + \left(g\boldsymbol{K}_0 + u^2\boldsymbol{K}_2\right)\boldsymbol{q} = \boldsymbol{f}. \tag{2.7}$$

In control theory, the state space representation is preferred over the second order differential equations, since the states of a system are important elements in the analysis of dynamical systems [45]. Furthermore, the representation is more appropriate for computational operations. Every linear system of ordinary differential equations of arbitrary order N can be transformed into a system of first order differential equations [49]. The equations of motion (2.6) can also be presented in state space form. The state space vector

$$\boldsymbol{x} = \left(\varphi, \delta, \dot{\varphi}, \dot{\delta}\right)^{\mathrm{T}} \tag{2.8}$$

consists of the generalized coordinates with their derivatives.

With the choice of states in (2.8) the standard form of the mechanical differential equation transforms to

$$\dot{\boldsymbol{x}} = \boldsymbol{A}\boldsymbol{x} + \boldsymbol{B}\boldsymbol{u} \tag{2.9}$$

with the system matrix $\boldsymbol{A}$ and the input matrix $\boldsymbol{B}$. The matrices of the second order matrix differential equation (2.6) are transformed into the state space representation by rearranging the stiffness and damping matrix entries accordingly. If the state vector is composed by increasing order of derivatives

$$\boldsymbol{x} = \left(\boldsymbol{q}, \dot{\boldsymbol{q}}, \ldots, \frac{\mathrm{d}^{\mathrm{N}-1}\boldsymbol{q}}{\mathrm{d}t^{N-1}}\right)^{\mathrm{T}}, \tag{2.10}$$

the state space matrices are computed by

$$\boldsymbol{A} = \begin{pmatrix} \boldsymbol{I} & \boldsymbol{0} \\ \boldsymbol{0} & \boldsymbol{M} \end{pmatrix}^{-1} \begin{pmatrix} \boldsymbol{0} & \boldsymbol{I} \\ -\boldsymbol{K} & -\boldsymbol{C} \end{pmatrix}, \tag{2.11}$$

$$\boldsymbol{B} = \begin{pmatrix} \boldsymbol{I} & \boldsymbol{0} \\ \boldsymbol{0} & \boldsymbol{M} \end{pmatrix}^{-1} \begin{pmatrix} \boldsymbol{0} & \boldsymbol{0} \\ \boldsymbol{0} & \boldsymbol{Z} \end{pmatrix}. \tag{2.12}$$

The forcing term is decomposed by $\boldsymbol{f} = \boldsymbol{Z}\boldsymbol{u}$, with the force distribution matrix bmZ. For the single input case, the input matrix $\boldsymbol{B}$ degenerates into an input vector $\boldsymbol{b}$ and the input variable vector $\boldsymbol{u}$ to the scalar input variable u.
Due to the dimension of the state vector, the benchmark bicycle model will also be called *4 states model* in subsequent chapters.

2.2 Bicycle Model with Tire Model

Equations of Motion

Instead of using non-holonomic constraints to model the ground contact relation of the tires, a tire model was introduced. By using a tire model additional forces and torques act at the respective generalized coordinates. As the non-holonomic bounds in lateral direction are discarded, an additional generalized coordinate per tire is added to the system. The state vector then reads

$$\boldsymbol{x} = \left(\varphi, \delta, v, r, \dot{\varphi}, \dot{\delta}\right)^{\mathrm{T}}. \tag{2.13}$$

This model will therefore be called *6 states model* in later sections. The lateral velocity v is the lateral velocity in the rear wheel contact point. The equations of motion, in Ott's [31] notation, are

v :

$$m_T(\dot{v} + ur) + m_T x_T \dot{r} - m_T h_T \ddot{\varphi} + m_H e_H \ddot{\delta} = F_{y1} + F_{y2} \tag{2.14}$$

r :

$$m_T x_T(\dot{v} + ur) + I_{Tzz|D}\dot{r} + I_{Txz|D}\ddot{\varphi} - G_T u\dot{\varphi} + I_{H\delta z_D}\ddot{\delta} - G_1 \sin\varepsilon\, u\dot{\delta} = lF_{y1} + M_{z1} + M_{z2} \tag{2.15}$$

φ :

$$-m_T h_T(\dot{v} + ur) + G_T ur + I_{Txz|D}\dot{r} + I_{Txx|D}\ddot{\varphi} + m_T h_T g\varphi + I_{H\delta x_D}\ddot{\delta} + G_1 \cos\varepsilon\, u\dot{\delta} - S_\delta g\delta = M_{x1} + M_{x2} \tag{2.16}$$

δ :

$$m_H e_H(\dot{v} + ur) + G_1 \sin\varepsilon\, ur + I_{H\delta z_D}\dot{r} + I_{H\delta x_D}\ddot{\varphi} - G_1 \cos\varepsilon\, u\dot{\varphi} - S_\delta g\varphi + I_{H\delta\delta}\ddot{\delta} + k_\delta\dot{\delta} + (c_\delta - S_\delta \sin\varepsilon g)\,\delta = -t_c F_{y1} + M_{x1}\sin\varepsilon + M_{z1}\cos\varepsilon + T_\delta \tag{2.17}$$

The lateral force of the front wheel F_{y1}, the lateral force of the back wheel F_{y2}, the overturning couple at the front wheel M_{x1}, the overturning couple at the rear wheel M_{x2} and the aligning torques M_{z1} and M_{z2} at the respective wheel are added as forcing terms. These terms are related to the generalized coordinates and are computed using a tire model.

Tire model

The non-holonomic constraints of the benchmark bicycle model lead to forces, which influence the bicycle's movements in order to sustain the non-holonomic bounds. To model a more realistic behavior of the bicycle, a tire model is used. The non-holonomic constraints are replaced by state related forcing terms. A tire model in general uses kinematic states as input and gives the forces and torques corresponding to the states at the output.

When exposed to external forces and torques, pneumatic tires form a contact patch with their contact partner, which is assumed as a perfectly flat horizontal plane in this thesis. Within this region the pressure and shear forces are transmitted. The distributed forces can be summarized to the respective equivalent normal force F_z, longitudinal force F_x and lateral force F_y. In order to generate the longitudinal and lateral forces, respective wheel slips κ_x and κ_y are needed.

The tire model uses these wheel slips κ_x and κ_y and relates them with the respective forces. The used tire model is the simple linear tire model Pacejka introduced in [9]. The normal force acts in the symmetry plane of the tire. A fictitious point F is introduced, which is located in the tire's symmetry plane at the road surface, see Fig.

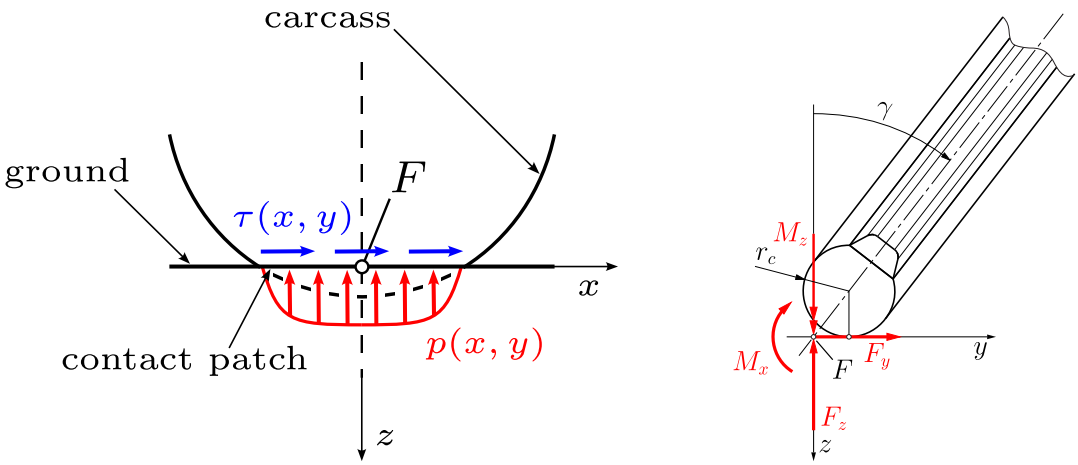

(a) Deformed upright tire with contact patch and stress distribution.

(b) Equivalent forces and torques acting on bicycle tires, adapted from [22].

Figure 2.2: Sketches for the tire model.

2.2. The distributed forces in the contact patch in Fig. 2.2a were transformed into an equivalent system of forces and torques at point F, sketched in Fig. 2.2a and 2.2b. The transformation of the pressure and shear stress distribution, $p(x, y)$ and $\boldsymbol{\tau}(x, y)$ respectively, into the equivalent forces and torques at the defined point F brings advantages for computations.

Kinematics

The lateral forces and the aligning torques are generated due to shear deformation of the contact patch. The lateral contact patch deformation is modelled by the wheel slip κ_y, where Pacejka's model [9] uses the side slip angle α and the camber angle γ to model wheel slip. The side slip angle α is the angle of the actual velocity vector $\boldsymbol{v} = (u, v)^{\mathrm{T}}$ to the wheel plane

$$\arctan(\alpha) = \frac{v}{u}, \tag{2.18}$$

where u is the longitudinal velocity inside the wheel plane and v the lateral velocity perpendicular to the wheel's plane. The camber angle γ in Fig. 2.3b is the inclination of the wheel plane to the normal vector of the road

$$\cos(\gamma) = \mathbf{e}_n \cdot \mathbf{e}_r. \tag{2.19}$$

The kinematic relations are apparent when looking at sketch 2.3 [9].

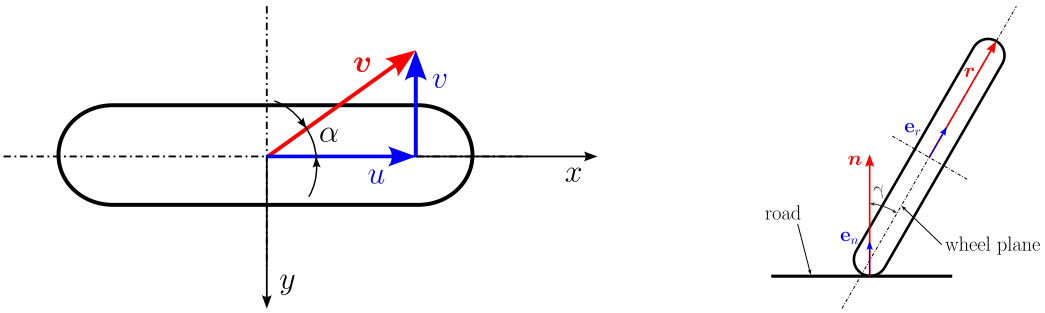

(a) Sketch to determine α. Top view of the tire with pure side slip.

(b) Sketch to determine γ. Tire pictured from behind with pure camber.

Figure 2.3: Sketches for the kinematic relations of side slip angle α and camber γ.

To compute the side slip and the camber angle at the front and rear wheel, kinematic relations expressed by the generalized coordinates are used. The kinematic quantities as well as the quantities needed for the tire model are illustrated in Fig. 2.4. The rear wheel side slip angle α_r and camber angle γ_r are computed by

$$\alpha_r = -\arctan\left(\frac{v_{|D}}{u_{|D}}\right) \approx -\frac{v_{|D}}{u}, \tag{2.20}$$

$$\gamma_r = \varphi. \tag{2.21}$$

The relation for α_r is linearised assuming side slip angles α_r using the forward velocity u and the lateral velocity of the rear wheel contact point $v_{|D}$. The rear wheel camber angle γ_r is equivalent to the roll angle of the bicycle model's frame.

In order to get to the actual side slip angle of the front wheel α_f, the ground steer angle δ_G is computed. This is done by projecting the steer angle δ on the road's surface. The full nonlinear relation with its derivation using a MBS formalism can be found in [31], where the linearised relation is given by

$$\delta_G = \delta \cdot \cos(\varepsilon). \tag{2.22}$$

The lateral velocity at the front wheel ground contact point is

$$v_{|C} = v_{|D} + l\, r - t_c \dot{\delta} \tag{2.23}$$

with the yaw rate r and steering rate $\dot{\delta}$. Using the defining relation of the side slip angle α (2.18) the front wheel side slip angle α_f is computed by

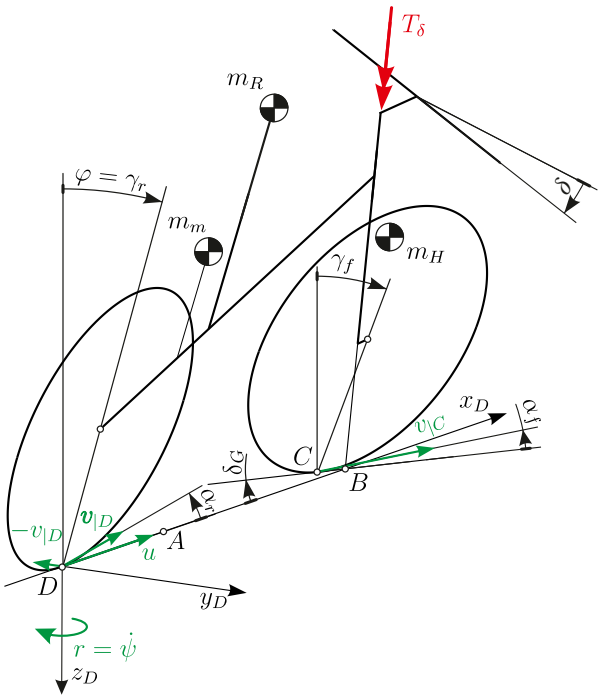

Figure 2.4: Bicycle while cornering with sketched state and tire variables; adapted from [22] using the denotations of Klinger [33].

$$\alpha_f = \delta_G - \arctan\left(\frac{v_{|D} + l\,r - t_c\dot{\delta}}{u_{|C}}\right) \approx \delta \cdot \cos(\varepsilon) - \frac{1}{u}\left(v_{|D} + l\,r - t_c\dot{\delta}\right). \tag{2.24}$$

The nonlinear relation of the front wheel camber angle γ_f can be found in [31]. The linearised relation for the front wheel camber angle is

$$\gamma_f \approx \varphi + \sin(\varepsilon)\delta. \tag{2.25}$$

Forces and Torques

The tire forces and torques can now be computed. The lateral forces are modelled by the side slip angle α and the camber angle γ for the used tire model. The lateral force at the respective tire is computed by

$$F_y = c_{F,\alpha} \cdot \alpha + c_{F,\gamma} \cdot \gamma. \tag{2.26}$$

The side slip angle and the camber angle get multiplied by the side slip stiffness for side force $c_{F,\alpha}$ and the camber stiffness for side force $c_{F,\gamma}$ respectively.

A similar relation is found for the aligning torque M_z of the respective wheel. Due to the asymmetric shear stress distribution in the contact patch, the lateral forces do not act in the plane of symmetry. By reducing the system of forces to the fictitious point F an equivalent torque occurs. The self aligning torque is computed, see [9], by

$$M_z = -c_{M,\alpha} \cdot \alpha + c_{M,\gamma} \cdot \gamma. \tag{2.27}$$

The torque stiffness constants $c_{M,\alpha}$ and $c_{M,\gamma}$ were used to compute the torque components originating from side slip and camber, respectively.

The overturning couple M_x is a fictitious torque due to relative movement of the fictitious point of contact F to the actual point of contact. As the normal forces will be reduced in the fictitious contact point, the overturning couple needs to be added in order to ensure the equivalence of the system of forces. The overturning couple of the tire model of Pacejka [9] only depends on the camber angle γ

$$M_x = -c_{M_x,\gamma} \cdot \gamma. \tag{2.28}$$

Tire Parameters

The dependency of F_y is modelled by the side slip stiffness $c_{f,\alpha}$ and camber stiffness $c_{f,\gamma}$, which are tire parameters determined by experiments or finite element analysis (FEA). The tire stiffnesses are multiplied by their respective normal forces F_z to obtain the respective actual stiffness coefficients for side forces

$$c_{F,\alpha} = c_{f,\alpha} \cdot F_z, \tag{2.29}$$
$$c_{F,\gamma} = c_{f,\gamma} \cdot F_z. \tag{2.30}$$

The coefficients $c_{M,\alpha}$ and $c_{M,\gamma}$ are related to the actual stiffnesses for side forces by the pneumatic trails $t_{\alpha 0} > 0$ and $t_{\gamma 0} < 0$. The pneumatic trails are the levers of the forces generating the torques [9] and are computed by

$$c_{M,\alpha} = c_{F,\alpha} \cdot t_{\alpha 0}, \tag{2.31}$$
$$c_{M,\gamma} = c_{F,\gamma} \cdot t_{\gamma 0}. \tag{2.32}$$

2.3 Addition of the SbW-System

The extraordinary part of the bicycle is the attached Steer-by-Wire system. A real-world prototype was developed as part of a final-year project at an upper secondary technical college. This design will be briefly outlined.

Construction

As mentioned in the introduction, the premise of a SbW system is to decouple the input unit from the output unit of the steering. Considering a bicycle's steering, this means disconnecting the handlebar from the fork and the front wheel. The decoupled units are then equipped with sensors and actuators to sense inputs and act with outputs on the respective subsystems. In the present design, the sensor and the actuator come in a single unit. Two stepper motors, one for the handlebar and one for the lower fork assembly, are proposed.[1] In order to supply the system with the necessary torques, planetary gearboxes were added. The output torque of the gearboxes is transferred to the respective assembly by a belt and pulley system. The stepper motors are mounted on bent sheet metal holders, which are clamped to the frame of the bicycle by 3D printed brackets. The sheet metal plates have slot holes in order to adjust the position of the stepper motors and to tension the belts. A sketch of the SbW system assembly is shown in Fig. 2.5.

The electric motors are used as sensors as well, since the electric current, which is proportional to the torque applied, the position, and the angular velocity can be measured. This system is used to sense the rider's input. Feedback torque for the rider as well as the steer torque are applied at the respective unit. By applying a feedback torque at the handlebar, the rider receives information about the system's state. It is a design criterion for SbW systems and will further be discussed in Chapter 5.

A more detailed insight into the design and the parts of the construction is given in [32]. The masses in table 2.1 are also adapted from [32]. Changes to the current status have been updated.

[1] There are some concerns regarding the type of motor. The chosen stepper motors are hybrid stepper motors. These motors are equipped with permanent magnets. There exists a desired position in which the rotor rests when no electric current is applied, the position of coincidence of the magnetic field of the rotor and stator [50]. If the motor is displaced, a holding torque depending on the current orientation is present. This torque could prevent small steer torques from being detected. Comparatively, Dialynas et al. [28] used brushless DC motors for their prototype. Some additional thoughts should be put into the selection of the motors.

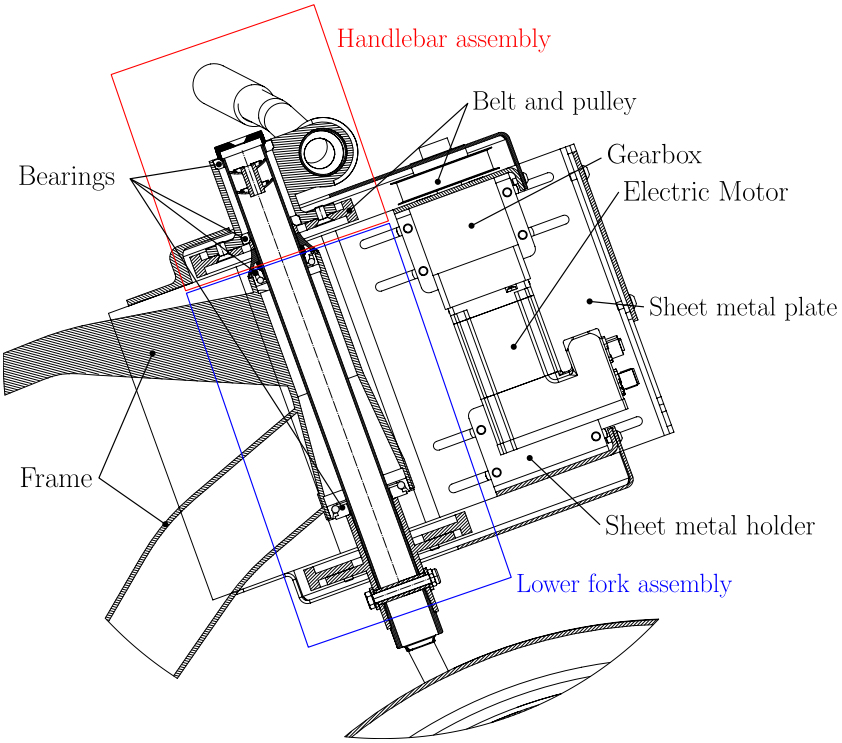

Figure 2.5: Sectional view of the proposed Steer-by-Wire system design. The handlebar motor with its components is depicted. The layout of the fork's drive train is the same.

Influence on Dynamics

The added mass of the SbW system influences the mass matrix. Since the system is mounted in front of the handlebar, the additional inertia tensor components Θ are significant, especially the terms of the SbW system with respect to the rear wheel contact point. The global dynamics of the entire system will therefore change. The inertia terms get added to the global mass matrix. The inertia tensor of the SbW system in its respective coordinate system is rotated and transformed in the rear wheel contact point D using the parallel axes theorem [51]. The mass and inertia properties of the design in 2.5 are given in the Appendix in table A.1.

The dynamics of the steer system also differ from the regular bicycle. Since the mechanical coupling between the handlebar and the fork has been cut, an additional DOF is added to the system. It is now crucial to differentiate between the steer angle of the handlebar δ_{HB} and the angle of the fork δ. Stiffness and damping terms as well as the polygonal effect of the toothed belt have not been included in the modelling section. The additional inertia of the rotating components were included accordingly. This thesis uses δ as the designated DOF. For this, the inertia terms of the angular variables connected to this DOF via a gear ratio need to be transformed. This is done by equivalence of kinetic energy [52] and the formulation with an equivalent moment of inertia Θ

Table 2.1: Mass properties of the modelled SbW assembly, adapted from [32]

Component	Mass in kg	Quantity	Note
Stepper motor and controller	1.3	2	Stator 1 kg, Rotor 0.3 kg
Planetary gearbox	0.9	2	-
Pulleys on fork	0.2	2	-
Pulleys on SbW system	0.2	2	-
Other components	1.5	1	-
Total mass	6.3	-	-

$$\begin{aligned} T &= \frac{1}{2}\Theta \cdot \dot{\delta}^2 = \frac{1}{2}\sum_i^N \Theta_i \cdot \dot{\omega}_i^2 = \frac{1}{2}\sum_i^N \Theta_i \cdot \left(\dot{\delta} \cdot i_{tot,i}\right)^2 \\ &= \frac{1}{2}\dot{\delta}^2 \sum_i^N \Theta_i \cdot i_{tot,i}^2 \rightarrow \Theta = \sum_i^N \Theta_i \cdot i_{tot,i}^2. \end{aligned} \tag{2.33}$$

The inertia term Θ_i is the component of the part rotating with ω_i and connected to the designated DOF δ by the total gear ratio $i_{tot,i} = \omega_i/\dot{\delta}$. The rotating parts of the motor and the gearbox 'gain' inertia in relation to the steer axis.

The influence on dynamics of the attached SbW system compared to the bicycle models without Steer-by-Wire system is shown in [32].

2.4 *SIMPACK* Model

The software *SIMPACK 2024x* from the company *Dassault Systems* was used as software to model the bicycle as MBS. *SIMPACK 2024x* uses an algorithm which defines the motion of a body relative to another body. The single bodies are connected via joints. The advantage of *SIMPACK 2024x* is that it solves the geometrically nonlinear equations. This allows the system to display more realistic dynamical behaviour even for larger values of φ, δ and ψ compared to the benchmark bicycle in [8] or section 2.1. The integration of additional dynamics into a multi-body model is considerably more straightforward than incorporating them into the previous models. Up to date, the MBS model uses constant forward speeds u, where an inclusion of longitudinal dynamics can be done by including a driving torque at the rear wheel and a respective tire model for longitudinal dynamics. The electric and magnetic dynamics of the motors also have not been modelled. These are mainly determined by the inductance L and the winding resistance R of the motors [50]. These two fundamental electric properties are relevant for the availability of the desired motor torque. These dynamics can be integrated by

simply adjusting the forcing terms in the model.

A linear tire model has been implemented to the MBS bicycle model, equal to the one in Chapter 2.2. The model is therefore not viable for large values of the side slip α and camber angle γ, since tires usually have strongly nonlinear characteristics for large values of camber and side slip [9]. The difference between the tire model implemented in the 6 states model and this one is that the transient side slip angle α' and transient camber angle γ' are used.

$$\frac{\sigma_\alpha}{u}\,\dot{\alpha}' + \alpha' = \alpha \tag{2.34}$$

$$\frac{\sigma_\gamma}{u}\,\dot{\gamma}' + \gamma' = \gamma \tag{2.35}$$

The lateral forces as well as the tire self-aligning torque are therefore time dependent. The overturning couple M_x is assumed to respond instantaneously to changes in camber [9].

As parameters of the first-order differential equations of the transient responses (2.34) and (2.35), relaxation lengths are introduced [9]. Experiments show that the relaxation lengths of the side slip σ_α and the camber σ_γ are similar [9]. The dependency of the relaxation length on the vertical load was not considered. Further simplification was done by choosing $\sigma_\alpha = \sigma_\gamma = \sigma$, due to the mentioned similarity. The lateral force and the self-aligning torque will build up faster for small relaxation lengths σ and high forward speeds u.

Due to the additional DOFs of the tires and other non-fully kinematically constrained bodies, the configuration and state space have a higher dimension than the benchmark bicycle and the bicycle model with tire model. This leads to additional eigenfrequencies and eigenmodes, which are generally of high frequency and damping. All of the above leads to a slight model mismatch, recognisable in the eigenvalue course shown in 2.5, and a state space mismatch.

The MBS model is not conservative. This is due to an absolute damping term which will damp vertical oscillations. The purpose of this damping is numerical, in order to prevent the system from additional oscillations and boost computational efficiency and precision. The velocity will therefore decrease in cornering manoeuvres, due to energy dissipation while transient effects of normal load transitions decay.

A snippet of the 3D modelling page of the *SIMPACK 2024x* MBS bicycle model is given in Fig. 2.6.

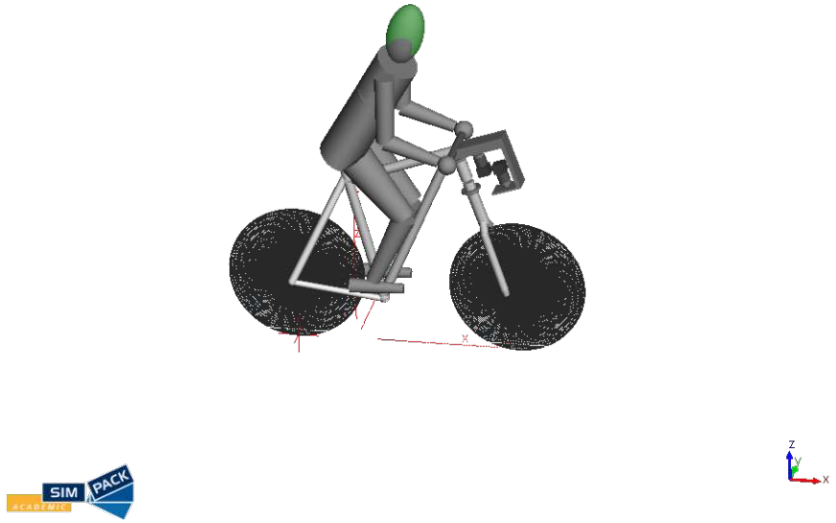

Figure 2.6: Screenshot of the *SIMPACK 2024x* graphical user interface with the multi-body model of the rider and the bicycle model with attached SbW system.

2.5 Characteristics and Stability

Stability Analysis

In this section, a closer look is taken at the system's behaviour in the lateral direction in the vicinity of the straight running condition $\varphi = \delta = \dot{\varphi} = \dot{\delta} = 0$. It is often stated that 'a system is stable'. This proposition is not correct but is often used colloquially. With that, usually the stability of an observed point of equilibrium at a given parameterisation is meant [53].
The bicycle's equations of motion are linearised in the straight running condition $\varphi = \delta = \dot{\varphi} = \dot{\delta} = 0$. A linear system of ordinary differential equations with constant coefficients is at hand. The stability behaviour of such systems is determined by their eigenvalues [54]. The linear time-invariant system

$$\dot{\boldsymbol{x}} = \boldsymbol{A}\boldsymbol{x} \tag{2.36}$$

is asymptotically stable and input-output stable as long as all eigenvalues of $\boldsymbol{A}$ have a negative real part

$$\operatorname{Re}\lambda\left(\boldsymbol{A}\right) < 0. \tag{2.37}$$

If the linearised system is asymptotically stable, the nonlinear system is also asymptotically stable for small perturbations [54].

The solutions of (2.36) are linear combinations of solution vectors $\boldsymbol{x}_i(t)$

$$\boldsymbol{x}(t) = \sum_{i=1}^{N} c_i \boldsymbol{x}_i(t). \tag{2.38}$$

The coefficients c_i are determined by initial conditions. The eigenvalues of $\boldsymbol{A}$ are computed by using an exponential ansatz for the single solution vectors

$$\boldsymbol{x}_i(t) = \mathrm{e}^{\lambda_i t} \boldsymbol{v}_i. \tag{2.39}$$

Inserting (2.39) in (2.36) gives

$$(\boldsymbol{A} - \boldsymbol{I}\lambda_i)\, \boldsymbol{v}_i = \boldsymbol{0}. \tag{2.40}$$

The exponent of the ansatz λ_i is called *eigenvalue* and the vector $\boldsymbol{v}_i$ the corresponding *eigenvector*. The eigenvalues determine the time course of the solution. The eigenvector gives the relative motion of the state variables to one another. In order to obtain non-trivial solutions for (2.40), the bracket has to vanish

$$|\boldsymbol{A} - \boldsymbol{I}\lambda_i| = 0. \tag{2.41}$$

Equation (2.41) is called *characteristic equation*. The eigenvectors $\boldsymbol{v}_i$ of the respective eigenvalues λ_i are computed by solving (2.40). If the eigenvalues and eigenvectors of two systems are equal, the dynamics are also identical.

The course of the eigenvalues over the forward speed u is pictured in Fig. 2.7. On the left side, the course of the real part and on the right side, the course of the imaginary part of the eigenvalues are shown.

A good correspondence of the eigenvalues of the different models is present in Fig. 2.7. At speeds $u \geq 15\,\mathrm{m/s}$, the real parts of the benchmark bicycle model are significantly lower than for the other models, as seen in 2.7a. The course of the imaginary part in Fig. 2.7b correlates with each other for the observed speed range. The eigenvectors to the eigenvalues shown in Fig. 2.7 are explained briefly.

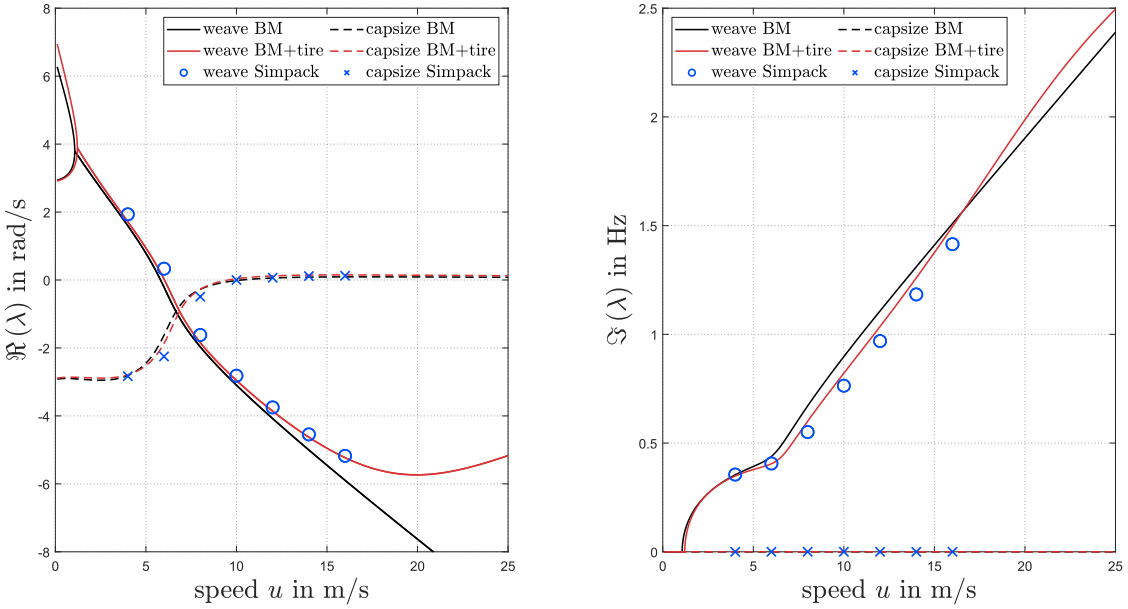

(a) Real parts of λ

(b) Imaginary parts of λ

Figure 2.7: Eigenvalue comparison between models.

Weave

The Weave mode is characterised by a complex conjugated pair of eigenvalues when excelling a certain speed, see 2.7b. The speed at which the branches connect and form the complex conjugated eigenvalue pair is at $u \approx 1.2\,\mathrm{m/s}$. The system's behaviour changes at this point due to a Hopf bifurcation [53]. The real parts of the eigenvalues are positive for low speeds up to the Weave-speed of $u_{\mathrm{Weave}} \approx 6\,\mathrm{m/s}$, where the eigenvalue crosses the $\mathrm{Re}\,\lambda = 0$ axis. With rising values of u, the imaginary part of λ is moving to higher frequencies while the real part decreases in the observed speed range. The bike performs an oscillatory roll-steer-yaw movement.

Capsize

This mode is stable for low speed ranges. The eigenvalues might cross the $\mathrm{Re}\,\lambda = 0$ axis, depending on the parameterisation. As seen in Fig. 2.7, the mode turns unstable at the Capsize speed $u_{\mathrm{Capsize}} \approx 10\mathrm{m/s}$ for the parameter set in this thesis. The mode stays unstable from there on in the observed speed range. This mode was named after the capsizing motion of ships. The bicycle performs a roll motion and falls in the lateral direction.

The bicycle is self-stable at forward speeds between u_{Weave} and u_{Capsize}. This speed range is called *autostable speed range*. Additional modes which are not discussed in this thesis,

but are well researched, are the Caster-mode, the Wobble-mode, and the Lean-mode of the rider [22], [31], [33], [55]. If one is interested in the bicycle model's behaviour for parameter variations such as the moment of inertia of the wheels, the tire stiffnesses, additional masses on bike baskets at the handlebar or above the rear wheel, or the influence of the rider's positioning on the bike, refer to [31], [33]. The stability behaviour of bicycle models in steady-state cornering manoeuvres is shown in [34].

Characteristics of the Benchmark Bicycle Model

In this section, additional dynamic aspects are mentioned which are important for rider modelling. Focus lies on the bicycle system with a single input, the steer torque T_δ (2.5). This assumption will be discussed in Chapter 3, but is necessary to mention for the following observations.

With the choice of the input variable, the system of differential equations can be Laplace transformed in order to perform transfer function analysis. In transfer function analysis, a harmonic excitation by the input variable is assumed [52]. The differential equation in form (2.6) then becomes

$$\begin{gathered} \boldsymbol{M}\ddot{\boldsymbol{q}} + \boldsymbol{C}\dot{\boldsymbol{q}} + \boldsymbol{K}\boldsymbol{q} = \boldsymbol{f} \\ \downarrow \mathcal{L}\{\ldots\} \downarrow \\ \left(\boldsymbol{M}s^2 + \boldsymbol{C}s + \boldsymbol{K}\right)\boldsymbol{Q}(s) = \boldsymbol{F}(s) = \boldsymbol{S}(s)\,\boldsymbol{Q}(s)\,. \end{gathered} \tag{2.42}$$

Vanishing initial conditions of the generalised coordinates and their derivatives $\dot{\boldsymbol{q}} = \boldsymbol{q} = \boldsymbol{0}$ are assumed. The dynamic stiffness matrix $\boldsymbol{S}$ is defined for harmonically excited systems [52]. The frequency domain forcing vector is $\boldsymbol{F} = (0, T_\delta)^{\mathrm{T}}$ with the steer torque as a single input. $\boldsymbol{Q}(s)$ is the vector of generalised coordinates in the frequency domain.

In this analysis, the benchmark bicycle model was used. The workflow for the other models is identical. The transfer function of the roll angle φ is

$$G_{\varphi T_\delta} = \frac{\varphi(s)}{T_\delta(s)} = K_\varphi \frac{(s+z_1)(s+z_2)}{(s+p_1)(s+p_2)(s^2-(p_3+p_4)\cdot s + p_3\cdot p_4)}. \tag{2.43}$$

In (2.43), $p_i \lesseqgtr 0$ are the poles and $z_i > 0$ are the zeros of the system. The poles, see Fig. 2.7, and zeros are generally parameter-dependent. The transfer behaviour therefore changes with varying speed.

Considering the transfer function of the steer angle δ

$$G_{\delta T_\delta} = \frac{\delta(s)}{T_\delta(s)} = K_\delta \frac{(s+z_3)(s-z_4)}{(s+p_1)(s+p_2)(s^2-(p_3+p_4)\cdot s + p_3 \cdot p_4)}, \tag{2.44}$$

it is noticeable that the denominator is identical for both terms in (2.43) and (2.44). A right half-plane zero z_4 appears in the equation. This indicates non-minimum-phase behaviour of the transfer function [56]. The zero is positive for all velocities, which means that the behaviour is independent of parameter variations. The non-minimum-phase behaviour of the benchmark bicycle's steer angle in the time domain can be observed in Fig. 2.8.

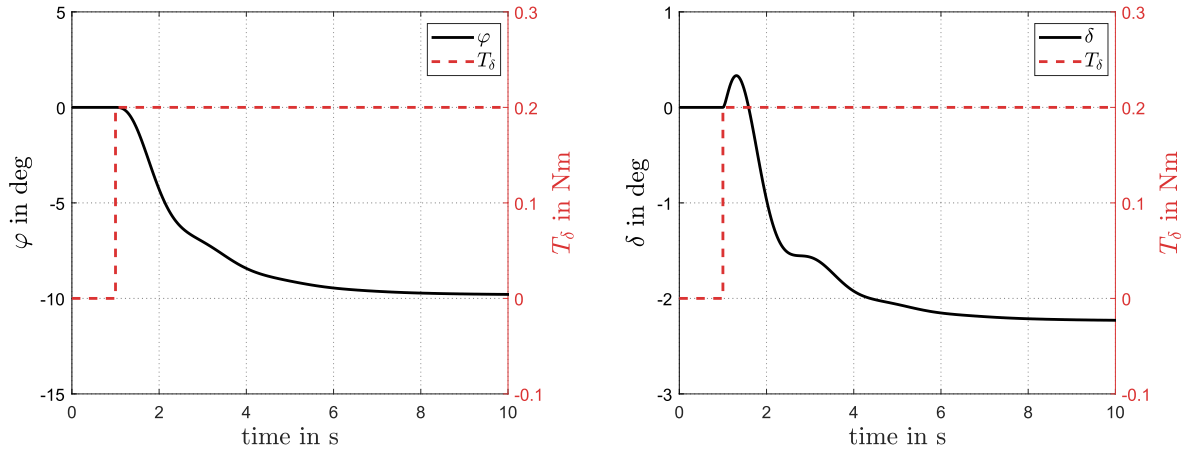

(a) Step response of the roll angle φ (b) Step response of the steer angle δ

Figure 2.8: Step responses of the roll angle on the left and the steer angle on the right of the benchmark bicycle model to a steer torque step input in the autostable speed range at $u = 7\,\mathrm{m/s}$.

On the one hand, the transfer function (2.43) shows minimum-phase behaviour in Fig. 2.8a, as the roll angle directly moves in a single direction. The steering angle in Fig. 2.8b, on the other hand, shows an initial counter movement to the same step steer torque input. This is the case if the respective transfer function possesses an odd amount of positive zeros [56]. The term non-minimum-phase originates from the system's behaviour in the frequency domain. The amplitude response, in this case, cannot be deduced from the phase response [57], as the phase gains disproportionately compared to minimum-phase systems. The counter movement of the steer angle is needed to move the pivot point of the bicycle to initiate the fall. The steer angle then proceeds to move to its asymptotic value, due to tire forces and moments, the influence of normal forces, as well as gyroscopic effects.

Looking at the relation of the yaw rate r and the steer angle [8] of the benchmark bicycle model

$$r = \frac{u \cdot \delta + t_c \cdot \dot{\delta}}{l} \cos(\varepsilon) \tag{2.45}$$

it can be concluded that the yaw rate, as well as the yaw angle and the lateral velocity, also have non-minimum-phase behaviour.

3 Rider Model

In this thesis, the roll angle φ was selected as the control variable. This statement is based on the following justifications:

- The roll angle has minimum-phase behaviour with the steer torque as input, see Fig. 2.8a.
- The roll angle is the quantity which gives immediate feedback in the visual, vestibular, and proprioceptive systems. The deviation from a desired position will therefore be felt with all senses.
- The amplitudes of the roll angle are larger than the steer angles and therefore more easily recognisable.
- The lateral acceleration is directly proportional to the roll angle [9].
- Looking at the lateral forces in steady-state cornering manoeuvres, the forces generated due to camber predominate the forces generated by the side slip. This is due to comparatively higher camber angles than side slip angles for two-wheeled vehicles.
- The head of the bicycle rider will laterally move from the point of contact of the bicycle with the road by $\Delta y_{Head} \approx h_{Head} \cdot \varphi$. Considering rider safety, the roll angle will be monitored to determine the current protrusion relative to the wheel's contact point.

As the input variable, the steer torque T_δ was used. This is supported by literature, as it is the most important input variable for bicycle riders [43].

Path Tracking Rider Model

A two-level rider model to track trajectories was used in this thesis. In order to follow a path, a rider uses information about the trajectory ahead and knowledge about the vehicle [15]. With the knowledge about the vehicle, the rider will anticipate the inputs to approximately follow the desired path. If the vehicle does not exactly meet the trajectory, the rider will perform further control inputs to move towards the desired trajectory.
In control-theoretic terms, the anticipation of the rider is labelled as *feedforward*, and the additional correction as *feedback* control. The control architecture of the rider model is depicted in Fig. 3.1. The following observations and relations are applicable for 'normal riding conditions'. The rider model is limited to moderate lateral accelerations and, as a consequence, moderate roll angles [15].

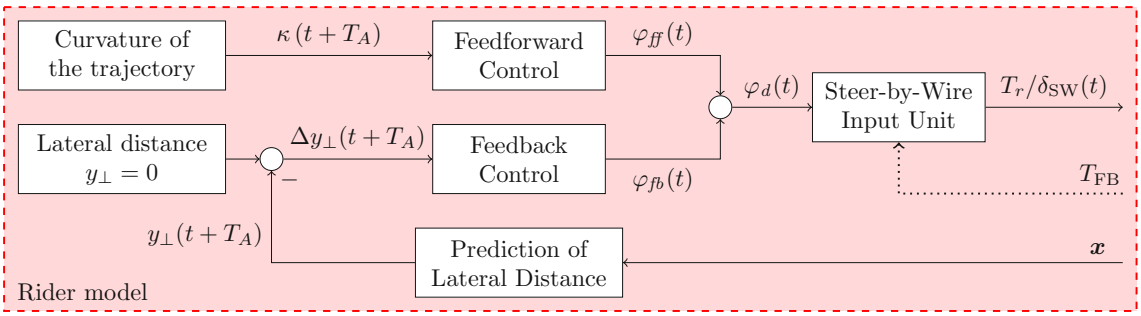

Figure 3.1: Rider model layout for the SbW bicycle model, adapted from [22].

The two-level model in Fig. 3.1 uses information about the trajectory, the curvature κ, and the lateral distance $y_\perp$ at a preview point located $s_A = T_A \cdot u$ in front of the bicycle to form a desired feedforward and feedback roll angle, φ_{ff} and φ_{fb}, respectively. There exist rider models which possess a control level to form a desired trajectory, which was not pursued in this thesis. The actual track coincides in this thesis with the desired trajectory. The track design therefore has a significant influence on the control performance of the rider model. The rider uses the curvature κ of point P_t, the distance $s_A = T_A \cdot u$ in front of the current heading at the track, to anticipate the inputs, see Fig. 3.2 for clarification. The curvature κ is the inverse of the track's curve radius ρ at the respective point. The curvature is a property of the curve and therefore is independent of the state of an observer. The feedback level uses the perpendicular distance $y_\perp$ between the track and the preview point P as input to form the feedback roll angle. This level uses information about the current state of the bicycle compared to the trajectory. The rider model then applies the input quantity, the steer torque T_r or the steering wheel angle δ_{SW} of the bicycle rider model or the car driver model, respectively, at the input unit. The bicycle rider model and the car driver model are discussed later in this chapter. The rider is provided with a feedback torque T_{FB} by the feedback unit of the SbW system. The input and feedback unit is discussed in Chapter 5.

3.1 Anticipatory Feedforward Control

In order to steer a vehicle in an anticipatory manner, it is necessary for a driver/rider to scan the trajectory ahead. If the view is limited by fog or trees, the driver/rider adjusts their velocity to meet the preferred preview distance s_A [15]. Instead of the preview distance, the anticipation or preview time T_A will be used. Horn [58] concluded that drivers control vehicles mostly by anticipation if the road is assembled by straights and curves connected by clothoids. Relatively few inputs are made to correct the heading of the trajectory. The feedforward roll angle φ_{ff} therefore is usually of higher magnitude compared to the feedback roll angle φ_{fb}. Different approaches to model the feedforward

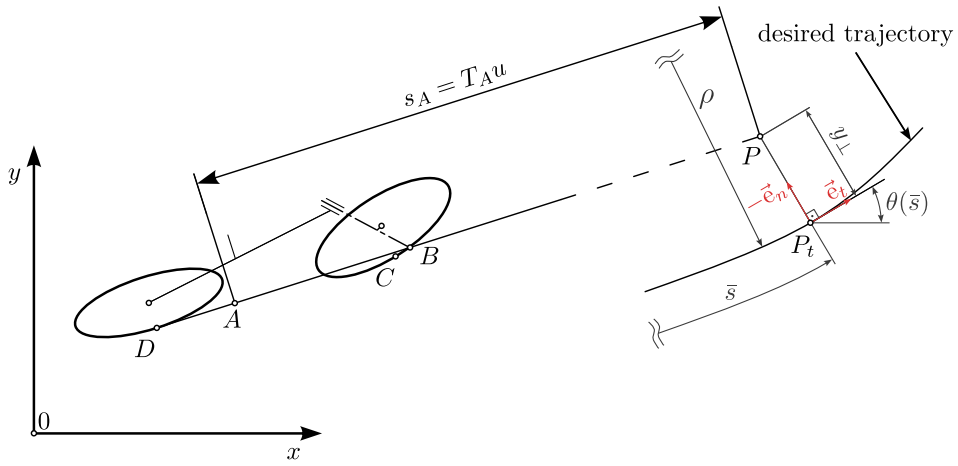

Figure 3.2: Sketch illustrating the anticipation with the variables to determine the feedforward and feedback control levels of the rider model, adapted from [22].

control of a bicycle are investigated.

Approach I

A driver model designed for car drivers is adapted to suit the input and output quantities of a bicycle rider. Mitschke [15] found a relation for the anticipatory feedforward level of a car driver. The relation in Mitschke's notation reads:

$$T_{2S}^2 \ddot{\delta}_{LS} + T_{1S} \dot{\delta}_{LS} + \delta_{LS} = V_{MS} \cdot \kappa \left(t + T_A\right) \tag{3.1}$$

The car driver therefore uses information about the trajectory, in the present model the curvature κ, to plan a steer angle course $\delta_{LS}(t)$ beforehand. The time constants T_{2S}, T_{1S}, the pre-gain V_{MS}, and the anticipation time T_A can be determined if one assumes that the driver solely steers the vehicle by anticipation. These constants mainly depend on vehicle properties, such as the side slip stiffness, the position of the COM, and so forth. The automobile's steering wheel angle is δ_{LS}. The anticipatory level therefore requires the driver to possess knowledge about the vehicle operated. Laplace transforming (3.1) gives:

$$\left((T_{2S}\, s)^2 + T_{1S}\, s + 1 \right) \delta_{LS} = V_{MS}\, \kappa(s) \mathrm{e}^{s\, T_A} \tag{3.2}$$

The factor V_{MS} can be approximated for cars [15] using (3.3).

$$V_{MS} \approx \frac{\delta\, u}{r} \tag{3.3}$$

Using the stationary form of the non-holonomic steer-yaw relation of the benchmark bicycle model (2.45), a term for the bicycle's stationary steer angle to curvature ratio V_{MS} is found:

$$V_{MS} \approx \frac{\delta\, u}{\frac{\delta\, u}{l}\cos\varepsilon} = l/\cos\varepsilon. \tag{3.4}$$

As bicycle riders do not plan manoeuvres with the steer angle in mind, (3.2) is adjusted to use the roll angle instead. This is done by using the transfer functions of the respective bicycle states to the steer torque. The transfer function between roll and steer angle:

$$G_{\varphi\delta} = \frac{\varphi(s)}{\delta(s)} = \frac{K_\varphi}{K_\delta} \cdot \frac{(s+z_1)\,(s+z_2)}{(s+z_3)\,(s-z_4)} \tag{3.5}$$

was used, which was derived by dividing $G_{\varphi T_\delta}$ (2.43) by $G_{\delta T_\delta}$ (2.44). The positive zero of $G_{\delta T_\delta}$ appears in the denominator of $G_{\varphi\delta}$, indicating unstable behaviour of (3.5).

This can be omitted by using stationary relations:

$$K_{\varphi\delta} = G_{\varphi\delta}|_{s=0} = -\frac{K_\varphi}{K_\delta} \cdot \frac{z_1 z_2}{z_3 z_4} \tag{3.6}$$

Inserting (3.6) into (3.2) and assuming stationary conditions, the term simplifies to:

$$\varphi = -\kappa(s) \cdot \mathrm{e}^{s\,T_A} \cdot \underbrace{\frac{l}{\cos\varepsilon} \cdot \frac{K_\varphi}{K_\delta} \cdot \frac{z_1 z_2}{z_3 z_4}}_{-K_{\varphi\kappa}}. \tag{3.7}$$

A new gain factor $K_{\varphi\kappa}$ is used as a combined parameter. Inverse Laplace transforming the relation gives:

$$\varphi(t) = \kappa(t + T_A) \cdot K_{\varphi\kappa}. \tag{3.8}$$

The poles and zeros of $G_{\varphi\delta}$ (3.5) and therefore the gain $K_{\varphi\kappa}$ are velocity-dependent. This further implies that $K_{\varphi\kappa}$ also provides the rider's knowledge about the vehicle.

Approach II

Another term for the anticipated roll angle related to a desired trajectory is derived using simple kinematics. Assuming the preview point P in Fig. 3.2 to move stationary with constant speed u along a circular track with radius ρ, the yaw rate around the circle's centre is:

$$r = \frac{u}{\rho} = u \cdot \kappa. \tag{3.9}$$

The bicycle also rotates with yaw rate r, as it follows the preview point P. The benchmark bicycle model does not provide a direct method to form a connection between the yaw rate and the desired roll angle. It is possible to follow the same path as in the previous approach, by using the steer angle as an intermediate variable and (2.45), as in the first approach, which is not desired as a bicycle rider is most likely not aware of the steer angle to yaw rate or roll angle ratio. This can be omitted by using the bicycle model with a tire model, as there exists a defined relation between the roll angle and the yaw rate, which a bicycle rider is more likely to be accustomed to. The desired roll angle for a respective curvature can then be computed by:

$$\varphi = \kappa(t + T_A) \cdot \underbrace{u \cdot G_{\varphi r}}_{K_\varphi \kappa}. \tag{3.10}$$

The transfer function $G_{\varphi r}$ is the transfer function between the roll angle φ and the yaw rate r. It can be computed by using the transfer function of the bicycle model with tire model with respect to the steer torque input $G_{\varphi r} = G_{\varphi T_\delta}/G_{r T_\delta}$. If the benchmark bicycle model's relation (2.45) is used in the kinematic relation (3.9), the exact same term as in Approach I is obtained. It is, nonetheless, more likely for a rider to approximate the desired roll angle for a specific cornering manoeuvre than the steer angle. Furthermore, a more general, kinematic derivation was presented in this approach compared to the derivation with a relation for a specific vehicle. The outcome, however, is the same.

To compare the relations, an approach of Pacejka [9] is used additionally. The yaw rate r with the forward speed u gives the lateral acceleration for the point moving along a circular track:

$$a_y = u\, r. \tag{3.11}$$

The lateral acceleration is closely related to the roll angle φ of bicycles. Pacejka [9] gives a relation for the roll angle at stationary cornering manoeuvres:

$$\varphi = \frac{u\,r}{g} = \frac{u^2\,\kappa}{g}. \tag{3.12}$$

Pacejka obtained the relation by considering the lateral and normal forces for stationary cornering manoeuvres. The ratio of roll angle to curvature is then:

$$K_{\varphi\kappa} = \frac{u^2}{g}. \tag{3.13}$$

The relationships of the forward gain $K_{\varphi\kappa}$ were compared in Fig. 3.3. The courses of $K_{\varphi\kappa,\mathrm{Tire}}$ were computed using Approach II and the transfer functions of the bicycle model with a tire model. The gain $K_{\varphi\kappa,\mathrm{BM}}$ used the benchmark bicycle model and Approach I. The values of $K_{\varphi\kappa,\mathrm{Simpack}}$ were obtained using *SIMPACK* and applying step torque inputs and dividing the corresponding results of the roll angles by the yaw rates in an evaluation window. Relation (3.13) is labelled as $K_{\varphi\kappa,\mathrm{Pacejka}}$ in Fig. 3.3.

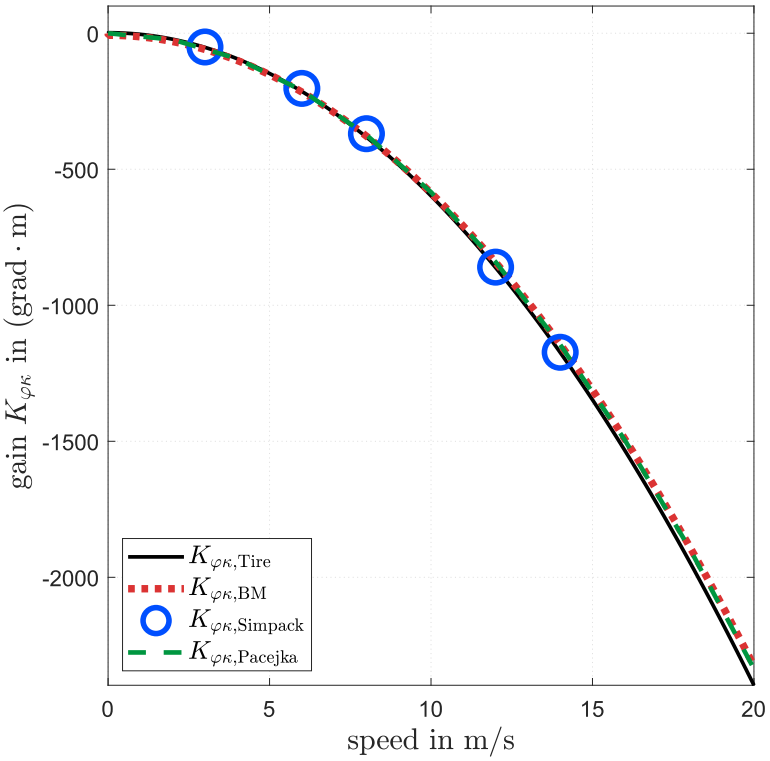

Figure 3.3: Comparison of different modelling approaches for the stationary gain $K_{\varphi\kappa} = \frac{\varphi}{\kappa}$.

All gains in Fig. 3.3 show similar courses for the observed speed range. The small deviation from the benchmark bicycle model is caused by the tire models of the higher-fidelity models. It is therefore of minor importance how the desired feedforward roll angle is obtained from the curvature by the rider model.

Notes on the Anticipation Time

The time T_A the rider looks ahead of the current position is dependent on the system's velocity. The current travel speed is estimated by the rider. Furthermore, there is a dependency on the system dynamics and the task to master. This was visualised by considering a 'J-Turn' manoeuvre and solely using feedforward control of the bicycle model. The 'J-turn' consists of a straight followed by a 180° turn with a constant radius. As the ideal rider model perfectly meets the track's curvature, two circular paths are compared. In order to initiate a turn, a bicycle moves to the opposite side at the beginning. This shifts the centre of the circular paths from each other. The circles are therefore not congruent. For physically reasonable manoeuvres, the desired and actual circular trajectories will intersect each other twice. The point of intersection can be controlled by the rider by adjusting the preview time. In Fig. 3.4, the effects of the different anticipation time constants are illustrated.

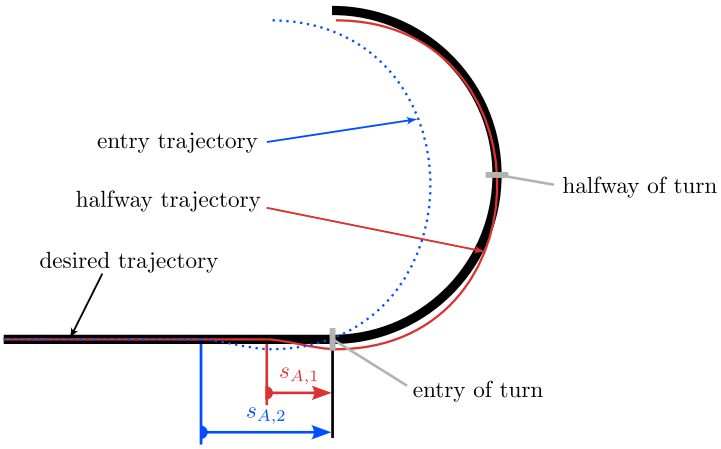

Figure 3.4: Possible assessments for the determination of the preview time illustrated for the J-turn manoeuvre. The previewed distance $s_{A,2}$ was chosen to hit the entry point of the curve while the anticipatory point of the blue line is located $s_{A,1}$ in front of the vehicle, which minimises the tracking error for the feedforward control.

The blue, dotted line in Fig. 3.4 is the trajectory of a bicycle model with the goal to meet the entry point of the curve. This case is important when a certain point in front of the rider needs to be hit. A large anticipation time $T_{A,2}$ is necessary. The red curve has a shorter anticipation time $T_{A,1}$. In this case, the target point on the trajectory is the halfway point of the J-turn. This is the task-dependent anticipation time, as it

is specifically designed to give a good result for the respective desired trajectory. For systems which possess faster dynamics, the necessary time to achieve a certain state will also decrease compared to slower systems.

The preview time is therefore dependent on the vehicle dynamics and the manoeuvre. A certain dynamical behaviour of the system and a set of manoeuvres were chosen for this thesis. A task-dependent anticipation time constant T_A is used. Reference values of the anticipation time are given by Haudum [22]. The stabilising dynamics of the bicycle rider model used by Haudum are different from the ones used here.

3.2 Compensatory Feedback Control

If the desired trajectory is not met by feedforward controls alone, the rider needs to apply additional corrective inputs. On the one hand, novice riders do not have knowledge about the vehicle and therefore cannot ride them in a feedforward manner. Experienced riders, on the other hand, will ride their respective vehicle mostly by feedforward control, as they are already aware of the dynamics [58]. In any case, disturbances acting from the outside on the system have to be compensated to return to the desired state. Examples of such disturbances are lateral wind gusts, road obstacles, and others. These disturbances will prevent the rider from following their desired path.

Considering the lateral control of a bicycle rider, the perpendicular lateral distance $y_\perp$ of the preview point P to the trajectory is used by the rider model to compute the feedback roll angle φ_{fb}. A relation is needed to model the rider model's additional roll angle for a given perpendicular deviation. McRuer [14] proposed a transfer function of a human operating a vehicle to possess lead-lag behaviour. This is based on experimental results of pilot handling experiments, analysed with system identification techniques [14]. The human lead-lag controller relation $G_r(s)$ reads:

$$G_r = \frac{\varphi_{fb}(s)}{y_\perp(s)} = V_m \cdot \frac{1 + T_v\, s}{1 + T_n\, s} \cdot \mathrm{e}^{-s\tau}. \tag{3.14}$$

The static gain V_m scales the overall amplitude of the transfer function. High values may cause instabilities, and low values will lead to slow reaction times and insufficient compensation. The lead time T_v helps to gain phase margin of the output to the input. Low values of T_v shift the lead effect to higher frequencies and therefore impact faster dynamics. The lag time T_n introduces an additional pole, which will give additional phase delay of the system output to the system input. Increasing T_n shifts the lag effect to lower frequencies, which reduces high-frequency amplification and stabilises slower systems. If it is increased, better transient behaviour is achieved but also becomes more

sensitive to noise. The model introduced by McRuer contains a sensory time delay τ. This should take human neuronal delays into account. The delay was neglected in this thesis, similar to Haudum [22], which simplifies (3.14) to:

$$G_r = \frac{\varphi_{fb}(s)}{y_\perp(s)} = V_m \cdot \frac{1 + T_v\, s}{1 + T_n\, s}. \tag{3.15}$$

Mitschke discusses (3.15) in [15] and gives typical values of phase margins, crossover frequencies, and prediction times for the driver control model design of the open-loop driver-car system. In this thesis, the controller parameters of Haudum [22] were used as a reference for an iterative process to find the parameters in this thesis. Haudum used the root locus method combined with a designed transfer function of the lateral displacement with respect to the steer torque.

The perpendicular lateral deviation $y_\perp$ is computed by using a line normal to the trajectory intersecting with the preview point P, see Fig. 3.2. The point P_t is the intersecting point at the trajectory. The perpendicular distance is computed by:

$$y_\perp = \left(\overline{P0} - \overline{P_t 0}\right) \cdot \mathbf{e}_n, \tag{3.16}$$

where $\overline{P0}$ is the position vector of the preview point and $\overline{P_t 0}$ the position vector of the intersection point at the trajectory. The trajectory is defined by a curvature course $\kappa(\bar{s})$. By integrating the curvature's course along the arc length coordinate $\bar{s}$, the trajectory's inclination $\theta(\bar{s})$ to the abscissa axis is obtained:

$$\theta(\bar{s}) = \int \kappa\,(\bar{s})\,\mathrm{d}\bar{s} \tag{3.17}$$

With the course of the inclination, the course of the normal vector:

$$\mathbf{e}_n(\bar{s}) = \begin{pmatrix} \sin(\theta(\bar{s})) \\ -\cos(\theta(\bar{s})) \end{pmatrix} \tag{3.18}$$

is computed. A linear relationship between curvature, inclination, and trajectory was used.

The lateral deviation $y_\perp$ will initially move in the opposite direction of the curve when turning, due to the non-minimum phase characteristics of the lateral dynamics, illustrated in the red and blue trajectory courses in Fig. 3.4 and observable in the result section in Fig. 6.1. This explains the small values of the static gain V_m used to achieve the results in Chapter 6, as non-minimum phase systems are prone to instability [45]. The compensation of a lateral deviation $y_\perp$ is therefore sluggish.

3.3 Remarks on Rider Modelling

It needs to be mentioned that the exact tracking of a trajectory was not the subject of this thesis. An easy-to-implement rider model was used to get a general feeling about the rider-vehicle interaction and investigate the designed components of the SbW system. More profound rider modelling techniques, such as model predictive control, would perform more realistic inputs. Perfect trajectory tracking is not possible due to the chosen system input. The trajectory planning level of a higher-level rider model was neglected, which could improve the tracking ability of the rider model when included. Splitting the anticipation time constant into two separate time constants, a feedforward anticipatory time constant $T_{A,ff}$ and a feedback anticipatory time constant $T_{A,fb}$, could improve the tracking performance, as an additional, yet simple, adjustment option is introduced.

3.4 Input Quantity of the Bicycle Rider Model

The input block in Fig. 1.1 needs inputs from the rider models to translate these inputs into reference values for the stabilisation controller, see Fig. 1.1. In order to achieve the desired roll angle φ_d, a bicycle rider will apply a steer torque T_δ at the handlebar. The steer torque required is obtained by using the desired stationary roll angle of the rider and the corresponding relation with the steer torque (3.19). This is assumed as knowledge about the vehicle, memorised by the rider.

$$K_{T_\delta \varphi} = \left(G_{\varphi T_\delta}\right)^{-1}\Big|_{s=0} = \left(\frac{T_\delta(s)}{\varphi(s)}\right)\Big|_{s=0} \tag{3.19}$$

As the rider knows which roll angle corresponds to which steer torque, a formulation for the necessary steer torque to achieve the desired roll angle φ_d at a certain forward velocity u is found:

$$T_\delta(t) = K_{T_\delta \varphi} \cdot \varphi_d(t) = K_{T_\delta \varphi} \cdot \left[\varphi_{ff}\left(\kappa(t+T_A)\right) + \varphi_{fb}\left(y_\perp(t+T_A)\right)\right]. \tag{3.20}$$

Assuming two different rider models, one used to the benchmark bicycle model and the other to the bicycle model with a tire model, two different steer torques are required for the same desired roll angle $\varphi_d(t)$. The steer torque to desired roll angle ratio over the forward speed u is illustrated in Fig. 3.5.

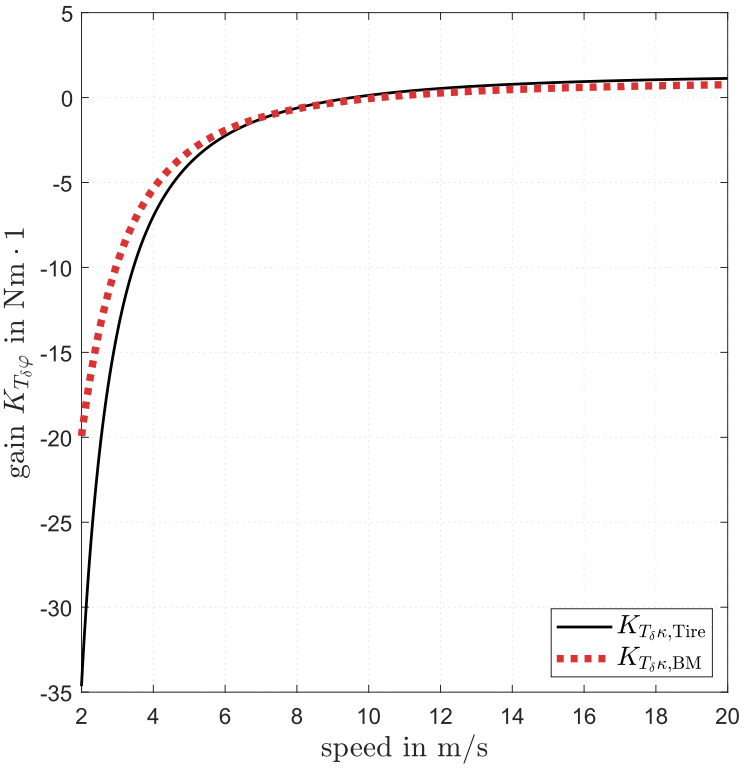

Figure 3.5: Relation between the applied steer torque of the rider model using different intrinsic bicycle models and the desired roll angle.

The gain $K_{T_\delta\varphi,\text{BM}}$ is the steady-state gain for the benchmark bicycle model. It is noticeable that the gain of the bicycle model with a tire model $K_{T_\delta\varphi,\text{Tire}}$ has higher magnitudes, in the majority of the observed speed range, than that of the benchmark bicycle model. This originates from the forces and torques of the tire model, which demand a higher steer torque from the rider model to meet the same roll angles.

Concluding, it can be said that the knowledge level of the bicycle mostly affects the amount of steer torque applied at the handlebar, as the knowledge of the vehicle to determine the feedforward roll angle is secondary. Only the feedback level of the rider control model will vary noticeably with improved knowledge, as the desired feedforward roll angle is similar for all models, see Fig. 3.3.

3.5 Input Quantity of the Car Driver Model

Instead of steer torques, a car driver uses the steering wheel angle δ_{SW} to operate cars. The feedforward steering wheel angle will be composed by the curvature of the track, similarly to the bicycle rider model in this thesis. The car driver model of Mitschke [15] uses the lateral acceleration to model the desired feedback steering wheel angle. Using the equivalence of lateral acceleration and the roll angle (3.12), the car driver model can react similarly to the bicycle rider model used in this thesis. Instead of modelling a relation between the steer torque and the desired roll angle, the car driver model uses a relation of the steering wheel angle δ_{SW} to a desired roll angle to operate the SbW vehicle:

$$\varphi_d \propto \delta_{SW}. \tag{3.21}$$

An appropriate, reasonable approach to model the mapping function between the steering wheel angle and the desired roll angle will be discussed in Chapter 5. The desired roll angles are computed in the same fashion as before, as the lateral and tilting dynamics of the bicycle models are maintained. The car driver model therefore needs to be aware of the characteristics of the bicycle models [46], discussed in section 2.5.

4 Stabilising Controller

The stabilising controller was designed using state feedback control techniques. State feedback control uses information about the system's states to influence the dynamics. The state feedback controller receives a reference variable y_d as the reference variable and applies a steer torque T_δ at the fork to track the reference variable accordingly. It needs to be investigated whether the bicycle models can be stabilised by the steer torque.

4.1 Assessment of Controllability

In order to exactly control the motion of a system, it has to be state controllable. Controllability is defined by the possibility to transform a system in an initial state $\boldsymbol{x}_0$ with an appropriate input variable $\boldsymbol{u}_{[0,t_e]}$ to an arbitrary end state $\boldsymbol{x}_e$ within the time span t_e [59].

Full state controllability is a more restricted property. If a system is fully state controllable, it is possible to reach the end point $\boldsymbol{x}_e$ by an arbitrary trajectory. The exact definition and the difference to regular controllability can be found in [59]. In this thesis, the distinction between these two definitions is not of importance.

Another differentiation has to be made for nonlinear and time-variant systems. For these types of systems, bijectivity [1] for the control of an arbitrary state $\boldsymbol{x}_a$ to the zero state $\boldsymbol{x}_0$ is not given [59].

There are several different criteria which could be used to determine the controllability of systems. A frequently used one is the controllability criterion of Kalman. Kalman uses a controllability matrix:

$$\boldsymbol{S}_S = \left(\boldsymbol{B}, \boldsymbol{AB}, \boldsymbol{A}^2\boldsymbol{B}, \ldots, \boldsymbol{A}^{n-1}\boldsymbol{B}\right) \tag{4.1}$$

which is quadratic for the single input case [59]. The system is fully state controllable if:

$$\operatorname{rank}(\boldsymbol{S}_S) = n, \tag{4.2}$$

[1] In this case, bijectivity expresses the directional independence of a control process between two desired states.

where n is the dimension of the system matrix $\boldsymbol{A}$. Haudum [22] also used the criterion in his thesis.

If the system is given in canonical form (4.3), the controllability can easily be assessed by looking at the state space matrices [2].

$$\frac{\mathrm{d}\tilde{\boldsymbol{x}}(t)}{\mathrm{d}t} = \operatorname{diag} \lambda_i \, \tilde{\boldsymbol{x}}(t) + \tilde{\boldsymbol{B}}\boldsymbol{u}(t) \tag{4.3}$$

The rows of the canonical input matrix $\tilde{\boldsymbol{B}}$ show which eigenvalue and therefore which eigenmode can be influenced by which system input u_i. If there exists a zero-row $\tilde{\boldsymbol{b}}_i = \boldsymbol{0}$, then the i-th eigenmode cannot be influenced, and the system is not fully state controllable. It can, however, still be state controllable if the not-controllable eigenvector is damped and the movements of the eigenmode decay.

For the low-fidelity 4- and 6-state models, the controllability can easily be obtained, as the system matrices are of low dimension and well-conditioned. Using Kalman's controllability criterion, the full rank of both systems is achieved in most cases. Two exceptions have to be made at distinguished velocities. Edelmann et al. [21] have shown with modal controllability methods that the benchmark bicycle model's Weave and Capsize modes both possess a velocity at which they are not controllable by a steer torque at the fork. The Weave's uncontrollable speed is $u_{\text{Weave,n.c.}} \approx 0.05\,\text{m/s}$, and the Capsize's is $u_{\text{Capsize,n.c.}} \approx 1.19\,\text{m/s}$ for the parameter set used in [21]. They have also used a measure of how well an eigenvector can be influenced by the respective input, where the steer torque is the best input to control the bicycle model's lateral dynamics. The stabilisation controller in this thesis will only act for velocities above the mentioned uncontrollable ones.

The MBS bicycle model's state space is higher-dimensional than the low-fidelity models, and the state matrix $\boldsymbol{A}$ is ill-conditioned. This makes the evaluation of Kalman's controllability criterion difficult due to numerical accuracy and rounding errors. The canonical form could not be computed using *Matlab*, as the problem is too ill-conditioned. Another method was pursued using singular value decomposition, which is less prone to numerical problems. All used criteria did not lead to a definite statement of the controllability of the MBS bicycle model. It is assumed that the controllability of the MBS bicycle model is given anyway, as the low-fidelity models possess controllability with the steer torque as the input variable, and Valenzano [32] already managed to stabilise the multi-body bicycle model using the steer torque.

[2] The tilde over the expressions should emphasise that these are transformed quantities compared to the regular state space representation.

4.2 Control Law for Stabilisation

As it is possible to control the MBS bicycle model with the steer torque, the task is now to find an appropriate relation to model the steer torque T_δ to achieve a desired system behaviour. State feedback with the pole placement method was used by Valenzano [32] to model the steer torque. The method was adapted in this thesis and is explained briefly. The bicycle model's equations of motion in state space are:

$$\dot{\boldsymbol{x}} = \boldsymbol{A}\boldsymbol{x} + \boldsymbol{b}u. \tag{4.4}$$

In order to manipulate the dynamics of the system, the input variable u is chosen to:

$$u = -\boldsymbol{k}^{\mathrm{T}}\boldsymbol{x} \tag{4.5}$$

which gives the opportunity to influence the location of the poles of the closed-loop system matrix $\boldsymbol{A}_{\mathrm{CL}}$:

$$\dot{\boldsymbol{x}} = \left(\boldsymbol{A} - \boldsymbol{b}\boldsymbol{k}^{\mathrm{T}}\right)\boldsymbol{x} = \boldsymbol{A}_{\mathrm{CL}}\boldsymbol{x} \tag{4.6}$$

by using the state feedback vector $\boldsymbol{k}^{\mathrm{T}}$. The state feedback vector can be computed by the characteristic equation of (4.6) if the pole locations are set. As a linear time-invariant system is defined by its eigenvalues, the state feedback vector in (4.6) influences the system's solution. In order to manipulate all eigenvalues, the system needs to be fully state controllable [59]. In Fig. 4.1, relation (4.6) is illustrated using block diagrams.

The achievable pole placement locations are limited by actuator limitations of the system. Kortüm and Lugner [54] give some guidelines on where to begin with the pole placements:

- The imaginary part of complex poles should not be altered. They should only be moved parallel to the real axis in the Gaussian plane.
- Unstable eigenvalues shall be mirrored along the imaginary axis. If the system's behaviour is still not satisfying, the poles can be moved to more negative real parts until the system behaves as desired.
- Eigenvalues which are already stable should not be touched to lower energy use.

A disadvantage of the pole placement method is its rather weak robustness.

Pole locations proposed by Valenzano [32] are used, which were selected considering the motor's restrictions of torque and angular velocities. Furthermore, Valenzano prescribed

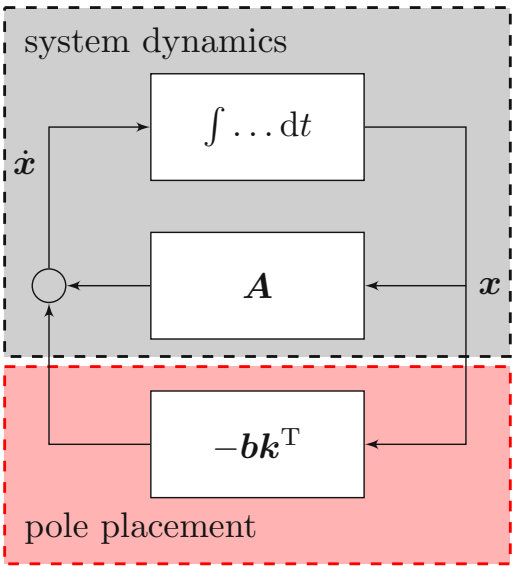

Figure 4.1: Sketch of a dynamic system with state feedback control using pole placement.

the pole locations following defined criteria given in [32]. The desired pole locations are illustrated in Fig. 4.2. The 'First setup' in Fig. 4.2 aims to give 'rapid' stabilising behaviour, where the 'Second setup' allows for more 'moderate' stabilising actions. The term 'rapid' is used as an abbreviation for a more stable set of poles, with a higher imaginary part whose course is less dependent on the forward speed. The term 'moderate' is the abbreviation for the set of pole locations which are more similar to the eigenvalues of a normal bicycle. The imaginary part of the Weave mode re-connects with the eigenvalue course of the open-loop system at lower forward velocities, see Fig. 4.2b. The pole locations nonetheless provide stable behaviour in the observed speed range in Fig. 4.2.

Using the control law (4.5) and the desired pole locations in Fig. 4.2, the bicycle model's straight running state $\varphi = \delta = \dot{\varphi} = \dot{\delta} = 0$ is stabilised.

As a model-based control strategy was pursued, the state feedback gains will be computed at a low-fidelity model. A good correspondence of the model for control parameter design and the controlled model is necessary for such an approach. The models match each other's dynamics well, as observable in Fig. 2.7.

Remarks on the Model-Based Control Design

Some remarks are made about the control performance[3] of the model-based approach pursued. In general, a good model coherence is given by the eigenvalue plot in Fig. 2.7, which is a great starting point for model-based controller design. As the high-fidelity

[3]Performance in this context is meant as accuracy of placement.

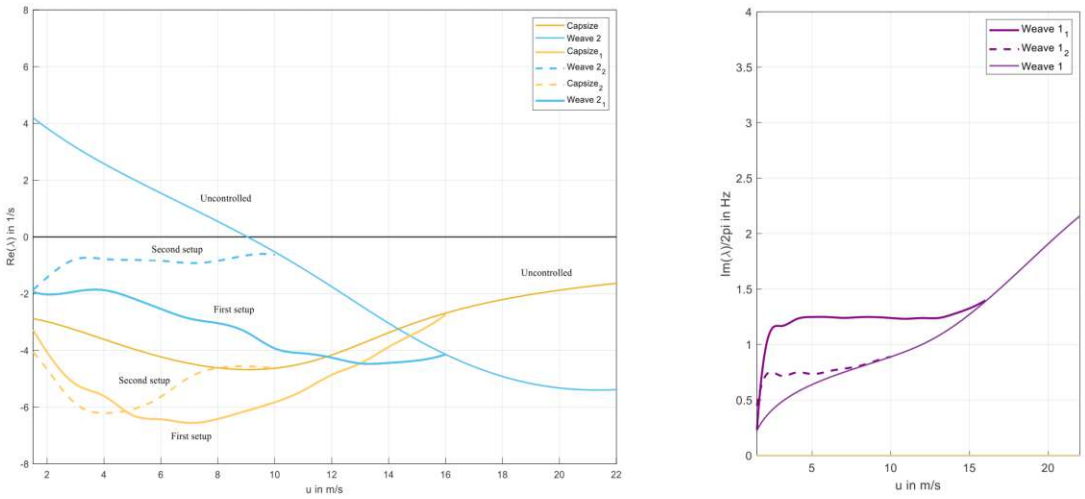

(a) Proposed real part of poles.

(b) Proposed imaginary part of poles.

Figure 4.2: Proposed pole locations, diagrams from [32].

multi-body bicycle model possesses a higher-dimensional state vector, a full state feedback control law cannot be obtained using the state feedback vector computed with the pole placement method and the low-fidelity bicycle models. As a consequence, only the states which are also present in the low-fidelity models were fed back, and a partial state feedback control is achieved. By ignoring part of the states of the state vector of the MBS bicycle model, the system is not fully state controllable [59], and the actual pole locations vary from the desired poles at the respective velocity u in Fig. 4.2.

The control performance of the pole placement method is now investigated at $u = 6\,\mathrm{m/s} \approx 22\mathrm{km/h}$. Both low-fidelity models, the benchmark bicycle model and the bicycle model with a tire model, are used for the state feedback vector computation to get a comparison of the placement accuracy between the two models. The results of the pole placement at the MBS bicycle model's Weave and Capsize eigenvalues, using the gains computed at the low-fidelity models, are illustrated in Fig. 4.3.

The plot 4.3a shows the pole placement accuracy using the 4-state feedback vector on the 6-state model and on the MBS bicycle model. In Fig. 4.3b, the pole placement performance using the 6-state feedback vector is shown. The actual poles of the closed-loop 6-state model are marked with red circles, the poles of the MBS bicycle model with blue crosses, and the desired poles with black triangles. Both state feedback vectors achieve asymptotically stable behaviour for all bicycle models. The accuracy of the pole placement, however, is highly dependent on the model used for the state feedback vector computation, as a comparison between Fig. 4.3a and Fig. 4.3b shows. The placement accuracy of the 4-state feedback vector in Fig. 4.3a is insufficient, as the desired system behaviour is not achievable. The Weave and Capsize eigenvalues are both placed far off the desired locations for this model. A better performance is given with the 6-state feed-

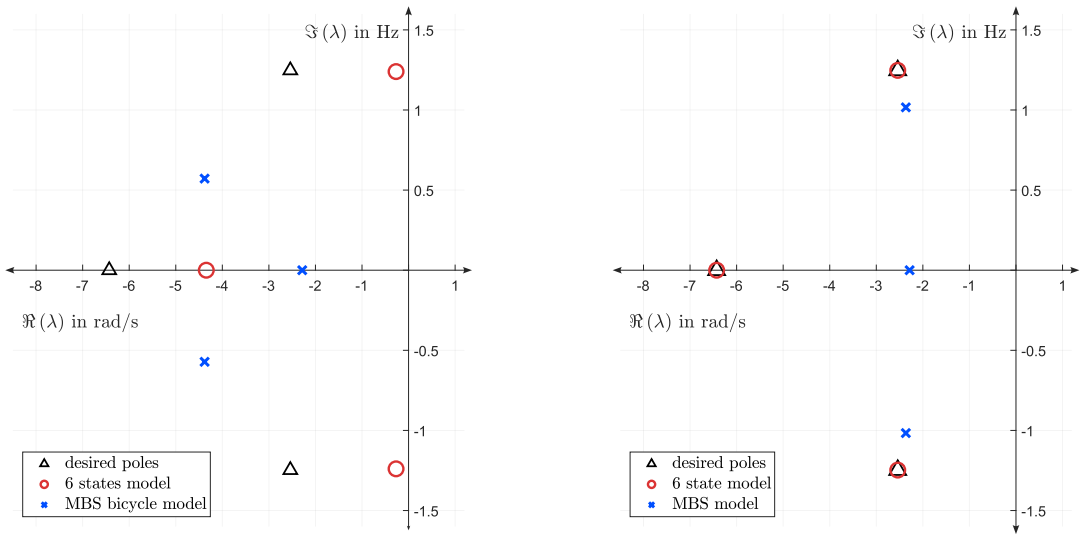

(a) Eigenvalues of closed-loop MBS model with the state feedback vector computed at the benchmark bicycle model.

(b) Eigenvalues of closed-loop MBS bicycle model with gains computed at the bicycle model with a tire model.

Figure 4.3: Closed-loop behaviour of the MBS model using state feedback from low-fidelity models.

back vector, where the Weave eigenvalues are placed closer to the desired. The Capsize eigenvalue is placed in a similar location using either method. If full state feedback is applied at the respective model, the pole placement method will place the poles in the near vicinity of the desired ones, as seen in Fig. 4.3b using the 6-state feedback vector at the 6-state model.

The poor placement quality can be attributed to a slight model mismatch, state-space discrepancies, and the limited robustness of the pole placement method. In Figure 4.3, only the Capsize and Weave eigenvalues are shown. However, the poles of the additional modes in the 6-state and MBS bicycle models are also influenced by the steer torque input. As a result, the energy supplied to the system through steer torque is distributed among all modes that can be controlled by it. This division of energy reduces the power available for positioning the Weave and Capsize poles, leading to decreased placement accuracy.

Lunze discusses a method in [59] to achieve optimised pole placement of chosen poles using partial state feedback. Lunze solves a matrix optimisation problem to compute the optimised partial state feedback vector. The disadvantage of this method is that all eigenvalues of the high-fidelity model would need to be known, and a weighting matrix needs to be designed, which is unfeasible for high-dimensional state spaces.

In summary, the system's poles are not in the desired positions using the partial state feedback, resulting in unexpected behaviour, as seen in Fig. 4.3.

Remarks on Digital Control

The stabilising controller will be run on a micro-controller or a similar device like the *Speedgoat*. These computers run on a certain clock frequency defined by the hardware used in these systems. A part of this cycle time is used for internal computations, input-output (IO) read and write times, storage operations, and many more. Since these operations may use alternating time spans and a guaranteed cycle time cannot be achieved, the frequency for IO operations is usually capped to create reproducible and predictive behaviour of the system. This frequency is called the *sampling frequency* f_s, where the inverse is the *sampling time* T_s:

$$T_s = \frac{1}{f_s}. \tag{4.7}$$

Furthermore, digital systems have a limited resolution on how they perceive the values of a sensor. The signal is therefore value- and time-discrete [60].

Since the physical bicycle is a continuous problem, the controller has a different perception of time. Methods of digital controls have to be used to take the different time scales into account. The concept of digital control is to transform a continuous system into a time-discrete form to design the controller. Due to discretisation, the system of differential equations is transformed into difference equations:

$$\begin{aligned} \dot{\boldsymbol{x}}(t) &= \boldsymbol{A}\boldsymbol{x}(t) + \boldsymbol{b}u(t) \\ \downarrow t \to kT_s \downarrow \\ \boldsymbol{x}(k+1) &= \boldsymbol{A}\boldsymbol{x}(k) + \boldsymbol{b}u(k) \end{aligned} \tag{4.8}$$

The time step variable k is the number of the computed cycle observed. In order to transform the discretised system into the frequency domain, the $\mathcal{Z}$-transformation is used. It is a sum transformation due to its discrete properties. The algorithm, limitations, and examples are given in [59]. The sampling time constant in this thesis is defined as $T_s = 150\,\text{Hz}$. Lunze gives guidelines in [59] on how the time constant should be chosen. As the highest frequency of the system is $\approx 2.5\,\text{Hz}$ in the observed speed range, as seen in Fig. 2.7, the sampling frequency needs to be:

$$f_s \geq 15\,\text{Hz} \tag{4.9}$$

according to the mentioned criteria in [59]. The input frequency of humans was also taken into account when selecting the sampling frequency. Due to neuromuscular delays, the human frequency bandwidth is limited to approximately $\approx 2\,\text{Hz}$. The *Speedgoat* system, developed by the company of the same name and available at the institute, supports refresh rates of 1000 Hz, ensuring that the chosen sampling frequency can be achieved.

The performance of discrete controllers lacks compared to continuous ones [59]. Consequently, the sampling frequency was set to $f_s = 150\,\text{Hz}$, as stabilisation was successfully achieved at this rate. Performance is expected to degrade significantly at lower sampling frequencies. If the pole placement was accurate at the continuous system, the sampling rate could be reduced to the 15 Hz mentioned above. However, since the pole placement is already inaccurate in the continuous case, see Fig. 4.3, further deviations in pole locations are expected at lower sampling frequencies, which could lead to insufficient stabilising behaviour or even instability of the closed-loop system.

In Fig. 4.4, the individual state feedback gain trajectories of the 6-state model at a forward velocity of $u = 6\,\text{m/s}$ are depicted for different sampling frequencies f_s. The desired pole locations remain identical for all frequencies, and each gain index corresponds to the respective state it feeds back.

In conclusion, the low-fidelity model-based state feedback controller using pole placement does not accurately position the poles in the continuous MBS model, as illustrated in Fig. 4.3. In the discrete system, the poles will generally be placed even further away, as the computed gains increase with decreasing sampling time, as shown in Fig. 4.4. The poles' inaccuracy will increase as a consequence, and the desired system behaviour cannot be achieved. The frequency at which the stabilising controller is unable to stabilise the system cannot be computed analytically.

4.3 Follow-Up Control of the Steer-by-Wire System

In order for the SbW system to follow the desired reference roll angle commands $y_d(t)$ of the input unit designed in Chapter 5, corresponding to the desired roll angle φ_d of the rider control model, a follow-up control approach needs to be incorporated into the control loop in Fig. 4.1. Two approaches for follow-up control were investigated. A method with a pre-amplification gain was implemented. A method utilising state shift techniques offers advantages for designing the steering feedback in the subsequent chapter. This method was explained in the Appendix and exhibits the same dynamic behaviour as the method discussed in this chapter.

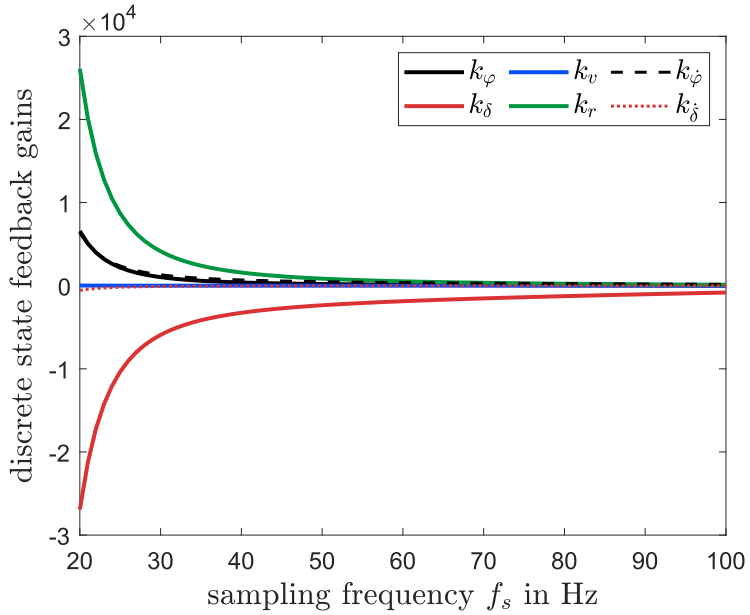

Figure 4.4: Course of the discrete state feedback gains computed at the bicycle model with a tire model at $u = 6\text{m/s}$ with respect to the sampling frequency of the discrete system.

To model the bicycle model's steer torque to allow follow-up control, the control algorithm:

$$u = K_w y_d - \boldsymbol{k}^{\mathrm{T}} \boldsymbol{x} \tag{4.10}$$

was used. The pre-amplification gain is K_w. The control loop uses the single control variable y_d, related to the rider model's desired roll angle, see Chapter 5. Substituting the control law (4.10) into (4.4) gives:

$$\frac{\mathrm{d}\boldsymbol{x}}{\mathrm{d}t} = (\boldsymbol{A} - \boldsymbol{b}\boldsymbol{k}^{\mathrm{T}})\boldsymbol{x} + \boldsymbol{b} K_w y_d. \tag{4.11}$$

As (4.6) stabilises the straight running condition, the pre-amplification gain K_w multiplied by the reference variable y_d is responsible for keeping the system in a stabilised state $\boldsymbol{x}_s$ different from the straight running condition. Using the output equation of control systems:

$$y = \boldsymbol{c}^{\mathrm{T}} \boldsymbol{x} + du + \boldsymbol{f}^{\mathrm{T}} \boldsymbol{z} \tag{4.12}$$

with the output vector $\boldsymbol{c}$, the feedthrough gain d, the disturbances $\boldsymbol{z}$, and the output disturbance vector $\boldsymbol{f}$, a relation to compute the pre-amplification gain can be designed.

As the system using the proposed pole locations in Fig. 4.2 is asymptotically stable, the output variable $y(t)$ will reach its desired state y_d:

$$\lim_{t\to\infty} y(t) \to y_d. \tag{4.13}$$

Using (4.13), considering vanishing dynamics at the point of equilibrium, and inserting (4.12) with $d = 0$ and $\boldsymbol{z} = \boldsymbol{0}$ into (4.11) gives:

$$\frac{\mathrm{d}\boldsymbol{x}}{\mathrm{d}t} = 0 = (\boldsymbol{A} - \boldsymbol{b}\boldsymbol{k}^{\mathrm{T}})\boldsymbol{c}^{\mathrm{T}} y_d + \boldsymbol{b} K_w y_d = \left((\boldsymbol{A} - \boldsymbol{b}\boldsymbol{k}^{\mathrm{T}})\boldsymbol{c}^{\mathrm{T}} + \boldsymbol{b} K_w\right) y_d. \tag{4.14}$$

The desired output variable $y_d \neq 0$, and the expression in the outer brackets therefore has to vanish. The pre-amplification gain can be computed by:

$$K_w = -\frac{1}{\boldsymbol{c}^{\mathrm{T}} \left(\boldsymbol{A} - \boldsymbol{b}\boldsymbol{k}^{\mathrm{T}}\right)^{-1} \cdot \boldsymbol{b}}. \tag{4.15}$$

In Fig. 4.5, the block diagram of the stabilising pole placement control loop with the added follow-up control is illustrated. The reference variable y_d is the interface to the input block designed in Chapter 5.

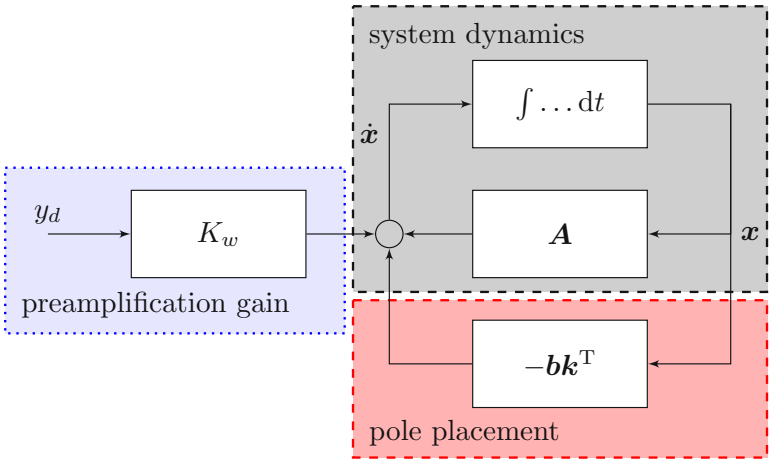

Figure 4.5: Block diagram of state feedback control with pre-amplification gain.

5 Steer-by-Wire Input and Feedback Design

Due to the mechanical decoupling of the handlebar from the fork, there is no defined relationship between the bicycle model's input and the output of the steering. The movement of the fork is determined by the dynamics of the stabilising controller. To allow the stabilising controller to receive the desired system states, a relationship between the reference variable y_d and the desired roll angle of the rider model φ_d must be established. Additionally, as one is used to steering feedback, a relationship to model the feedback torque at the respective input also needs to be designed. The design of the Steer-by-Wire input and feedback block will be distinguished between the bicycle rider model and the car driver model.

In Fig. 5.1, the structure of the Steer-by-Wire system is pictured. The 'Stabilising Controller', which applies a steer torque at the bicycle model's fork, was already discussed in Chapter 4. The 'Input and Feedback Block' receives an input signal from the rider control model, a steer torque T_δ or a steering wheel angle δ_{SW} corresponding to the desired roll angle of the rider model. The input part of the 'Input and Feedback Block' then maps the received input to a respective reference variable y_d for the Stabilising Controller. The stabilising controller then applies the steer torque at the fork to move the bicycle model to the desired state. The feedback part of the 'Input and Feedback Block' computes a feedback torque and applies the torque at the input unit, see Fig. 3.1 and Fig. 1.1. As the feedback torque is not a necessity for the system to function, the 'Input and Feedback Block' input of the states $\boldsymbol{x}$, used to compute the feedback torque, and the output of the feedback torque F_{FB} are dotted.

Two different input units, a handlebar and a steering wheel for the bicycle rider model and the car driver model, respectively, were investigated in this thesis. As discussed in Chapter 3, the bicycle rider model and the car driver model use different input quantities to operate a vehicle. As a consequence, two different algorithms for the input units need to be designed.

Both bicycle riders and car drivers are used to steer torque feedback. The steer torque feedback supplies the rider with information about the road, the tires, and a rough estimation of several dynamical states [61]. The feedback torque for the bicycle rider can be associated with the fork's actual state. Three different approaches to model the feedback torque were investigated for the bicycle rider. For the car driver, a relation for the feedback torque was found, which gives equivalent feedback torques for similar

lateral accelerations in stationary cornering manoeuvres as investigated steering systems for automobiles in [24].

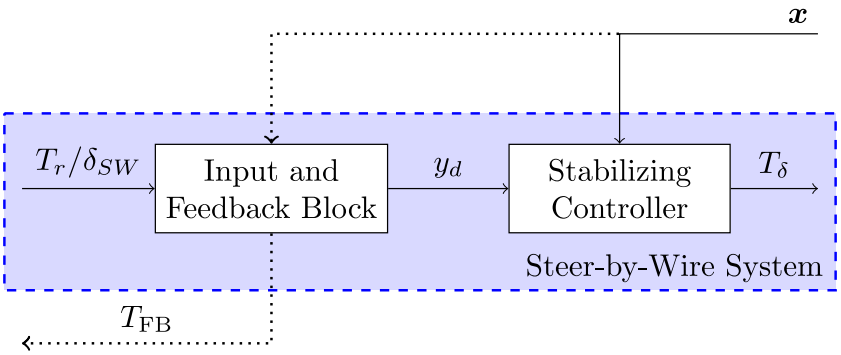

Figure 5.1: Structure of the Steer-by-Wire system between the rider control model and the bicycle model, see Fig. 1.1.

5.1 Bicycle Rider Model

The bicycle rider model is a benchmark case for the Steer-by-Wire bicycle, as it should be possible to simulate a 'normal bicycle ride' using the system. The non-minimum phase and resulting countersteer behaviour, one is used to when riding a bicycle, should be preserved.

5.1.1 Input Design

As emphasised, the bicycle rider will perform input actions by applying the rider steer torque T_r at the handlebar. This torque needs to be measured or computed when pursuing this approach. The relation between the fork's steer torque T_δ and the stationary roll angle φ is known for the low-fidelity bicycle models and can be expressed by the static gain of the transfer function:

$$G_{\varphi T_\delta}|_{s=0} = \left.\frac{\varphi(s)}{T_\delta(s)}\right|_{s=0} = K_{\varphi T_\delta}. \tag{5.1}$$

The relationship depends on the bicycle model used to derive the transfer function, as illustrated in Figure 3.5. In Fig. 5.2, the necessary steer torque T_δ of the bicycle model with a tire model to sustain stationary roll angles at a specific forward speed is plotted. In Fig. 5.2a, the dependency of the steer torque on the stationary roll angle φ is shown for different velocities. As linearised equations of motion were used, the dependency of the steer torque on the roll angle at a certain forward velocity u is a linear function. Fig.

5.2b shows the dependency of the steer torque for a respective roll angle on different forward speeds. The plotted lines are not linear, as the system's behaviour changes when varying the parameter u.

In this thesis, the functions shown in Fig. 5.2 were used to determine the desired roll angles based on the steering torques applied by the rider. The Steer-by-Wire system then hands the desired roll angle quantities computed by this relation in the form of a reference variable to the stabilising controller.

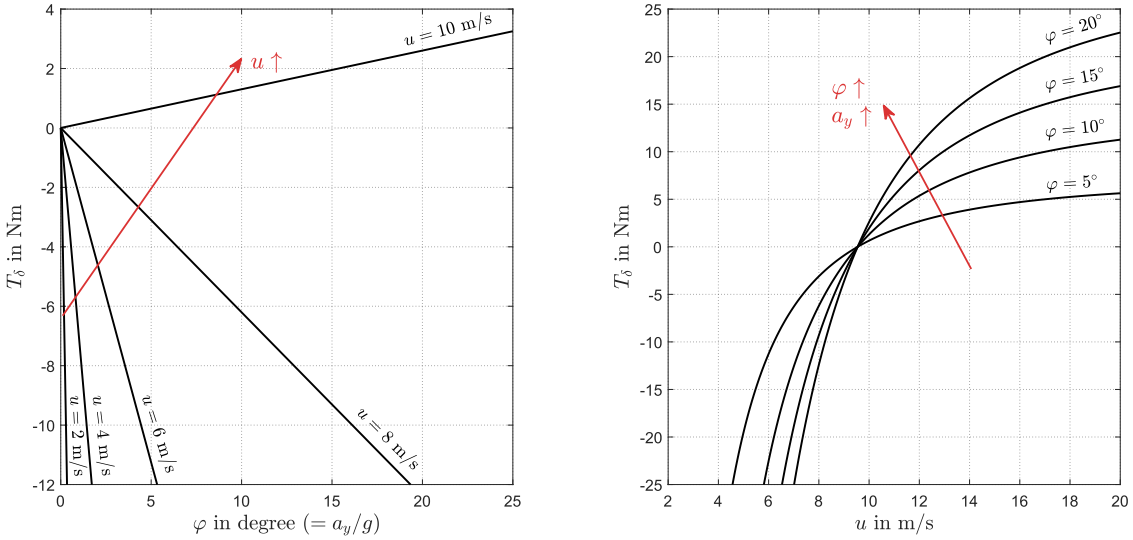

(a) Course of the steer torque over the roll angle (=scaled lateral acceleration) at five different speeds.

(b) Course of the steer torque over the forward velocity for four different roll angles (=scaled lateral acceleration).

Figure 5.2: Steer torque courses of the bicycle model with a tire model with respect to forward velocity u and roll angle φ.

5.1.2 Feedback Design

Three different approaches will be discussed. It generally will be distinguished between a *relative* and *absolute* formulation of the feedback torque. The relative formulation refers to actual states of the fork of the bicycle model, and the steer torque is computed accordingly. The absolute formulation uses a decoupled relationship between the fork and the input unit's steer quantities. Here, model-based approaches to determine the steer feedback torque are used, and the advantages of it for the car approach will be discussed. It would also be possible to electrically couple the feedback motor of the input unit with the output unit, where the torque of the output unit then will be mirrored to the input unit.

Relative Formulation - Approach I

Similar to the approach of Appelman [27], a PD tracking controller is used. This method is mechanically equivalent to replacing the head tube by a virtual torsional spring-damper combination between the fork and the handlebar, see Fig. 5.3. The coupling is unidirectional, as solely the steering quantities of the fork influence the handlebar. The fork's movement is influenced by the torque computed by the stabilisation controller.

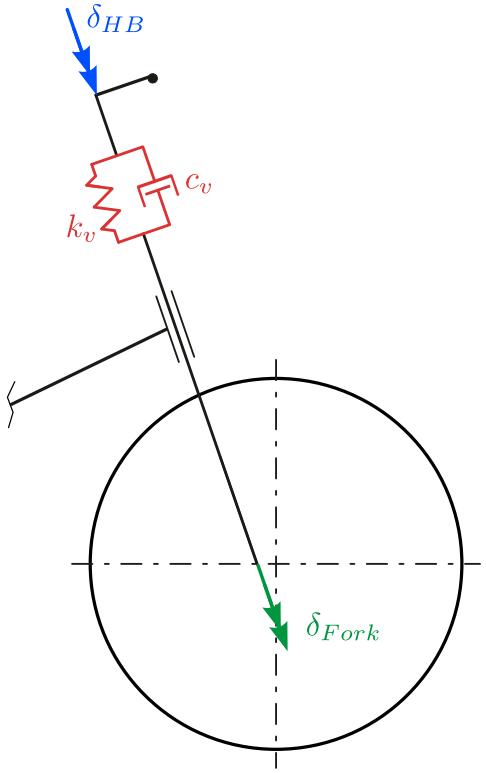

Figure 5.3: Equivalent mechanical model of the PD path tracking controller with virtual torsional spring constant k_v and virtual torsional damping constant c_v between the handlebar steer angle δ_{HB} and the fork's steer angle δ_{Fork}.

The term 'PD tracking' originates from control theory and means that the difference in angle and angular velocities of the two different steering angles will be considered. The consequent torque at the handlebar $T_{PD,HB}$ was computed with [27]:

$$T_{PD,HB} = (\delta_{HB} - \delta_{Fork})\, k_v + \left(\dot{\delta}_{HB} - \dot{\delta}_{Fork}\right) c_v = \Delta\delta\, k_v + \Delta\dot{\delta}\, c_v. \tag{5.2}$$

The equation of motion of the handlebar in the straight riding condition $\varphi = \dot{\varphi} = r = 0$ is:

$$I_{\delta,HB}\ddot{\delta}_{HB} = T_r - T_{PD,HB} = T_r - \underbrace{\left(\delta_{HB} - \delta_{Fork}\right) k_v - \left(\dot{\delta}_{HB} - \dot{\delta}_{Fork}\right) c_v}_{T_{PD,HB}} . \tag{5.3}$$

If the fork is moved by a steer torque by the stabilising controller, a steer angle and steer rate difference will occur, and an additional feedback torque will be applied by the Steer-by-Wire system at the handlebar. This will move the handlebar to follow the fork. A remaining steer angle error $\Delta\delta = \delta_{HB} - \delta_{Fork}$ persists for steady-state cornering (5.2). With equation (5.3), the rider's torque T_r could be computed by using the measured steer angle course and the respective derivatives [52].

The non-minimum phase dynamics of the steer angle remain for a suitable choice of the parameters k_v and c_v, see Fig. 6.4a. The parameters used for plot 6.4a are given in the Appendix.

Appelman [27] did not use the pole placement method with follow-up control but instead 'tunneled' the handlebar tracking torque and added the torque of the stabiliser to receive the steer torque at the fork.

Absolute Formulation 1 - Approach II

Although the riding experience in 'Relative Formulation - Approach I' is similar to that of a conventional bike, one might argue that disturbances at the fork should not be sensed by the rider. The fork movements and the movements of the handlebar then need to be decoupled, leading to the absolute formulations. The first approach uses the desired value of the fork angle $\delta_{d,\mathrm{Fork}}$ instead of the actual fork angle δ_{Fork} and the actual steer rate $\dot{\delta}_{Fork}$ in the PD tracking control equation:

$$I_{\delta,HB}\ddot{\delta}_{HB} = T_r - T_{PD,HB} = T_r - \underbrace{\left(\delta_{HB} - \delta_{d,\mathrm{Fork}}\right) k_v}_{T_{PD,HB}} . \tag{5.4}$$

The desired steering rate $\dot{\delta}_{d,\mathrm{Fork}}$ vanishes, as no steer movements are done in the desired state. The feedback formulation (5.4) will immediately push the handlebar into the position needed for stationary cornering manoeuvres using (5.3). Jerky movements will be the result, as the feedback torque has bigger amplitudes due to the initially bigger difference of $\delta_{HB} - \delta_{d,\mathrm{Fork}}$ compared to $\delta_{HB} - \delta_{Fork}$ in (5.3). The feedback torque therefore will peak initially, and the non-minimum phase behaviour using (5.4) is cut short compared to the one in (5.3), but existent. The movements necessary to stabilise the bicycle will not be felt at the handlebar.

Absolute Formulation 2 - Approach III

For this approach, it will be distinguished between the actual bicycle model, which is subject to disturbances, and a 'digital twin', where a stabilised low-fidelity bicycle model is used. This method will use the equations of motion of a stabilised low-fidelity bicycle model (4.11) and compute an undisturbed course of states $\tilde{\boldsymbol{x}}$, as the disturbances acting at the actual bicycle model are not modelled for the digital twin. The stabilised low-fidelity bicycle model will be stabilised by the same state vector feedback control as the actual bicycle to receive equivalent dynamics.

The equations of motion of the undisturbed quantities are:

$$\frac{\mathrm{d}\tilde{\boldsymbol{x}}}{\mathrm{d}t} = \left(\boldsymbol{A} - \boldsymbol{b}\boldsymbol{k}^{\mathrm{T}}\right)\tilde{\boldsymbol{x}} + \boldsymbol{b}K_w y_d. \tag{5.5}$$

With (5.5), the time course of the undisturbed system is computed. The undisturbed time course of the stabilised low-fidelity bicycle model's fork steer angle $\tilde{\delta}_{\mathrm{Fork}}$ and steer angle rate $\dot{\tilde{\delta}}_{Fork}$ can be extracted. The feedback torque then is computed by:

$$T_{PD,HB} = \left(\delta_{HB} - \tilde{\delta}_{Fork}\right) k_v + \left(\dot{\delta}_{HB} - \dot{\tilde{\delta}}_{Fork}\right) c_v. \tag{5.6}$$

A dynamical feedback behaviour, which is similar to the one of the actual bicycle, is received. The non-minimum phase behaviour of the handlebar steer angle remains.

For the real-world application, the integration of the equations of motion will be challenging, as sensor noise and drifts are present, which is non-existent at the inputs of the *Matlab* model.

5.2 Car Driver Model

The 'Car Driver Model' is another example of how the Steer-by-Wire system could be operated. There are no defined relationships available which map a regular car drive to a bicycle ride. The relationships therefore need to be designed from scratch. Dynamical phenomena which define operating a car are incorporated into the modelling of the Steer-by-Wire system's input and output block.

5.2.1 Input Design

The steering wheel angle δ_{SW} is used as the input quantity to the SbW system. The steering wheel will not follow the steering angle of the fork. A car driver is used to achieving a certain lateral acceleration a_y for a steering wheel angle δ_{SW} at a forward speed u for stationary cornering manoeuvres. If the velocity u is increased, the steering wheel angle δ_{SW} also needs to be increased to sustain the curvature κ of the cornering manoeuvre. This behaviour is known as *understeer* behaviour. Conventional cars possess this behaviour for 'normal' stationary cornering conditions.

This behaviour is simulated by designing a suitable input-output relation or mapping function. In Fig. 5.4, a linear relation between the steering wheel angle δ_{SW} and the desired roll angle φ_d was assumed. The relation is given in a general form using a normalised scaling factor and a normalised squared velocity, as the final parameters need to be obtained by experimental investigations. The parameters used are given in the Appendix.

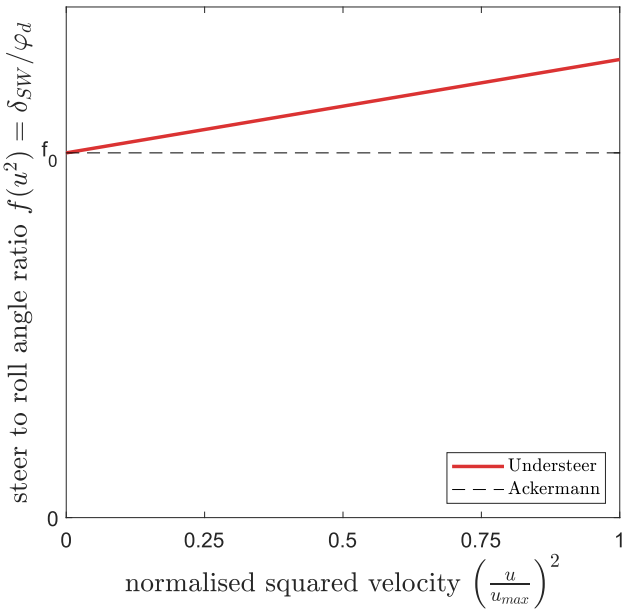

Figure 5.4: Designed input-output relation for steady-state cornering between the steering wheel angle δ_{SW} and the desired roll angle φ_d.

The relation in Fig. 5.4 uses the squared velocity u^2 as it is proportional to the lateral acceleration a_y and is defined independently of the curvature. A maximum velocity $u_{\max}$, in our case the maximum velocity of the observed speed range in Fig. 2.7, was used to normalise the relation. A steering angle of $\delta_{SW} \approx 50\,\text{deg}$ and a steering wheel rate of $\dot{\delta}_{SW} \approx 100\,\text{deg/s}$ should not be exceeded for 'normal' driving manoeuvres. The steering angle $\delta_{SW} \approx 50\,\text{deg}$ is used together with the results of the manoeuvre in Fig. 6.1e to

design the diagram in Fig. 5.4. The simulation shown in 6.5b was used to determine the parameter of the input relation given in the Appendix.

5.2.2 Feedback Design

The steering wheel angle has different dynamics than the fork's steering angle. A relative approach was therefore not pursued. Instead, an absolute formulation was designed which is able to give road feedback. The equivalent mechanical model of the absolute formulation is illustrated in Fig. 5.5. A virtual, torsional spring-damper combination was placed between the handlebar and the bicycle model's frame.

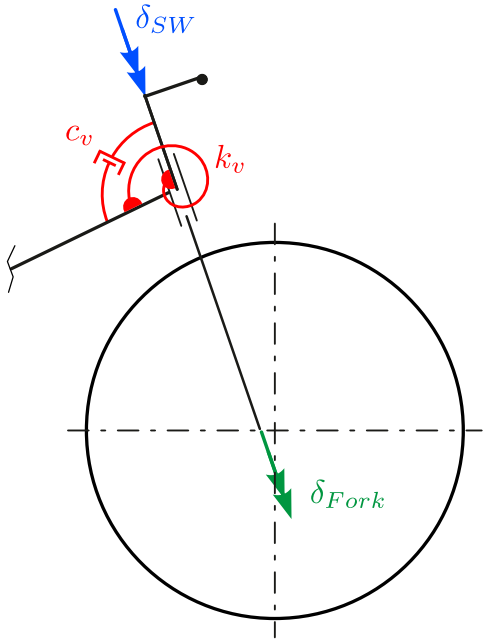

Figure 5.5: Equivalent mechanical model of the steer feedback system using an absolute approach.

The virtual, torsional stiffness coefficient is labelled by k_v and the virtual, torsional damping coefficient by c_v. The parameter k_v was determined using the relations between steering wheel torque and lateral accelerations of passenger cars in [24]. The steering wheel's angle is associated with the desired roll angle given by the input relation in Fig. 5.4. The virtual, torsional stiffness coefficient then can be computed by associating the steering wheel angle with the steering wheel torque at the respective lateral acceleration or roll angle. The feedback torque T_{FB} then is computed by:

$$T_{FB} = -k_v(u) \cdot \delta_{SW} - c_v \cdot \dot{\delta}_{SW}. \tag{5.7}$$

The virtual, torsional stiffness coefficient k_v depends on the velocity, as the mapping function in Fig. 5.4 between the steering wheel angle and the lateral acceleration is also velocity-dependent. The virtual, torsional damping coefficient c_v was then computed to receive critically damped behaviour of the equation of motion:

$$I_{\delta,SW}\ddot{\delta}_{SW} + c_v\,\dot{\delta}_{SW} + k_v\,\delta_{SW} = T_r. \tag{5.8}$$

The inertia term of the steering wheel $I_{\delta,SW}$ is a design parameter. The torque the car driver model needs to supply at the steering wheel to sustain the steering wheel angle, rate, and acceleration using the feedback torque law (5.7) can be computed with (5.8).

An idea to incorporate road feedback into the feedback torque should be mentioned at last. This can be achieved by using the state shift method for follow-up control, which is explained in Appendix A.4. A distinction between the torque needed to supply a given stationary state and the torque needed to stabilise the stationary state is possible. The torque necessary to stabilise the stationary state T_s can simply be added to the feedback torque formulation (5.7):

$$T_{FB} = -k_v(u)\cdot\delta_{SW} - c_v\cdot\dot{\delta}_{SW} + i_v\cdot T_s \tag{5.9}$$

An additional, virtual gear ratio i_v was introduced, which can be used to increase or decrease the stabiliser torques that are fed back.

One might think of more sophisticated approaches. The simple relation chosen in (5.7) does not capture all the features a steering system may provide to its operator. Finne and Ström [62] mentioned five steering feel attributes of regular cars which should be provided in a SbW system:

- On-centre
  Torque felt for driving straight ahead.
- Off-centre
  Torque which builds up when turning the steering wheel.
- Return control
  Predictable and stable return of the steering wheel to its neutral position after a turn.
- Damping feel
  Providing a calm feel.

- Friction feel
  Friction torque which takes a part of the stationary torque when cornering.

For a better steering feel, the just-named components of the steer torque can be added in later investigations.

6 Results

6.1 Simulation Preface

A short introduction to the simulation process is given before the respective results are shown and discussed. The maneuvers are carefully selected and are supposed to highlight the performance of the bicycle rider and car driver models and the interaction with the Steer-by-Wire system. The functionality of the proposed Steer-by-Wire system design is investigated and tested in the simulations.

Simulation Layout

In order to simulate the proposed layout of the rider model operating the Steer-by-Wire bicycle, illustrated in Fig. 1.1, a co-simulation was implemented. The rider model and the Steer-by-Wire system were designed in *Matlab*. The equations of motion of the benchmark bicycle model and the bicycle model with tire model are programmed into *Matlab*, where the low-fidelity model-based stabilizing controller with follow-up control and the model-based input and output relations of the Steer-by-Wire system are set up. The feedback and feedforward roll angles and the respective input quantity of the rider model in use are also computed in *Matlab*, where the respective relations mentioned in Chapter 3 are implemented.

The multi-body bicycle model is simulated using *SIMPACK 2024x*. The nonlinear equations of motion are solved using a variable time-step integration algorithm. The different trajectories are modeled using the 'Track' option in *SIMPACK 2024x*. *SIMPACK 2024x* provides functions to easily obtain the values of the curvature $\kappa(t+T_A)$ and the lateral deviation $y_\perp(t+T_A)$ at the preview point, see Fig. 3.2.

Matlab is the host of the co-simulation. *Matlab* requests and transmits quantities from and to *SIMPACK 2024x* at the defined sampling frequency $f_s = 150\,\text{Hz}$. The chosen value of the sampling frequency was discussed in Chapter 4. *SIMPACK 2024x* sends the value of the states $\boldsymbol{x}(t)$, the curvature $\kappa(t+T_A)$, and the lateral deviation $y_\perp(t+T_A)$ at the requested time stamps to *Matlab*. As the variable time-step integration algorithm will not reliably hit the sampling time steps, *SIMPACK 2024x* interpolates the values of the states at the transfer time stamps using adjacent integration points. *Matlab* then computes the rider model's desired roll angle using the curvature and the lateral deviation. The desired roll angle is transformed to the respective input quantity of the rider model, which is then applied at the input unit of the Steer-by-Wire system. The

input unit then computes the reference value y_d, by using the defined input relationships discussed in 5, for the stabilizing controller with follow-up control and the feedback torque for the rider. The stabilizing controller then computes the necessary steer torque T_δ to stabilize the actual state and move the system to the desired input variable y_d. This steer torque is then transmitted back to *SIMPACK 2024x* and applied at the fork of the multi-body bicycle model for the next sampling time step T_s. *SIMPACK 2024x* then starts over and solves the equations of motion. The whole procedure repeats periodically with the sampling frequency.

Parameter Selection

The chosen parameters of the bicycle are equal to those of Klinger [33], and the SbW system was parameterized using Valenzano's values [32]. The forces and torques, camber stiffness $c_{F,\gamma}$ and $c_{M,\gamma}$, respectively, of the front and rear wheel were halved in comparison to Klinger's values in order to lower the weave and capsize speed. The used parameter set is given in tabular form in the Appendix in Table A.1.

The pole locations for the pole placement method of the stabilization controller are the same as the ones in Fig. 4.2, as Valenzano optimized them to follow a desired course over the velocity. Both setups, 'First setup' being a rapid and 'Second setup' being a moderate set of pole locations, were used for a simulation. The pole location set used for a result is given in the respective results description. The gain vector $\boldsymbol{k}$ was computed using the bicycle model with tire model, as the pole placement was more accurate using the 6-state model for the model-based controller design, see Fig. 4.3b. The follow-up control using the pre-gain K_w was used for reference variable tracking. The pre-gain is given by (4.15) and the pole locations at the respective velocities. The state feedback gain vector $\boldsymbol{k}$ and the pre-gain K_w were evaluated at integer-valued velocities in the observed velocity range in Fig. 4.2a and gathered in a lookup table in *Matlab*.

Both models, the bicycle rider model and the car driver model, were implemented and tested. The layout of the rider model is given in Fig. 3.1. The feedforward roll angle φ_{ff} determined by the rider model considering the curvature $\kappa(t+T_A)$ in front of the bicycle, is the 4-state model, which corresponds to the line $K_{\varphi\kappa}$ in Fig. 3.3. The preview time T_A and the parameters of the rider feedback control model, which models the additional feedback roll angle φ_{fb} to compensate for a lateral deviation $y_\perp$, in (3.15), namely V_m, T_v, and T_n, were carefully selected by an iterative approach. Haudum's computed values [22] were used as a starting point for the process, as the bicycle rider model therein features different pole locations for the stabilization task and therefore cannot simply be adapted. The rider feedback control model parameters, as well as the anticipation time constant, are maneuver-dependent and given in the respective maneuvers section in the Appendix. The feedforward roll angle φ_{ff} and the feedback roll angle φ_{fb} are added to one another to form the desired roll angle $\varphi_d = \varphi_{ff} + \varphi_{fb}$. The bicycle rider model applies a steer torque T_r referring to the desired roll angle at the input unit. The

relation between the rider steer torque T_r and the desired roll angle was modeled using the bicycle model with tire model, where the relation is illustrated in Fig. 3.5. It was assumed that the car driver model uses a steering angle δ_{SW} proportional to a desired roll angle φ_d. The relation in Fig. 5.4 is used by the car driver model to perform the steer angle inputs, referring to the desired roll angles, at the input unit.

The steer torque or steering wheel angle of the bicycle rider model or the car driver model, respectively, are the input in the 'Input and Feedback Block', see Fig. 1.1 and 5.1. The input section of the 'Input and Feedback Block' maps the quantity applied by the respective rider model to a reference variable y_d for the stabilizing controller. The bicycle rider model's input torque is mapped using the relation between the applied rider steer torque T_r and the respective steady-state roll angle φ of the 6-state model, see Fig. 5.2. The car driver model's steering wheel input is mapped to the reference variable y_d for the stabilizing controller using the designed input-output relation simulating understeer behavior, illustrated in Fig. 5.4. The parameter $f(u^2)$ of Fig. 5.4 is given in the respective maneuvers section in the Appendix.
The feedback torque $T_{PD,HB}$ is computed for the bicycle rider model using the relative formulation (5.2). The non-minimum phase behavior of the handlebar is therefore preserved. The virtual torsional stiffness constant k_v and the virtual torsional damping constant c_v, illustrated in Fig. 5.3, are given in the maneuvers section in the Appendix. The car driver model feedback torque is computed using (5.8). The virtual torsional stiffness constant k_v and the virtual torsional damping constant c_v, illustrated in Fig. 5.5, are given in the maneuvers section in the Appendix.

Trajectory Design

The considered maneuvers contain simple trajectories assembled by straights, clothoids, and curves of constant radii. In order to stay in an approximately linear region of the nonlinear equations of motion of the multi-body bicycle model, the maximum roll angle during a maneuver should not exceed approximately 25 degrees. Presuming stationary conditions, this relates to a maximum lateral acceleration of $a_{y,max} \approx 4.3\,\mathrm{m/s}$; the maximum curvature of the trajectory to a given forward speed u was then computed by

$$\kappa_{max}(u) = \frac{a_{y,max}}{u^2}.$$

A roll angle of 25 degrees also corresponds to the angle at which the pedal, of the city bike in the vehicle dynamics laboratory, hits the ground when resting in the lowest position. The velocity at which the simulations were performed is given in the respective plots.

Three different maneuvers are considered. The first maneuver is a 'J-turn', which consists of a straight followed by a 180-degree curve to the right followed by another straight. The rider needs to initiate a single turn by applying a steer torque or performing a steering wheel motion, for the bicycle rider model or the car driver model respectively, and then track the trajectory with a constant radius, while the stabilizing controller moves to and stabilizes the consecutive roll angle demands of the rider. Stationary conditions should be present somewhere during the turn, as the maneuver possesses a region of constant curvature.

The second maneuver is a figure of eight. This trajectory consists of two connected loops and begins with a straight section. The transition into the curve is achieved using a clothoid. At the apex, the trajectory has a constant radius before another clothoid decreases the curvature again. The second loop mirrors the first and is connected by a straight section. The rider therefore needs to exit the first turn correctly, briefly has the chance to redirect on the straight, and then start the subsequent cornering maneuver. Two approximately stationary situations should be present during cornering. A similar maneuver is taught when pursuing a motorcycle license.

The third maneuver is a single lane change maneuver. This consists of a straight followed by a curve in a certain direction followed by another curve in the opposite direction to re-direct towards the initial heading. Due to the rapid change of direction, the maneuver will not reach stationary states and is therefore considered transient. This maneuver is present in everyday cycling operations when overtaking, switching lanes, or merging onto bike lanes.

6.2 Simulation Results

The parameter sets of the rider control model, as well as the trajectory design parameters, are given in Appendix A.3 in the respective maneuver section.

Qualitative Maneuver Comparison

The question asked in this section is whether the rider control model is able to follow different trajectories. A related aspect is how much the rider needs to adjust their control parameters to complete the maneuver successfully. These questions should be answered by the simulation results shown in Fig. 6.1, where comparisons of the traveled trajectories and the desired ones are shown. The adjustment of the rider control model parameters in order to master the maneuver is given in Appendix A.3 in the respective maneuvers section.

The desired track is shown in black, solid lines in the plots on the left side of Fig. 6.1. The actual trajectories of the respective points are shown in colors and dotted or dashed lines. On the right side, the curvature of the track and the lateral deviation of the

preview point perpendicular to the track is shown, whereas the curvature is plotted on the left ordinate and the lateral deviation of the preview point on the right ordinate. Note that these are the input values to the rider control model.

The lateral dynamic behavior is similar to that of the steering angle (2.45), which exhibits non-minimum phase characteristics, as shown in Fig. 2.8b. This counter-movement appears in all curve entry maneuvers in Fig. 6.1, where peaks in the path deviation $y_\perp$ appear in the opposite direction of the curvature.

At the curve exit, the rapid change in curvature leads the rider model to generate abrupt changes in roll angle demands and input quantities, as described by (3.20) and (3.21). The stabilization controller of the Steer-by-Wire bicycle model follows these demands with the dynamics defined by the chosen rapid set of poles for pole placement, or the 'First setup' given in Fig. 4.2. Due to the system's dynamics, it does not immediately reach the desired state defined by the rider model. As a result, the feedback rider control model generates additional roll angle corrections, leading to oscillations at the curve exit, which are visible in Fig. 6.1. These oscillations of the lateral displacement $y_\perp$ slowly decay over time. This sluggish response is caused by the limited tuning range of the feedback rider control parameters due to the non-minimum phase behavior [45], [46].

Furthermore, the path deviation of the preview point $y_\perp$, as illustrated in Fig. 3.2, generally deviates more from the desired trajectory than the front and rear wheel contact points of the bicycle model, as seen e.g. in Fig. 6.1e.

The 'J-turn' trajectory is a maneuver that provides a curve suitable for stationary cornering conditions. After the initial counter-movement, the preview point remains close to the track between seconds 3 and 5 in Fig. 6.1b. The rider corrects the trajectory after the initial lateral deviation $y_\perp$ to align with the trajectory. However, the rider control model reacts too rapidly, causing the rider to move to the outside [1] of the curve. The lateral deviation then approaches a quasi-stationary value. Fully stationary conditions are not reached as the stationary part of the curve of the trajectory ends beforehand. A rider control model better suited for handling non-minimum phase behavior is likely to reach stationary conditions. The rider model parameters, provided in Table A.3, serve as a reference for comparing the parameters of the rider control model of other maneuvers. The forward speed of the maneuver is $u = 7\text{m/s}$, whereas the bicycle model is in the autostable speed range. The stabilizing controller therefore is mainly utilized for tracking purposes and changing the system's dynamics. The high speed was chosen as this maneuver is usually performed by passenger cars on broad runways to test cornering abilities, vehicle dynamics, and chassis designs.

The results of the figure of eight maneuver are shown in plots 6.1c and 6.1d. Again, the non-minimum phase behavior of $y_\perp$ is present. A similar reaction as in the 'J-turn' is observable during the first cornering maneuver. The rider initially cuts the turn and

[1] In this context, 'outside' means the opposite side of the trajectory, on which the center of the circle of curvature of the previous curve lies. 'Inside' is therefore located at the side of the curve's center.

then corrects the trajectory to end up outside of the desired path. During the straight, the rider model is slowly correcting the trajectory to meet the desired track. For the second turn, a slight initial lateral deviation is present. The counter-movement of $y_\perp$ is therefore far less pronounced. The rider will ride along the outside of the curve. At the curve's exit, the rider cuts inside and then redirects towards the trajectory while riding the straight section, visible in Fig. 6.1c. The rider model parameters are given in A.4. The task-dependent anticipation time T_A is equal to the anticipation time of the 'J-turn' maneuver, as both maneuvers possess a similar trajectory design, whereas the sequence of straight-clothoid-curve is meant. The maneuver demands a more moderate reaction of the rider control model compared to the 'J-turn', as the static gain's magnitude $|V_m|$ is smaller, and the lead time constant T_v and the lag time constant T_n are higher. This hints that a moderate reaction of riders proves to be useful for this maneuver at the respective speed compared to the 'J-turn' maneuver. The constant forward speed of the maneuver is $u = 4\text{m/s}$, whereas the bicycle model is unstable if not stabilized by the stabilizing controller of the SbW system. The stabilizing controller therefore needs to be utilized for tracking and stabilizing purposes. The low speed was chosen as this maneuver is usually performed at moderate speeds, since it is a training maneuver for cornering of motorcycle riders.

The 'Single Lane Change' was chosen as a transient maneuver and is shown in 6.1e. It resembles an overtaking maneuver by a bicycle rider. Looking at the curvature course in 6.1f, one can see that the maneuver consists of three clothoids, where the curvature varies linearly. The counter-movement of $y_\perp$ at the curve's entry is again present. Large values of the perpendicular deviation of the preview point to the track are existent. These result from the transient nature of the maneuver, where the vehicle has a higher tendency to be positioned at a steep angle relative to the track. The front and rear wheel trajectories, however, are located closer to the trajectory, observable in Fig. 6.1e. The maneuver is almost solely traveled on the outside of the trajectory. The maneuver's exit is cut, and the compensation of the lateral deviation is therefore on the inside of the maneuver's track. The rider model parameters are given in Table A.5. A shorter anticipation time constant T_A is observed compared to the other maneuvers, meaning the rider model starts reacting closer to the trajectory features. The static gain's magnitude $|V_m|$ and the lag time constant T_n are the smallest of the maneuvers considered. The lead time constant T_v is the highest of the maneuvers. The rider therefore tries to react as fast as possible to lateral deviations, reasoned by the high lead time constant, while accepting higher settling times, reasoned by the low static gain magnitude and the high lag time constant. The constant forward speed of the maneuver is $u = 6\text{m/s}$, whereas the bicycle model is at the lower stability boundary, the weave speed, of the uncontrolled bicycle model. The stabilizing controller therefore needs to be utilized for tracking and stabilizing purposes. The speed was chosen as it resembles a cruising speed at a bicycle lane.

The bicycle rider model is suited to follow the maneuvers' trajectories. The influence of

the maneuvers on the rider control parameters is discussed, and an interpretation was given. It needs to be mentioned that the lateral bicycle control model is not capable of removing persisting control errors. This is because neither the system nor the controller provides global integral behavior. An additional I-term could be added to the controls, which would turn the feedback rider model (3.15) into a real PID controller. This would, however, contribute to the reaction of the controller to the initial undershoot and will favor oscillations. One could think of switching on the additional integral behavior if a certain threshold of lateral deviation is surpassed, which is commonly used in driver model applications for passenger vehicles.

Different Vehicle Dynamics with Same Rider Models

The stabilizing controller of the Steer-by-Wire system is able to alter the dynamics of the system by the press of a button. It now should be investigated how the reaction of a rider used to a certain vehicle dynamic could look like if the system suddenly switches its dynamic. As a consequence, the rider model is not used to the dynamics, and the tracking ability will suffer. This scenario represents a rider who is used to a specific bicycle and is sat on a different kind of bicycle expressing different dynamical responses.

The dynamics are altered by switching between the 'First setup' to the 'Second setup' in Fig. 4.2. The parameters of the feedback rider model are given in Table A.4. The feedback rider model parameter set was selected using the pole locations of the 'First setup' of Fig. 4.2, which will be called 'rapid' setup for the subsequent observations. The 'Second setup' in Fig. 4.2 will be called 'moderate' setup, as the stabilizing controller's follow-up tracking performance takes longer to reach the desired values.

As a track, the figure of eight maneuver was chosen. This maneuver shows how the rider model enters the curve, approaches stationary conditions, exits the curves, and deals with control errors during straight sections, where the rider model is able to realign with the desired trajectory. Furthermore, the rider model was able to perform the maneuver for both pole location sets using the same rider model parameters. As this task resembles a motorcycle rider training exercise for cornering, the maneuver was deemed suitable for a simulation investigating rider model reactions. The desired track is shown in black, solid lines in the plots on the left side of Fig. 6.2. The actual trajectories of the respective points are shown in colors and dotted or dashed lines. On the right side of Fig. 6.2, the desired roll angle φ_d and the actual roll angle φ_{act} are shown. The desired roll angle shows the rider model's reaction taking into account the trajectory and the actual vehicle's state. The rider model's reaction will be more severe if the vehicle is not behaving as predicted. The actual roll angle illustrates the follow-up tracking behavior of the different pole location sets used to model the state feedback vector control law.

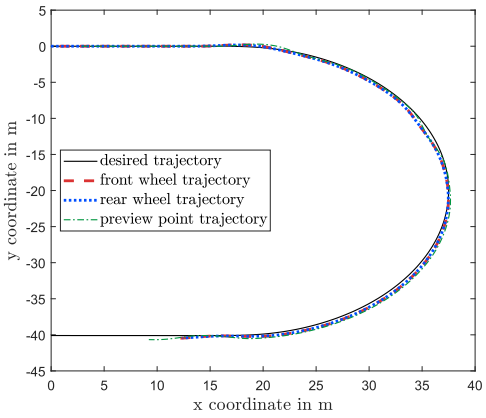

(a) 'J-turn' track.

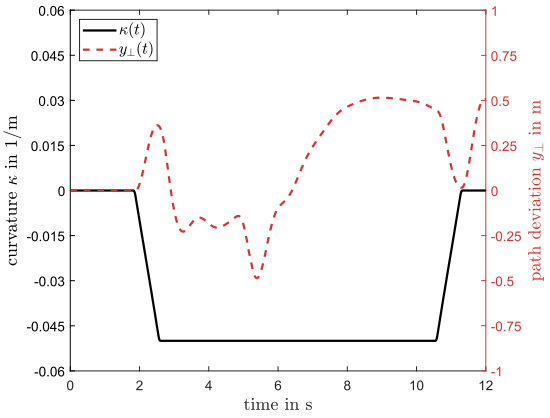

(b) 'J-turn' κ and $y_\perp$.

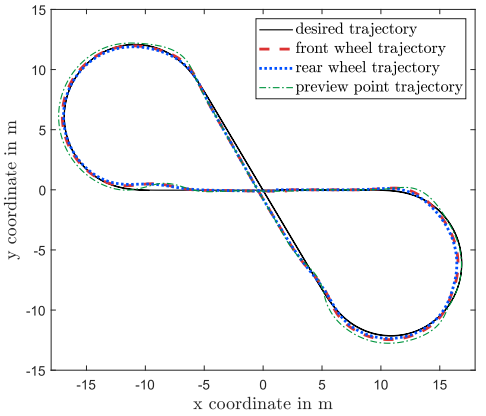

(c) 'Eight' track.

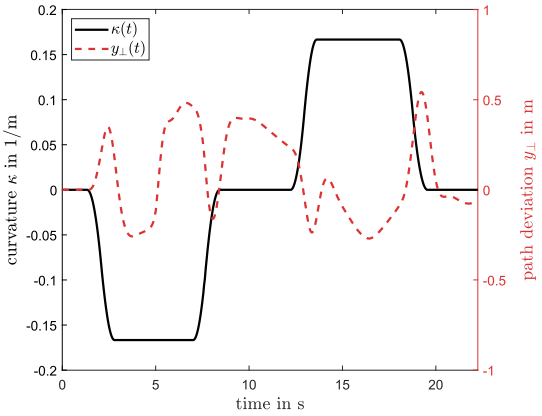

(d) 'Eight' κ and $y_\perp$.

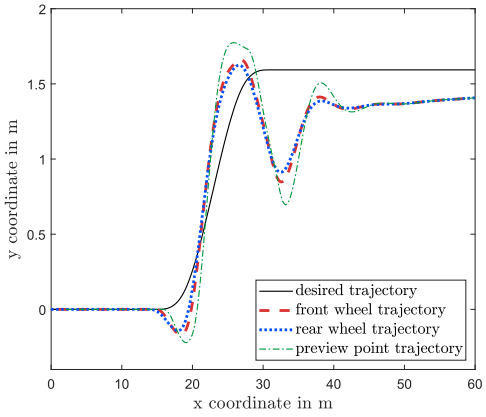

(e) 'Lane change' track.

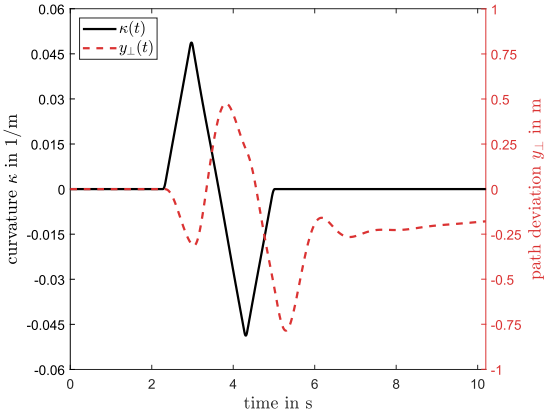

(f) 'Lane change' κ and $y_\perp$.

Figure 6.1: Trajectories of the different maneuvers on the left and on the right side the respective quantities the rider model uses to plan input actions.

The trajectory in Fig. 6.2a of the rider using the rapid pole location set for the pole placement of the stabilizing controller was already discussed in the previous result section. The roll angle course in Fig. 6.2b is added, compared to the results in Fig. 6.1. A very good tracking performance is achieved by the follow-up control of the stabilization controller. This statement is made, as the actual roll angle closely follows the roll angle demands. The stabilization controller does not tend to oscillate. This is an advantage for the rider controller, as the oscillations of the perpendicular deviation $y_\perp$ in Fig. 6.1d solely originate from the rider model's inputs. The trajectory course, as well as the roll angle courses of the rapid setting, will be used as a reference for comparison with the moderate pole location set.

The rider model used to the rapid pole location set of the stabilization controller is not able to operate the Steer-by-Wire using the moderate pole location set of the stabilization controller in an optimal manner. While the rider model can still roughly follow the trajectory, as shown in Fig. 6.2c, precise control is compromised. The first corner is cut noticeably, as the roll angle demand φ_d in Fig. 6.2d is higher than the one for the rapid pole location set of the stabilization controller. This is due to the reason that the moderate setup of the stabilization controller is tracking the desired roll angle commands worse than the rapid setup. The rider model demands higher feedback roll angles as a consequence, as the bicycle model is not in the state the rider model expects. Once caught up, the actual roll angle overshoots the desired roll angle, as the stabilization controller using the moderate setup is less damped than the rapid one, observable when comparing Fig. 6.2d with Fig. 6.2b. The rider model feedback level senses the overshoot and corrects the desired roll angle to realign with the trajectory. The moderate set of pole locations of the stabilization controller paired with the rider model used to the rapid dynamics will induce oscillations, as seen between second 3 and 10 and at the exit of the second cornering maneuver in Fig. 6.2d, as the rider model is unaware of the settling time of the moderate stabilization controller.

The relationships developed in this thesis enable the modeling of rider control models with varying levels of knowledge about the operated vehicles. The level of knowledge can be adjusted using the rider control model parameters V_m, T_n, T_v, and T_A. It is shown that a rider model used to two-wheeled vehicles is generally able to operate all kinds of two-wheeled vehicles, as the rider model is aware of the tilting dynamics. For the rider model to operate the vehicle in an optimal manner, knowledge about the specific vehicle needs to be considered by tuning the rider model control parameters. Furthermore, the ability of the Steer-by-Wire system to alternate the bicycle model dynamics is shown. The anticipation time T_A is particularly influenced by the chosen pole location for the state feedback control method, as the rise time of the stabilization controller determines when the rider model must initiate control actions to ensure accurate path tracking. In a real-world prototype, a rider's learning curve could be recorded, chronologically illustrating the human ability to adapt to different vehicle dynamics, obtained by switching the pole location set during a ride.

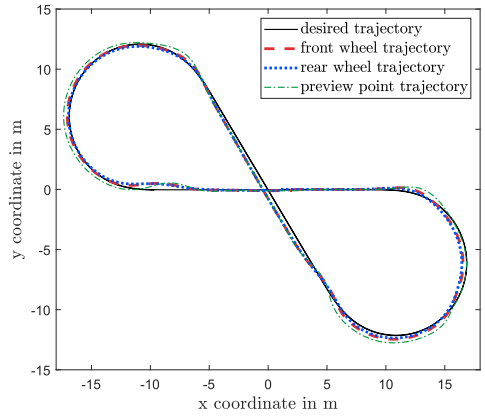

(a) Rapid stabilizer trajectory.

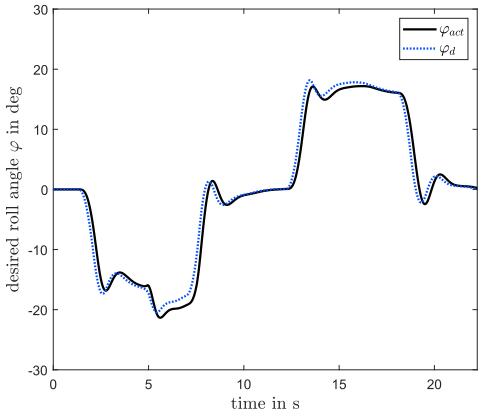

(b) Rapid stabilizer roll angles.

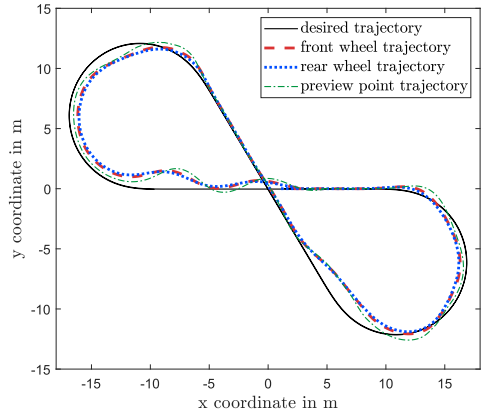

(c) Sluggish stabilizer trajectory

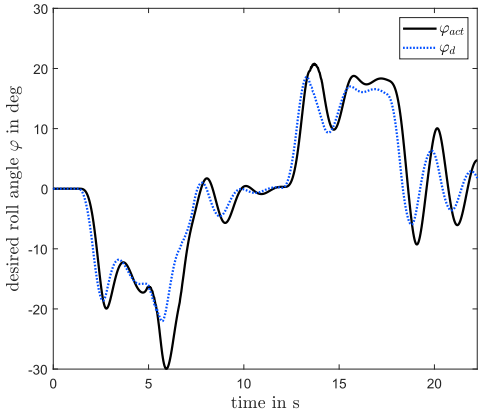

(d) Sluggish stabilizer roll angles.

Figure 6.2: Trajectories of the figure of eight maneuver using different stabilizing controller pole location sets and the same rider model parameters. The rapid settings are on the top side of the figure and the results using the moderate pole location set on the bottom. The parameters of the rider model were optimized for the rapid pole location set of the stabilizing controller.

Same Vehicle Dynamics with Different Rider Model Parameters

The possibility to model a novice and an expert rider by adjustment of the rider model parameters was already discussed. As the human internally adjusts its parameters over time to operate a vehicle in a desirable fashion, most humans are able to achieve good tracking performance once accustomed to a bicycle. In this section, the ability of the rider control model to model human preferences is investigated. Some might react quickly to path deviations, where others are more calm and patient towards deviations from their desired trajectory. The rider model control parameters are given in Table A.6 in the Appendix. The rapid set of pole locations in Fig. 4.2 is used.

As a track, the figure of eight maneuver was chosen. The reasoning on why this maneuver was used is equivalent to the reasoning of the previous result section.

A benchmark rider model set was selected, where the rider model parameter set used to obtain the results in Fig. 6.1c, 6.1d, 6.2a, and 6.2b is selected. Additionally, Fig. 6.3b is added to provide insights into the composition of the desired roll angle φ_d of the benchmark rider model. The sum of the feedforward roll angle φ_{ff} and the feedback roll angle φ_{fb} gives the desired roll angle φ_d. The different rider model parameter sets use these results for comparison. The curvature κ and the lateral deviation $y_\perp$, plotted in the left pane of Fig. 6.3, are the quantities used by the rider model to compute the rider model's desired roll angles φ_{ff} and φ_{fb}, respectively, shown in the right pane of Fig. 6.3.

All the parameter sets achieve a globally equivalent tracking performance. The maxima and minima of the lateral deviation $y_\perp$ are at similar time marks in the plots in the left pane of Fig. 6.3. The rider models therefore all possess knowledge of the system they operate. The difference in the tracking performance of the investigated rider model parameter sets lies in the details.

The course of the lateral deviation $y_\perp$ of the patient rider in Fig. 6.3c provides a smoother course than the reference in Fig. 6.3a. This can be seen when comparing the courses at second 6 and 10. The course of the path deviation of the patient rider model provides no bumps at these time marks. A smoother ride therefore is provided for the patient rider model. The maxima and minima of the path deviation possess a slightly bigger magnitude, as the rider model accepts a bigger lateral deviation before initiating further inputs to realign with the trajectory. This statement is supported by the smooth course of the feedback roll angle φ_{fb} in Fig. 6.3d.

The path deviation of the hectic rider's parameter set is prone to oscillations. The course of $y_\perp$ in Fig. 6.3e provides more peak-like structures than the course of the reference rider in Fig. 6.3a. Such peaks are evident at second 4 and 6 in Fig. 6.3e and Fig. 6.3f. The tendency of the rider model to perform oscillating input is observable in Fig. 6.3e and Fig. 6.3f at the end of the second turn at around $t \approx 18\,\mathrm{s}$. The hectic rider model provides a rough ride, as oscillations in the roll angle course also mean oscillations of the lateral acceleration (3.12). The rider provides better tracking capabilities, as the magnitudes of the maxima and minima of the path deviation in Fig. 6.3e are smaller.

The rider model proves to be suitable for showing basic characteristics of different riders by adjusting the control parameters. This was demonstrated by analyzing the rider model's response to lateral deviations from the trajectory of a selected desired trajectory. Three different reactions emerged, which could be directly attributed to the modifications in the rider model parameter sets.

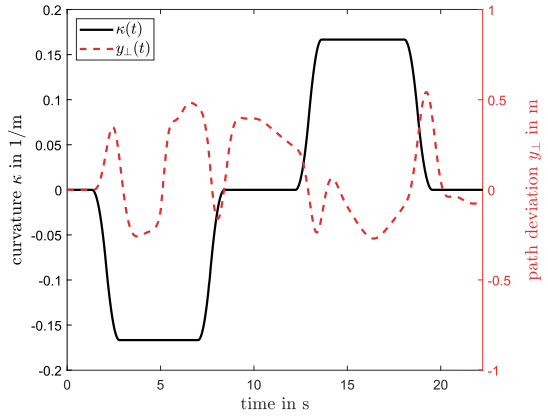

(a) κ and $y_\perp$ of 'normal' rider.

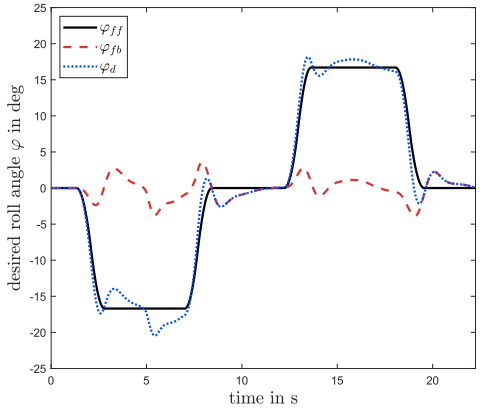

(b) Desired roll angles 'normal' rider.

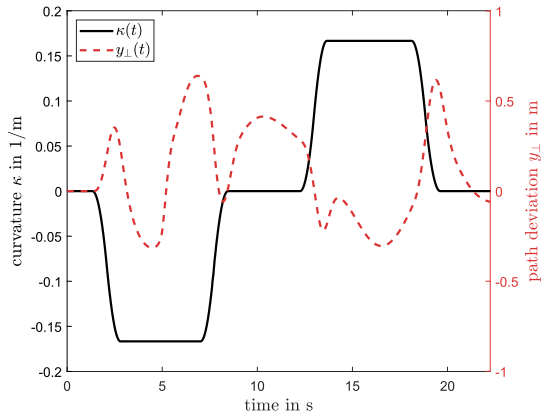

(c) κ and $y_\perp$ of 'patient' rider.

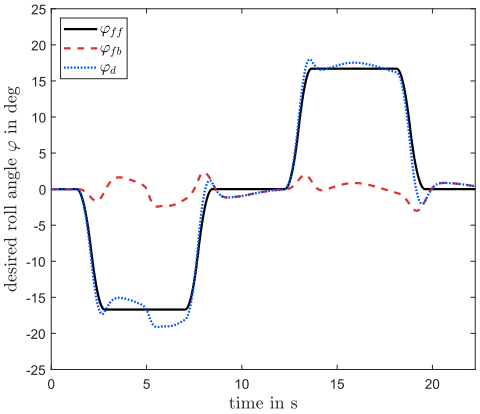

(d) Desired roll angles 'patient' rider.

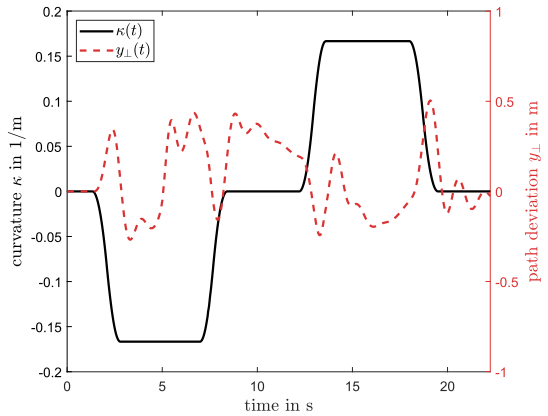

(e) κ and $y_\perp$ of 'hectic' rider.

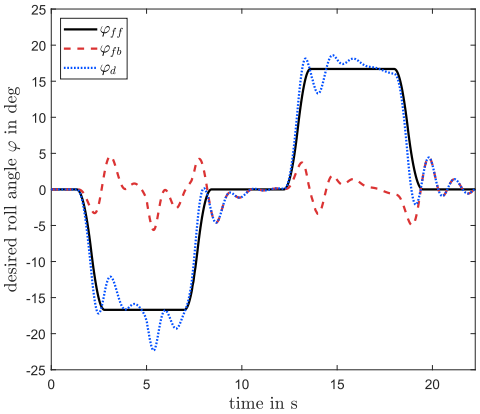

(f) Desired roll angles 'hectic' rider.

Figure 6.3: Trajectories of the rider model with different feedback parameters.

'Bicycle Rider' Input and Feedback

This section examines the capabilities of the input and feedback block for the bicycle rider model, as shown in Fig. 5.1 and Fig. 1.1. The input block receives a steering torque T_r as its input. The corresponding output reference variable y_d for the stabilization controller and the computed feedback torque T_{FB} are critically analyzed regarding their performance and the plausibility of the input and output quantities.

To obtain these results, the single lane change maneuver was used. This maneuver was chosen because the bicycle does not approach stationary states during the cornering process. The dynamic characteristics of the designed relations in Chapter 5 can therefore be evaluated through the inputs of the rider control model. A brief consideration of the static behavior of the input-output relationship is also included. The rider model control parameters are the same as those used in the single lane change maneuver in the section "Qualitative Maneuver Comparison" of this chapter and are listed in Table A.5. Therefore, the trajectory shown in Fig. 6.1e also represents the trajectory of the bicycle model in this section. The rapid pole locations in Fig. 4.2 are used.

The rider will initiate a turn by applying a steer torque T_r at the handlebar. The steer torque is computed using the handlebar steer angle δ_{HB} and its derivatives (5.3). The rider's steer torque is then mapped to the respective reference variable of the stabilizing controller y_d, using the function in Fig. 5.2. The reference variable y_d will then be tracked by the stabilizing controller. The steer angle of the fork δ follows the dynamic behavior forced by the stabilizing controller. By using the approach (5.2) 'Relative Formulation - Approach I', discussed in Chapter 5, the feedback torque is computed by the difference in steering angle and steering rate between the handlebar and the fork and applied at the handlebar. The virtual torsional stiffness constant k_v and the virtual torsional damping constant c_v are given in Table A.7 in the Appendix.

The input design uses the relation between steer torque and the referred stationary roll angle φ_d (5.1) of the 6-state bicycle model. A design criterion for the virtual torsional stiffness and damping constant of the feedback torque was to retain the non-minimum phase behavior of the handlebar steering angle. This behavior was achieved by using the parameters listed in Table A.7 as shown in Fig. 6.4a. The time courses of the handlebar steering angle δ_{HB} and the fork's steering angle δ_{Fork} are almost congruent. The difference between the two angles $\Delta\delta = \delta_{HB} - \delta_{\text{Fork}}$ is plotted using the scale at the right ordinate in Fig. 6.4a. There is at least an order of magnitude between the scales of the left and the right. This should emphasize the remarkable tracking performance of the used method. For stationary cornering conditions, an angle difference $\Delta\delta$ will remain, as the feedback torque T_{FB} using (5.3) needs to possess the same magnitude with a different sign as the steer torque T_r to receive a stationary handlebar and fork

steering angle.

The rider steer torque T_r is modeled by relation (5.1). The feedback torque achieves moving the handlebar in an equivalent way as the fork is moved by the steer torque computed by the stabilizing controller. The feedback torque therefore mimics the torque coming from the tire forces and moments, the gyroscopic forces and torques, and the external influences in a reasonable way. The input variable y_d is computed correctly, as the Steer-by-Wire system is able to follow the trajectory using the rider torque applied by the rider.

Summarized, it can be said that the presented input and feedback block design for the Steer-by-Wire model shows reasonable steer angle tracking which retains the non-minimum phase behavior and provides the rider with a suitable feedback torque.

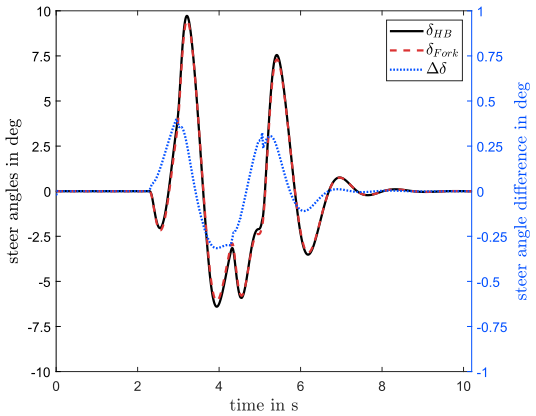

(a) Performance of the PD feedback tracking model.

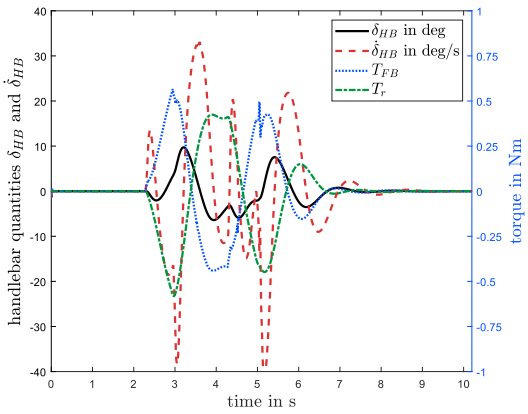

(b) Bicycle rider input and feedback quantities.

Figure 6.4: Courses of the rider's input quantities and the behavior of the system equipped with the PD tracking. The maneuver is the single lane change shown in Fig. 6.1e and 6.1f.

'Car Driver' Input and Feedback

The design of the input and feedback block using the car driver model's inputs is investigated at last. The car driver model's input unit features a steering wheel, as discussed in Chapter 3, where the driver controls the Steer-by-Wire bicycle model through the steering wheel angle δ_{SW}. This raises a well-justified question: is it possible to ride a bicycle without using steering inputs directly related to the movement of the bicycle model's front fork?

To evaluate the input and feedback design block for the car driver model, the single lane change maneuver was selected as the test trajectory. The reasoning why this maneuver was used is identical to that of the previous section. The rider control parameters are equivalent to those used for the bicycle rider control model and are given in Table A.5. The rapid pole locations in Fig. 4.2 and the 6-state model are used to determine the state feedback vector for the stabilizing controller. The trajectory of the bicycle model is shown in Fig. 6.1e.

The rider model is assumed to have exceptional knowledge of both the vehicle and the input and feedback block. It therefore understands how each steering wheel angle δ_{SW} refers to which stationary roll angle φ. The input function processes the rider's steering wheel input $\delta_{SW}(t)$ and converts it into a reference variable y_d for the stabilizing controller, following the relationship defined in Fig. 5.4. The value of $f(u^2 = (6\,\mathrm{m/s})^2)$ is provided in Table A.8. The stabilizing controller then applies the steer torque necessary to move the system to the respective desired state with the desired dynamic chosen by the desired pole locations.

The feedback torque at the steering wheel was modeled using an absolute ansatz in Chapter 5. Since the steering wheel angle is linked to the desired roll angle through the input function in Fig. 5.4, it is also related to the lateral acceleration (3.12). Given that the steering torque in passenger cars is proportional to lateral acceleration [24], the feedback torque of the Steer-by-Wire system can be designed to be proportional to the steering wheel angle (5.7). The proportionality is modeled by using a virtual torsional stiffness constant k_v. To ensure a damped response in the equation of motion for the steering wheel system (5.8), a virtual torsional damping constant c_v was used. The virtual torsional stiffness constant k_v and virtual torsional damping constant c_v were carefully selected by an iterative approach and are listed in Table A.8 in the Appendix.

Looking at the desired roll angle course φ_d in Fig. 6.5a and the steering wheel angle course δ_{SW} in Fig. 6.5b, the proportionality defined by the designed input-output function in Fig. 5.4 is recognizable. The steering wheel amplitudes appear reasonable, as the input-output factor $f(u^2 = (6\,\mathrm{m/s})^2$ was selected to ensure that the amplitudes are comparable to those experienced when driving a passenger car on country roads under normal conditions. The steering wheel rate $\dot{\delta}_{SW}$ is also in a reasonable range for human operators. If the amplitudes of the steering wheel angle and the steering wheel rate need to be adjusted, the parameter $f(u^2)$ can be modified to provide a different roll angle to steering wheel ratio. Comparing the fork steering angle in Fig. 6.4a and the steering wheel angle in Fig. 6.5b, it should be emphasized that the steering wheel angle does not provide the typical behavior a bicycle steering system supplies. This is evident as the steering wheel angle is related to the desired roll angle of the rider, where the stabilizing controller will apply the torque necessary to move the bicycle model in the predefined dynamic towards the desired state.

The steering wheel feedback torque in Fig. 6.5b has the opposite sign to the steering wheel angle. This results from relation (5.7) in Chapter 5, which uses a virtual torsional stiffness constant k_v to model the torque, which therefore provides restraining properties. This behavior is familiar from operating passenger cars and is one of the key properties a Steer-by-Wire system should provide to drivers, as highlighted by Finne and Ström [62]. To ensure a damped, non-oscillating restraining response, the virtual torsional damping coefficient c_v was added to (5.7). The amplitudes of the steer torque are reasonable considering the simulation results of stationary cornering maneuvers of passenger road cars by Pfeffer [24].

It was shown that it is possible for the designed Steer-by-Wire system to use input quantities not related to the actual steering of the bicycle model. This was achieved by choosing an input-output relation which maps the steering input by the rider, in this case the steering wheel angle δ_{SW}, to an appropriate bicycle model state, in this case the desired roll angle φ_d. The stabilizing controller of the Steer-by-Wire system then performs the necessary inputs to follow the desired roll angle course. The designed input relation is valid, as the steering wheel angles and steering wheel rate of the car driver model appear reasonable. The feedback torque is also reasonable as it fits the steer torque of stationary cornering maneuvers according to findings of Pfeffer [24]. The fine-tuning of the parameters k_v and c_v as well as the input-output relationship $f(u^2)$ needs to be done by investigations at a real-world prototype.

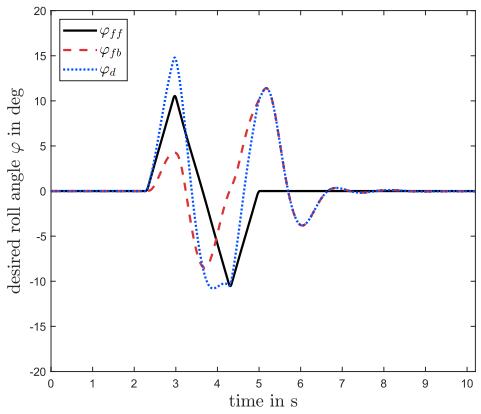

(a) Desired roll angles of the car driver model. The desired values are equal to the bicycle rider model.

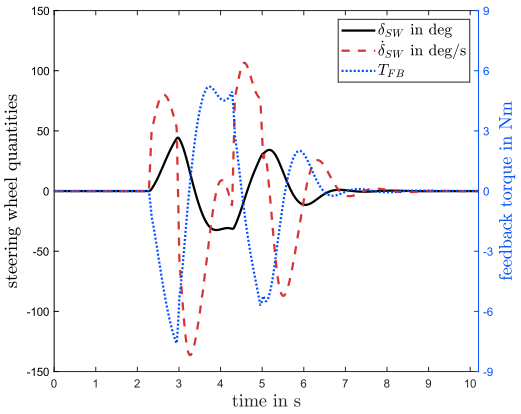

(b) Input values of the car driver model and course of the feedback action of the SbW system.

Figure 6.5: Courses of the car driver model input quantities and the behavior of the steer feedback system. The maneuver is the single lane change shown in Fig. 6.1e and 6.1f.

7 Conclusion

7.1 Conclusion

This thesis addressed the central research question of how a Steer-by-Wire (SbW) system for a bicycle can be designed and tested a-priori. To answer this question, the individual components of the SbW system were modelled, and a path-tracking rider model was developed to generate desired vehicle states. The work builds on an existing SbW bicycle model, which was extended with a stabilising controller and a follow-up algorithm to enable trajectory tracking. The results demonstrate the feasibility of the proposed design and provide insights into the system's behaviour under various conditions.

The design of the SbW system was enhanced with a stabilising controller that applies a steer torque to the fork, ensuring stability in straight-running conditions. A follow-up algorithm was integrated to enable the system to track reference variables, such as desired roll angles computed by the rider model. Two distinct rider models were developed: a bicycle rider model that applies a steer torque T_r and a car driver model that prescribes a steer angle course δ_{SW}. These models were designed to compute reference variables based on the trajectory's curvature and the lateral displacement at a preview point. Additionally, a feedback torque was introduced to provide proprioceptive feedback to the rider, enhancing the system's usability and realism.

The proposed system was tested through selected manoeuvres, confirming its ability to follow trajectories and validating the reasonableness of the designed input and feedback quantities. The bicycle models used in this work—ranging from a benchmark model with non-holonomic tyre constraints to a high-fidelity multi-body model with transient tyre dynamics—exhibited similar dynamic behaviour. This similarity was confirmed by the resemblance of eigenvalues across different velocities, supporting the use of model-based control approaches.

Unlike traditional rider models that actively stabilise the vehicle, the proposed rider model relies on the SbW system's stabilising controller. This approach simplifies the rider model's design while maintaining effective trajectory tracking. The feedforward control approach, revisited from Haudum [22], was extended with an additional perspective. The investigation revealed that various methods for modelling the relationship between trajectory curvature and stationary roll angle yielded practically equivalent results for the given bicycle model parameters. The feedback control, based on McRuer's model [13], effectively reduced lateral deviations but exhibited limitations, such as the persistence of stationary control errors due to the lack of integral behaviour in the system.

The controllability of the multi-body bicycle model via steer torque T_δ could not be definitively established. Additionally, discrepancies in pole placement accuracy were observed when applying state feedback vectors derived from low-fidelity models to the high-fidelity multi-body model. These challenges highlight the importance of model fidelity in control design and suggest areas for future research.

The findings of this thesis have several implications for the design and testing of SbW systems. The proposed system demonstrates the feasibility of using a stabilising controller and follow-up algorithm for trajectory tracking, providing a foundation for further development of SbW technologies. The rider models developed in this work offer a novel approach to path tracking, leveraging the SbW system's stabilising capabilities. Future research could explore the integration of neuromuscular dynamics to enhance the realism of the rider model. The challenges encountered in controllability analysis and pole placement underscore the need for advanced modelling techniques and control strategies to bridge the gap between low- and high-fidelity models.

7.2 Outlook

Some thoughts should be put into the choice of the motors. Hybrid stepper motors use permanent magnets, which generate a restraining torque even without applied electric current, as the rotor wants to minimise the magnetic reluctance. This restraining torque may provide small steer torques to be measured. The steer torques present in the simulations show that it is necessary to measure small values of steer torque, as even small input steer torques can lead to significant roll angle amplitudes.

The rider model introduced was able to follow trajectories in an acceptable way. The interaction of the rider accompanied by the designed input unit with the stabilising controller gives promising results. The rider model, nonetheless, has difficulties to follow trajectories, as the anticipation time T_A as well as the rider model control parameters are manoeuvre dependent. The implemented rider model is linear, which is why it is not particularly well suited for non-minimum phase systems. It is up to be investigated if a real rider on the Steer-by-Wire bicycle faces similar difficulties when riding along a trajectory. If the model occurs to possess a similar behaviour as the implemented rider model, it will be interesting to find how well the behaviours of the real rider matches the rider model. If a real rider is able to follow trajectories much more precisely and is able to remove the non-minimum phase dynamics of the system by using additional input variables, it will be interesting to conclude on what inputs a rider uses and how the rider applies them to get a reasonable tracking performance.

Appelman [27] uses a different formulation for the follow-up control of the stabilising controller. The torque applied by the rider directly gets transferred to the fork, which

allows the rider to initiate trajectories using the rider's desired dynamic. The stabilisation controller then stabilises the manoeuvres initiated by the rider. This provides a more accustomed riding experience, where the method proposed in this thesis brings the possibility to include the car driver model and remove disturbances on the fork from the handlebar. The reaction of the rider to the prescribed dynamics of the bicycle needs to be investigated on a real-world prototype, where the method proposed by Appelman [27] could be implemented as comparison.

The stabilising controller currently uses the state feedback gains computed at the 6-state model. This gives poles in the rough vicinity of the desired poles for the MBS bicycle model. The problem at hand is the use of dynamic states which are hard to measure or even observe, namely the roll angle φ and the lateral velocity of the rear wheel contact point $v_{|D}$. It is therefore desirable to design a control law which uses states that are easy to measure. For example, an output vector feedback, which can be done by matrix transformations [57].

List of Figures

List of Tables

Bibliography

[1] M. Hamer, "Brimstone and bicycles," *vol. 185*, pp. 48–49, 2005.

[2] D. Limebeer and R. Sharp, "Bicycles, motorcycles, and models," *IEEE Control Systems Magazine*, vol. 26, no. 5, pp. 34–61, 2006.

[3] Bundesministerium für Verkehr, Innovation und Technologie, *Der Radverkehr in Zahlen*, Last accessed on 12.11.2024, New York, 2010. [Online]. Available: https://www.bmk.gv.at/themen/mobilitaet/fuss_radverkehr/publikationen/riz.html.

[4] W. Rankine, "On the dynamical principles of the motion of velocipedes," *The Engineer*, pp. 2,79,129,153,175, 1869.

[5] F. Whipple, "The stability of the motion of a bicycle," *Q. J. Pure Appl. Math.*, vol. 30, pp. 312–348, 1899.

[6] M. Carvallo, "Théorie du movement du monocycle, part 2: Théorie de la bicyclette," *J. LÉcole Polytechnique*, vol. 6, pp. 1–118, 1901.

[7] D. Limebeer and R. Sharp, "Bicycles, motorcycles, and models," *IEEE Control Systems Magazine*, vol. 26, no. 5, pp. 34–61, 2006. DOI: 10.1109/MCS.2006.1700044.

[8] J. Meijaard, J. Papadopoulos, A. Ruina, and A. Schwab, "Linearized dynamics equations for the balance and steer of a bicycle: A benchmark and review," *Proceedings of The Royal Society A: Mathematical, Physical and Engineering Sciences*, vol. 463, pp. 1955–1982, Jun. 2007. DOI: 10.1098/rspa.2007.1857.

[9] H. Pacejka, *Tyre and Vehicle Dynamics* (Automotive engineering). Elsevier Science & Technology, 2006, ISBN: 9780750669184.

[10] V. Cossalter, *Motorcycle Dynamics*. Vittore Cossalter, 2006, ISBN: 9781430308614.

[11] R. Lot and J. Sadauckas, *Motorcycle Design: Vehicle Dynamics Concepts and Applications*. Roberto Lot, 2021, ISBN: 9791220098533.

[12] J. Kooijman and A. Schwab, "A review on bicycle and motorcycle rider control with a perspective on handling qualities," *Vehicle System Dynamics*, vol. 51, Nov. 2013. DOI: 10.1080/00423114.2013.824990.

[13] D. McRuer and D. Graham, "Pilot-vehicle control system analysis," AIAA GUIDANCE and CONTROL CONFERENCE, CAMBRIDGE, MASSACHUSETTS, 1963.

[14] D. McRuer and D. Graham, "Human pilot dynamics in compensatory systems," *AIR FORCE FLIGHT DYNAMICS LABORATORY RESEARCH AND TECHNOLOGY DIVISION, Technical Report*, vol. AFFDL-TR-65-15, 1965.

[15] M. Mitschke and H. Wallentowitz, *Dynamik der Kraftfahrzeuge* (VDI-Buch). Springer Fachmedien Wiesbaden, 2014, ISBN: 9783658050689.

[16] R. Sharp, "Optimal stabilization and path-following controls for a bicycle," *Proceedings of The Institution of Mechanical Engineers Part C-journal of Mechanical Engineering Science - PROC INST MECH ENG C-J MECH E*, vol. 221, pp. 415–427, Apr. 2007. DOI: 10.1243/0954406JMES529.

[17] R. Sharp, "On the Stability and Control of the Bicycle," *Applied Mechanics Reviews*, vol. 61, Nov. 2008. DOI: 10.1115/1.2983014.

[18] A. L. Schwab, J. Kooijman, and J. P. Meijaard, "Some recent developments in bicycle dynamics and control," 2008.

[19] C. Findlay, J. K. Moore, and C. Perez-Maldonado, "Siso control of a bicycle-rider system," 2006.

[20] R. Hess, J. Moore, and M. Hubbard, "Modeling the Manually Controlled Bicycle," *IEEE Transactions on Systems, Man, and Cybernetics - TSMC*, vol. 42, May 2012.

[21] J. Edelmann, M. Haudum, and M. Plöchl, "Bicycle Rider Control Modelling for Path Tracking," *IFAC-PapersOnLine*, vol. 48, no. 1, pp. 55–60, 2015, 8th Vienna International Conferenceon Mathematical Modelling, ISSN: 2405-8963. DOI: https://doi.org/10.1016/j.ifacol.2015.05.070. [Online]. Available: https://www.sciencedirect.com/science/article/pii/S2405896315000713.

[22] M. Haudum, "Entwurf und Simulation eines Fahrermodells," M.S. thesis, TU Wien, Vienna, 2012.

[23] D. Gabriel, D. Baumgärtner, and D. Görges, "On the Development of a Path Tracking Controller by combining Optimal Preview Control and Pursuit Control Methods," *The Evolving Scholar*, Jan. 2023. DOI: 10.24404/63FC7FE222B9278B7D0866F9.

[24] P. Pfeffer and M. Harrer, *Lenkungshandbuch: Lenksysteme, Lenkgefühl, Fahrdynamik von Kraftfahrzeugen* (ATZ/MTZ-Fachbuch). Springer Fachmedien Wiesbaden, 2013, ISBN: 9783658009779.

[25] M. Bartolozzi, A. Niccolai, C. Lucci, and G. Savino, "Motorcycle emergency steering assistance: A systematic approach from system definition to benefit estimation and exploratory field testing," *Accident Analysis & Prevention*, vol. 188, p. 107 116, 2023, ISSN: 0001-4575. DOI: https://doi.org/10.1016/j.aap.2023.107116. [Online]. Available: https://www.sciencedirect.com/science/article/pii/S000145752300163X.

[26] Y. Marumo and M. Nagai, "Steering control of motorcycles using steer-by-wire system," *Vehicle System Dynamics*, vol. 45, pp. 445–458, May 2007.

[27] N. Appelman, "Dynamics and Control of a Steer-by-Wire Bicycle," M.S. thesis, Delft University of Technology, Delft, 2012.

[28] G. Dialynas, R. Happee, and A. Schwab, "Design and implementation of a steer-by-wire bicycle," International Cycling Safety Conference, vol. 11, 2018.

[29] Österreichischer Automobil-, Motorrad- und Touring Club (ÖAMTC), *Zahl der Fahrradunfälle in vergangenen zehn Jahren stark angestiegen*, https://www.oeamtc.at/presse/zahl-der-fahrradunfaelle-in-vergangenen-zehn-jahren-stark-angestiegen-61039866, Last accessed on 28.12.2024, 2023.

[30] K. Åström, R. Klein, and A. Lennartsson, "Bicycle dynamics and control: Adapted bicycles for education and research," *Control Systems, IEEE*, vol. 25, pp. 26 –47, Sep. 2005. DOI: 10.1109/MCS.2005.1499389.

[31] C. L. Ott, "Untersuchung des Wobble-Modes bei Fahrrädern– Theorie und Fahrversuch," M.S. thesis, TU Wien, Vienna, 2011.

[32] L. Valenzano, "MODELLING AND ENHANCED STABILITY OF A STEER BY WIRE BICYCLE," M.S. thesis, Politecnico di Torino, Torino, 2024.

[33] F. Klinger, "Theoretische Untersuchungen zum High-Speed-Wobble-Phänomen bei Rennrädern," M.S. thesis, TU Wien, Vienna, 2013.

[34] W. Müller, "Modellbildung und querdynamische Untersuchung eines Fahrrades," M.S. thesis, TU Wien, Vienna, 2011.

[35] B. Angrosch, "Fahrradstabilität unter besonderer Berücksichtigung des Lenkungsflatterns," M.S. thesis, TU Wien, Vienna, 2010.

[36] A. E. Dressel, "Measuring and Modeling the Mechanical Properties of Bicycle Tires," Ph.D. dissertation, University of Wisconsin-Milwaukee, 2013.

[37] A. van Lunteren and H. Stassen, "On the influence of drugs on the behavior of a bicycle," ser. Sixth Annual Conference on Manual Control, Air Force Institute of Technology, 1970.

[38] J. Moore, "Human control of a bicycle," Ph.D. dissertation, University of California DAVIS, Aug. 2012. DOI: 10.6084/m9.figshare.4244963.

[39] M. Plöchl and J. Edelmann, "Driver models in automobile dynamics application," *Vehicle System Dynamics*, vol. 45, no. 7-8, pp. 699–741, 2007.

[40] J. S. Brunner, Y.-C. Ni, A. Kouvelas, and M. A. Makridis, "Microscopic simulation of bicycle traffic flow incorporating cyclists' heterogeneous dynamics and non-lane-based movement strategies," *Simulation Modelling Practice and Theory*, vol. 135, p. 102 986, 2024, ISSN: 1569-190X. DOI: https://doi.org/10.1016/j.simpat.2024.102986.

[41] C. Schmidt, A. Dabiri, F. Schulte, R. Happee, and J. Moore, *Essential Bicycle Dynamics for Microscopic Traffic Simulation: An Example Using the Social Force Model*, Feb. 2024. DOI: 10.59490/65a5124da90ad4aecf0ab147.

[42] A. Schwab, P. Lange, R. Happee, and J. Moore, "Rider control identification in bicycling using lateral force perturbation tests," *Proceedings of the organization of Mechanical Engineers, Part K: Journal of Multi-body Dynamics*, vol. 227, pp. 390–406, Dec. 2013. DOI: 10.1177/1464419313492317.

[43] J. Kooijman, A. Schwab, and J. Moore, "Some observations on human control of a bicycle," vol. 4, Jan. 2009.

[44] A. Aoki, "Experimental study on motorcycle steering performance," *SAE Transactions*, vol. 88, pp. 946–961, 1979.

[45] J. Lunze, *Regelungstechnik 1* (Springer-Lehrbuch). Springer Berlin, 2020, ISBN: 978-3-662-60745-9.

[46] J. Edelmann and M. Plöchl, "Electronic stability control of a narrow tilting vehicle," *SAE International Journal of Materials and Manufacturing*, vol. 4, pp. 1006–1013, Jun. 2011. DOI: 10.4271/2011-01-0976.

[47] H. Gattringer, A. Reiter, A. Müller, D. Wagner, and T. Mauernböck, "Dynamical Modeling and LQR Control of a Gyroscopically Stabilized Bicycle," *PAMM*, vol. 18, no. 1, 2018. DOI: https://doi.org/10.1002/pamm.201800406.

[48] E. Hanavan, *A Mathematical Model of the Human Body* (A Mathematical Model of the Human Body Bd. 32,Nr. 3). Aerospace Medical Research Laboratories, Aerospace Medical Division, Air Force Systems Command, 1964.

[49] M. Drmota, *Mathematik 2 für MB, WI-MB und VT*, LVA-Nr. 104.299, TU Wien, Institute of Discrete Mathematics and Geometry, 2020.

[50] D. Schröder and R. Kennel, *Elektrische Antriebe - Grundlagen: Mit durchgerechneten Übungs- und Prüfungsaufgaben* (Springer-Lehrbuch). Springer Berlin Heidelberg, 2021, ISBN: 9783642304712.

[51] K. Magnus and H. H. Müller-Slany, *Grundlagen der Technischen Mechanik* (Springer-Link Bücher), ger, 7. Wiesbaden: Vieweg+Teubner Verlag, 2005.

[52] J. Edelmann, *Skritpum zur Vorlesung Maschinendynamik*, LVA-Nr. 303.082, TU Wien, Institute of Mechanics and Mechatronics, 2023.

[53] H. Troger and A. Steindl, *Nonlinear Stability and Bifurcation Theory: An Introduction for Engineers and Applied Scientists*. Springer Vienna, 1991, ISBN: 9780387822921.

[54] W. Kortüm and P. Lugner, *Systemdynamik und Regelung von Fahrzeugen : Einführung und Beispiele*, ger. Berlin [u.a.]: Springer, 1994, ISBN: 3540572759.

[55] P. Ingenlath, "Mehrkörpersimulationsgestützte Fahrradentwicklung," Ph.D. dissertation, RWTH Aachen, 2019.

[56] J. B. Hoagg and D. S. Bernstein, "Nonminimum-phase zeros - much to do about nothing - classical control - revisited part ii," *IEEE Control Systems Magazine*, vol. 27, no. 3, pp. 45–57, 2007. DOI: 10.1109/MCS.2007.365003.

[57] S. Jakubek, *Grundlagen der Regelungstechnik*, LVA-Nr. 325.038, TU Wien, Institute of Mechanics and Mechatronics, 2021.

[58] A. Horn, "Fahrer-Fahrzeug-Kurvenfahrt auf trockener Straße," Ph.D. dissertation, TU Braunschweig, 1985.

[59] J. Lunze, *Regelungstechnik 2 : Mehrgrößensysteme, Digitale Regelung*, ger, 10th ed. 2020. Berlin Heidelberg: Springer Berlin Heidelberg Imprint: Springer Vieweg, 2020, ISBN: 3662607603.

[60] M. Kaltenbacher and H. Ecker, *Skriptum zur Vorlesung Mess- und Schwingungstechnik*, LVA-Nr. 303.009, TU Wien, Institute of Mechanics and Mechatronics, 2021.

[61] A. Balachandran and J. C. Gerdes, "Designing steering feel for steer-by-wire vehicles using objective measures," *IEEE/ASME Transactions on Mechatronics*, vol. 20, no. 1, pp. 373–383, 2015. DOI: 10.1109/TMECH.2014.2324593.

[62] A. Finne and L. Ström, "Road Feedback in a Steer-by-Wire System for a Passenger Car – enhancing the feeling of being connected," M.S. thesis, Linköping University, Göteborg, 2022.

[63] M. Horn, *Regelungstechnik*, TU Graz, Institute of Automation and Control, 2018.

Appendix

A.1 Geometric and Inertial Parameters of the Bicycle, the Rider and the Steer-by-Wire System

Geometric and inertial parameters of the observed bicycle model. The parameters originate from previous thesis and were gathered from [22], [31], [32], [33].

Parameter	Symbol	Value	Unit
Wheelbase	l	1.095	m
Castor angle	ϵ	19	°
Geometric trail	t_c	0.0692	m
Front wheel			
Radius	r_f	0.3355	m
Mass	m_f	1.95	kg
Inertia tensor	$\begin{bmatrix} I_{fxx\|f} & 0 & 0 \\ 0 & I_{fyy\|f} & 0 \\ 0 & 0 & I_{fzz\|f} \end{bmatrix}$	$\begin{bmatrix} 0.063 & 0 & 0 \\ 0 & 0.127 & 0 \\ 0 & 0 & 0.063 \end{bmatrix}$	kgm^2
Rear wheel			
Radius	r_r	0.3355	m
Mass	m_r	2.35	kg
Inertia tensor	$\begin{bmatrix} I_{rxx\|r} & 0 & 0 \\ 0 & I_{ryy\|r} & 0 \\ 0 & 0 & I_{rzz\|r} \end{bmatrix}$	$\begin{bmatrix} 0.065 & 0 & 0 \\ 0 & 0.130 & 0 \\ 0 & 0 & 0.065 \end{bmatrix}$	kgm^2
Front assembly			
Mass	m_H	4.423	kg
Center of mass x	a_H	0.6522	m
Center of mass z	h_H	−0.6331	m
COM offset	e_H	0.0259	m
Inertia tensor	$\begin{bmatrix} I_{Hxx\|H} & 0 & I_{Hxx\|H} \\ 0 & I_{Hyy\|H} & 0 \\ I_{Hzz\|H} & 0 & I_{Hzz\|H} \end{bmatrix}$	$\begin{bmatrix} 0.633 & 0 & -0.023 \\ 0 & - & 0 \\ -0.023 & 0 & 0.130 \end{bmatrix}$	kgm^2
Main frame			
Mass	m_m	9.9759	kg
Center of mass x	x_m	0.2397	m
Center of mass z	h_m	−0.6006	m
Inertia tensor	$\begin{bmatrix} I_{mxx\|m} & 0 & I_{mxz\|m} \\ 0 & I_{myy\|m} & 0 \\ I_{mxz\|m} & 0 & I_{mzz\|m} \end{bmatrix}$	$\begin{bmatrix} 0.69 & 0 & -0.0004 \\ 0 & 1.37 & 0 \\ -0.0004 & 0 & 0.76 \end{bmatrix}$	kgm^2

Parameter	Symbol	Value	Unit
Rider			
Mass	m_R	73.44	kg
Center of mass x	x_R	0.4304	m
Center of mass z	h_R	-1.099	m
Inertia tensor	$\begin{bmatrix} I_{Sxx\|S} & 0 & I_{Sxz\|S} \\ 0 & I_{Syy\|S} & 0 \\ I_{Sxz\|S} & 0 & I_{Szz\|S} \end{bmatrix}$	$\begin{bmatrix} 9.0721 & 0 & 0.5336 \\ 0 & - & 0 \\ 0.5336 & 0 & 1.7972 \end{bmatrix}$	kgm^2
SbW assembly			
Mass	m_S	6.30	kg
Center of mass x	x_S	0.9821	m
Center of mass z	h_S	-0.9865	m
Inertia tensor	$\begin{bmatrix} I_{Sxx\|S} & 0 & I_{Sxz\|S} \\ 0 & I_{Syy\|S} & 0 \\ I_{Sxz\|S} & 0 & I_{Szz\|S} \end{bmatrix}$	$\begin{bmatrix} 0.0250 & 0 & -0.009 \\ 0 & 0.048 & 0 \\ -0.009 & 0 & 0.0271 \end{bmatrix}$	kgm^2

Table A.1: Geometric and Inertial Parameters of the Bicycle Models.

A.2 Tire Parameters

The stiffness constants for side force and moment and the crown radius are given in table A.2.

Parameter	Symbol	Value	Unit
Front wheel			
Side slip stiffness for side force	$c_{f,\alpha}$	12.61	N/rad
Camber stiffness for side force	$c_{f,\gamma}$	0.43	N/rad
Side slip stiffness for moment	$c_{m,\alpha}$	0.344	Nm/rad
Camber stiffness for moment	$c_{m,\gamma}$	0.019	Nm/rad
Crown radius	r_c	0.018	m
Rear wheel			
Side slip stiffness for side force	$c_{f,\alpha}$	10.31	N/rad
Camber stiffness for side force	$c_{f,\gamma}$	0.401	N/rad
Side slip stiffness for moment	$c_{m,\alpha}$	0.258	Nm/rad
Camber stiffness for moment	$c_{m,\gamma}$	0.013	Nm/rad
Crown radius	r_c	0.018	m

Table A.2: Tire parameters.

A.3 Parameters used in Simulations

The chosen parameters for the respective maneuvers in the result section are listed.

Qualitative Maneuver Comparison

Parameter of 'J-turn' Maneuver

A sketch of the 'Jturn' track design is shown in figure A.1. The parameters of the maneuver and the rider are given in table A.3.

Table A.3: 'J-turn' maneuver settings.

Quantity	Value	Phys. Unit	Note
T_A	0.3	s	
V_m	-0.045	1/m	
T_v	2.9	s	
T_n	0.43	s	
l	15	m	
ρ	20	m	
l_{Circ}	57.84	m	
$l_{Clothoide}$	5	m	
u	7	m/s	

Parameter of 'Eight' or 'Infinity' Maneuver

A sketch of the track design is shown in figure A.2. The parameters of the maneuver and the rider are given in table A.4.

Parameter of 'Single Lane Change' Maneuver

A sketch of the 'Single Lane Change' track design is shown in figure A.3. The parameters of the maneuver and the rider are given in table A.5.

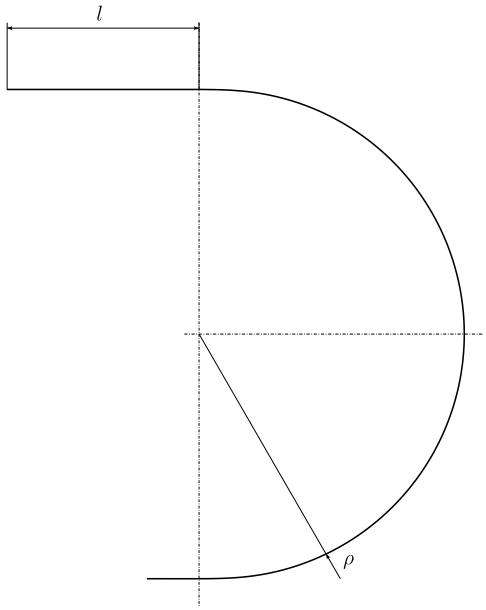

Figure A.1: Maneuver design parameters of the 'J-turn' maneuver. The clothoid length $l_{Clothoide}$ is the arc length of the clothoide, the linking element between the straight and curved elements. The clothoids radius varies linearly between 0 and the constant curve radius ρ. The length l_{Circ} is the arc of the curve.

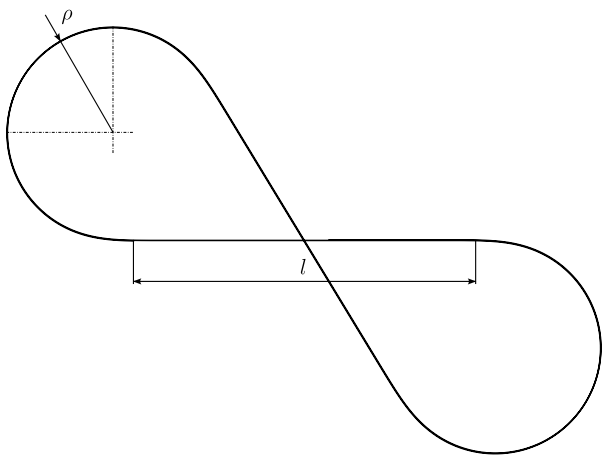

Figure A.2: Maneuver design parameters of the 'Eight' or 'Infinity' maneuver. The clothoid length $l_{Clothoide}$ is the arc length of the clothoide, the linking element between the straight and curved elements. The clothoids radius varies linearly between 0 and the constant curve radius ρ. The length l_{Circ} is the arc of the curve.

Table A.4: 'Infinity' maneuver settings.

Quantity	Value	Phys. Unit	Note
T_A	0.3	s	
V_m	-0.025	1/m	
T_v	4.3	s	
T_n	0.53	s	
l	18.75	m	
ρ	6	m	
l_{Circ}	22	m	
$l_{Clothoide}$	3	m	
u	4	m/s	

Table A.5: 'Single Lane Change' maneuver settings.

Quantity	Value	Phys. Unit	Note
T_A	0.2	s	
V_m	-0.022	1/m	
T_v	10	s	
T_n	0.6	s	
l	15	m	
ρ	20	m	
$l_{Clothoide}$	4	m	
u	6	m/s	

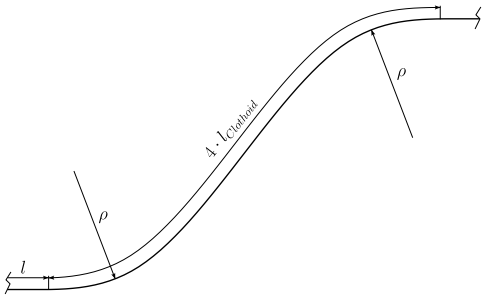

Figure A.3: Maneuver design parameters of the 'Single Lane Change' maneuver. The clothoid length $l_{Clothoide}$ is the arc length of the clothoid. The clothoids radius varies linearly between 0 and the maximum radius ρ. The maximum radius is reached after $l_{Clothoid}$. Afterwards the length of $2 \cdot l_{Clothoid}$ is necessary to reach the maximum radius in the opposite direction.

Same Vehicle Dynamics with different Rider Model Parameters

The parameters of the rider models are given in table A.6.

Table A.6: Rider model parameters to mimic different types of riders.

Rider	Quantity	Value	Unit
'Normal'	T_A	0.3	s
	V_m	-0.025	1/m
	T_v	4.3	s
	T_n	0.53	s
'Patient'	V_m	-0.2	1/m
	T_v	4.0	s
	T_n	0.6	s
	T_A	0.3	s
'Hectic'	V_m	-0.32	1/m
	T_v	4.0	s
	T_n	0.4	s
	T_A	0.3	s

'Bicycle Rider' Input and Feedback

The chosen parameters of the bicycle rider input and output relation are listed in table A.7. The parameters of the maneuver and the rider are given in table A.5.

Table A.7: Values of the virtual torsional stiffness constant k_v and the virtual torsional damping constant c_v of the input and feedback block suitable for the bicycle rider model.

Quantity	Value	Unit	Notes
k_v	80	Nm/rad	Virtual stiffness constant
c_v	1	Nm s/rad	Virtual damping constant

'Car Driver Input' and Feedback

The chosen parameters of the car driver models input and output relation are listed in table A.8. The parameters of the maneuver and the rider are given in table A.5.

Table A.8: Values of the steering wheel - roll angle ratio $f(u^2)$, virtual torsional stiffness constant k_v and the virtual torsional damping constant c_v of the input and feedback block suitable for the car driver model.

Quantity	Value	Unit	Notes
$f(u = 6\,\mathrm{m/s})$	3	1	δ_{SW}/φ_d ratio
k_v	25.8	Nm/rad	Virtual stiffness constant
c_v	3.4	Nm s/rad	Virtual damping constant

A.4 State Shift Follow Up Control

Another approach for the follow up control of the stabilizing controller is to modify the state vector for the state feedback by subtracting the desired state $\boldsymbol{x}_d$ from the actual state $\boldsymbol{x}$ [63]

$$\boldsymbol{\xi}(t) = \boldsymbol{x}(t) - \boldsymbol{x}_d(t) \tag{A.1}$$

The tracking error ξ is therefore the deviation of the desired to the actual states. Rearranging (A.1) with (4.5) and inserting in (4.4), one gets

$$\frac{\mathrm{d}(\boldsymbol{\xi} + \boldsymbol{x}_d)}{\mathrm{d}t} = \frac{\mathrm{d}\boldsymbol{\xi}}{\mathrm{d}t} = (\boldsymbol{A} - \boldsymbol{b}\boldsymbol{k}^{\mathrm{T}})\boldsymbol{\xi} + \boldsymbol{A}\boldsymbol{x}_d \tag{A.2}$$

which gives the same dynamics as the original controlled system (4.4) with additional shift of the arbitrary desired state vector (A.2). The desired state vector now appears in (A.2) as a particular solution of the system. Assuming the asymptotically stable system in the desired state $\boldsymbol{x} = \boldsymbol{x}_d$ or $\boldsymbol{\xi} = \boldsymbol{0}$ at $\lim_{t\to\infty} \xi(t)$ one notices that

$$\frac{\mathrm{d}\boldsymbol{\xi}}{\mathrm{d}t} = \boldsymbol{A}\boldsymbol{x}_d,$$

This is a contradiction when thinking about the definition of asymptotically stable states, where all of the initial dynamics of the system are decayed. Since $\boldsymbol{A}$ is, by definition, regular and the desired state is arbitrarily chosen,

$$\frac{\mathrm{d}\boldsymbol{\xi}}{\mathrm{d}t} = \boldsymbol{A}\boldsymbol{x}_d = 0$$

cannot be satisfied. Remedy is provided by adding the control input u_d needed to get the system into the desired stationary state $\boldsymbol{x}_d$. The algebraic equation to determine the control input is

$$\frac{\mathrm{d}\boldsymbol{\xi}}{\mathrm{d}t} = 0 = \boldsymbol{A}\boldsymbol{x}_d + \boldsymbol{b}u_d. \tag{A.3}$$

Equation (A.3) is the relation between a control input u_d and the associated stationary state [63].

All of the above can be summarized in the control law

$$u = u_d - \boldsymbol{k}^{\mathrm{T}}\left(\boldsymbol{x} - \boldsymbol{x}_d\right) \tag{A.4}$$

and the associated differential equation together with (4.4)

$$\frac{\mathrm{d}\boldsymbol{x}}{\mathrm{d}t} = (\boldsymbol{A} - \boldsymbol{b}\boldsymbol{k}^{\mathrm{T}})\boldsymbol{\xi} + \boldsymbol{A}\boldsymbol{x}_{\boldsymbol{R}} + \boldsymbol{b}u_d. \tag{A.5}$$

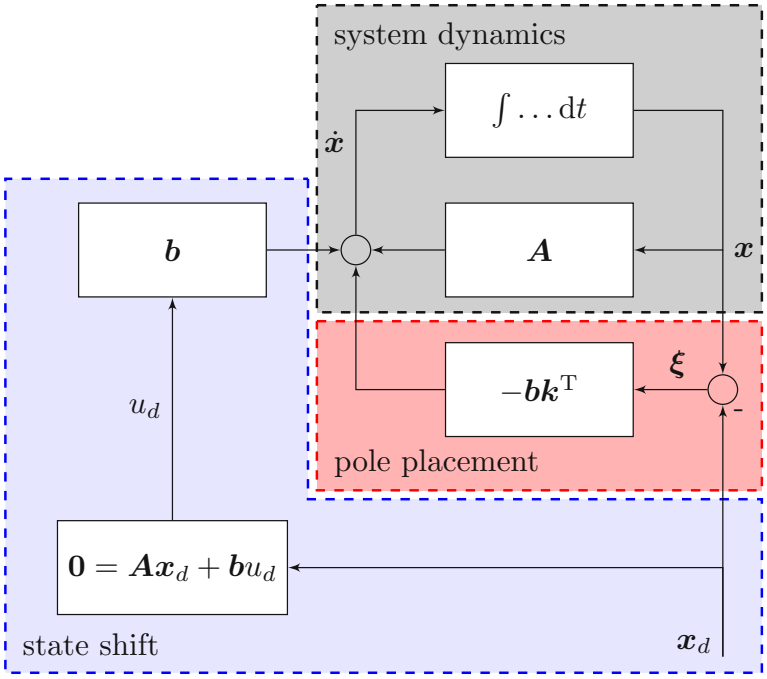

Figure A.4: Block diagram of state feedback control with state shift.

Relationship between the State Shift and Pre-Amplificatoin Gain Control Approach

Since both control approach have the same dynamics and vanishing control errors, the used relations (A.4) and (4.11) need to be equivalent. Considering the same system in both cases and presupposing asymptotically stable behaviour of the controlled system

$$\lim_{t\to\infty} \boldsymbol{x}(t) \to \boldsymbol{x}_d \leftrightarrow \lim_{t\to\infty} y(t) \to y_d \tag{A.6}$$

holds. The output variable y and the states x_i are related through (4.12). Equating (A.4) with (4.11) and using (4.12) one is left with

$$K_w \boldsymbol{c}^{\mathrm{T}} \boldsymbol{x}_d = \boldsymbol{k}^{\mathrm{T}} \boldsymbol{x}_d + u_d. \tag{A.7}$$

Multiplying both sides by $\boldsymbol{b}$ from the left and recalling (A.3) equation (A.7) is transformed to

$$\left(\boldsymbol{A} - \boldsymbol{b}\boldsymbol{k}^{\mathrm{T}} + \boldsymbol{b} K_w \boldsymbol{c}^{\mathrm{T}}\right) \boldsymbol{x}_d = 0. \tag{A.8}$$

The stationary state $\boldsymbol{x}_d$ is arbitrary and the pre-amplification factor K_w can be computed.